A novel explicit solution for twisting control of smart laminated cantilever composite plates/beams using inclined piezoelectric actuators

Soheil Gohari*, S. Sharifi, Zora Vrcelj

*Tel: +61423656484
College of Engineering and Science, Victoria University, Melbourne, VIC 8001, Australia

Email Addresses: soheil.gohari@live.vu.edu.au, soheil.gohari7@gmail.com (S. Gohari), sharifi.te@gmail.com (S. Sharifi), Zora.Vrcelj@vu.edu.au (Z. Vrcelj)

Abstract. In the present work, a novel explicit solution is proposed for obtaining twisting deformation and optimal shape control of smart laminated cantilever composite plates/beams using inclined piezoelectric actuators. The linear piezoelectricity and plate theories were adapted for the analysis. A novel double integral multivariable Fourier transformation method and discretised higher order partial differential unit step function equations were employed. For the first time, an exact solution is developed to analyse electro-mechanical twisting moments in smart composite structures. Since there are no published benchmark results for verification, a series of simple, accurate and robust finite element (FE) analysis models and realistic electro-mechanical coupled FE procedures are developed for the effective prediction of the structural behaviour of the smart laminated piezo-composite structures under arbitrary loads. In addition to the novelty of the explicit solution, more comprehensive FE simulations of smart structures and step-by-step guidelines are discussed. The effect of various parameters including electro-mechanical twisting coupling, layup thickness, actuators size, placement, and inclination angle, electrical voltage, stacking sequence, and geometrical dimension was taken into account. The comparison of results showed an excellent agreement. Unlike the earlier studies, the proposed method does not require the characteristic and trial deflection function to be predetermined.

Key Words: Twisting control; Electro-mechanical twisting coupling; Explicit solution; Finite element method (FEM); Inclined piezoelectric actuators; Smart laminated cantilever composite plates/beams.

1.Introduction

Laminated and asymmetric composite structures are being used considerably in aerospace, automotive, civil, mechanical and structural engineering applications due to their high stiffness and strength to weight ratio, low density, and temperature resistance[1][2][3]. Laminated plates and beams are usually applied to achieve the desired stiffness and lightness for parts of load-bearing engineering structures[4][5]. For instance, laminated cantilever composite plates are adopted widely in various engineering applications such as airplane wings, corrugated plates, reinforced concrete slabs, decks of contemporary steel bridges, boom arms of industrial cranes, and flight control surfaces[6][7][8]. Piezoelectric materials have recently drawn much attention due to their low power consumption, high material linearity, and quick response when induced by external forces[9][10][11]. Piezoelectric materials can be integrated with laminated composite structures to provide smart-intelligent composite systems. Numerous smart engineering structures incorporated with smart devices such as piezoelectric sensors and actuators have proved to be superior to their conventional counterparts. Static analysis of advanced composite structures under axial, transverse, twisting, and torsional loads in addition to the torsional actuation due to piezoelectric materials has potential application in mechanical systems, helicopter rotor blades, and/or blades for turbomachinery[12]. Some other applications of piezoelectric materials in smart and adaptive engineering structures are acoustical noise reduction, damage identification, structural health monitoring, vibration suppression, deflection control in missile fines, and airfoil shape changes[13][14][15]. One of the great advantages of piezoelectric materials is their ability to respond to changing environment and control structural deformation, which has led to the new generation of aerospace structures like morphing airplanes[11]. Among piezoelectric materials, bounded piezo-ceramic actuators are commonly used for shape control of online monitoring systems.

Piezoelectric actuators can also be embedded in laminated composite structures to induce structural stiffness system to the advantage [16][17][18].

Failure and deformation analysis of load-bearing structures made of isotropic/composite structures with/without piezoelectric materials have been studied broadly by several researchers using analytical methods, FEM and experimental work[19][20][21]. Milazzo [22] developed a FE model for the large deflection analysis of multi-layered smart plates. Sartorato et al [23] worked on a FE formulation for smart composite shells. This smart shell FE formulation was used as a benchmark for his work on dynamic analysis of laminated curved isotropic and orthotropic structures integrated with piezoelectric layers. The presented FE model was then verified with experimental and numerical findings available in open literature. Milazzo [22] developed a family of two dimensional (2D) refined equivalent single layer models for vibration analysis of multilayered and functionally graded smart magneto-electro-elastic plates. The single layer FE model presented in his work was validated against available benchmark three dimensional (3D) solutions. Zhang et al [24] developed a linear electro-mechanically coupled FE model for thin-walled smart composite laminates bounded with macro-fibre composite (MFC) actuators. Their proposed method was compared with numerical and experimental results. In a similar study, Zhang and Schmidt [25] formulated a FE model based on the large rotation shell theory for static and dynamic analysis of thin-walled smart piezoelectric composite laminates. Plattenburg et al [26] studied analytically, numerically, and experimentally vibration excitation of a thin plate with free boundary conditions and with multiple bounded piezoelectric actuator patches. Numerically and experimental studies were undertaken by Lin and Nien [27] on static and dynamic shape deformations of laminated plates integrated with piezoelectric actuators and subjected to unknown loads. Their study demonstrated the effectiveness of piezoelectric actuators on the shape and deflection control of composite laminates. Other experimental and numerical studies concerning the deflection and shape control of smart laminated cantilever and simply-supported composite plates and beams, as well as unattached laminates, can be found in Refs [27][28][29][30]. The FE simulation of composite structures with/without piezoelectric actuators have been studied by several researches using FE commercial software. Gohari et al[31][32]studied the mechanical deformation of laminated composite domes under internal pressure using finite element simulation and compared it with theoretical results based on classical shell theory. There are also numerous studies regarding the FE simulation of laminated thin/thick composite cylindrical shells under arbitrarily static[33][34][35]and dynamic[36][37]loads. There are several studies regarding the FE simulation of composite plates induced by piezoelectric actuators[38][39].

There are few research works presenting the effect of flexural-torsion loads on composite structures with or without piezoelectric elements. Considering torsional-bending coupling mode of beams, a very limited published benchmark results are available. Sakawa and Luo[40], adapted a shear deformable theory for modelling of a mass-coupled beam considering the internal beam damping in which a motor shaft was used to create actuation torque. The effect of warping torsion on natural frequency of a composite beam, when considering the transverse shear deformation for various beam aspect ratios, was investigated in multiple studies[41][42][43]. In addition, the vibration analysis of a beam adopting Timoshenko's beam theory and excluding the effect of warping torque was studied by Banerjee and Williams [44].

There are a few researchers who studied the torsion-bending behaviour of smart structures analytically, numerically, and experimentally. Park et al.[45] developed new models for prediction of the torsion-bending and couple extension in a beam using piezoelectric patches

with arbitrary orientation with respect to the beam axis. The model was based on a Newtonian shear lag formulation, neglecting the through-thickness strain variation in the actuator patches. However, the strain variation through-thickness of the beam was assumed to be linear. A new model to predict the effect of coupled extension and torsion-bending in a beam incorporated with piezoelectric actuators was then developed by Park and Chopra[46]. Their experimental results showed accuracy when the piezoelectric actuators had the inclination angles up to 45 degrees with respect to the beam axis. In another similar study by Chen and Chopra[47], the static bending and torsion response of a fraud-scale helicopter rotor blade was investigated. Takawa et al.[48] used the piezoelectric actuators with 90-degree inclination angle with respect to the beam principle axis to control the torsional vibration mode of the beam. Thirupathi et al.[49] investigated the effect of piezoelectric actuators on the blades for turbomachinery application using FEM. The quadrilateral shell FE model with eight nodes and curved edges was adapted for the numerical analysis of piezoelectric actuated blades. Subsequently, the results were verified using experimental findings and a good agreement between numerical and experimental results was observed. In their experimental work, the piezoelectric actuated blades were modelled as piezo-ceramic cantilevered bimorph beam.

It can be observed from available literature that most of the studies on smart piezo-composite laminates were based on experimental and/or numerical approach. In addition, there are no explicit solutions for the twisting analysis of smart cantilever composite structures induced by electrical twisting moment. There are also very limited number of studies on the torsion and deflection of beams in which the effect of different parameters, such as electro-mechanical twisting coupling, layup thickness, piezoelectric actuators size, placement, and inclination angle, electrical potential intensity, stacking sequence, and geometrical dimension, were not taken into account. Furthermore, some theories adapted for the analysis of smart structures displacement fields result in significant computational time required due to a large number of degrees of freedom [50]. Smart cantilever composite plates and beams are important structural elements, but their exact analytical evaluation is one of the most difficult problems in the theory of elasticity. Multi-scale and approximation solutions, typically adapted for analytical evaluation of smart composite laminates, are complex and require characteristic and trial deflection functions to be predetermined.

In the present work, a new explicit solution is proposed for obtaining twisting-bending deformation and optimal shape control of smart laminated cantilever composite plates and beams using inclined piezoelectric actuators. The linear piezoelectricity and plates theories are adapted for the analysis. The results are then compared with the numerical results by using finite element method (FEM). A series of simple, accurate and robust FE analysis models and realistic electro-mechanical coupled FE procedures are developed for the accurate and reliable prediction of the structural behaviour of smart laminated cantilever piezo composite structures under arbitrary electro-mechanical loads. The ABAQUS FE package is adopted for this purpose. MATLAB was also employed to obtain structural twisting-bending deformations of smart cantilever piezo composite plates/beams for the explicit evaluation of the results. Calculation of required optimal voltages to suppress the twisting-bending deformation was based on classical trial and error techniques.

2.Mathematical modelling

Consider a cantilever laminated composite plate composed of N orthotropic layers and with a total layup thickness of H. Each layer can be incorporated with arbitrarily positioned inclined piezoelectric actuators (see Fig.1). Considering the material linearity for small displacements,

the Kirchhoff hypothesis leads to the general form of displacement fields as shown in Eqs.1a-c[51]. For composite laminates and piezoelectric layers/patches, some initial assumptions for mathematical modelling are made as follows[51][52]:

- Fibers distribution throughout the matrix is uniform;
- There is a perfect bonding between fibers and matrix, avoiding fibers dislocations and disarrangements through the matrix and no slip occurs between the lamina interfaces;
- The matrix is perfectly fabricated with no voids and impurity;
- The lamina is not initially pre-stressed, thus, there are no residual stresses in presence of matrix and fibers; and
- The matrix and fibers behave linearly within elastic domain.

For the smart part of the laminates, the linear piezoelectricity theory is adapted with assumptions made as follows[52]:

- The strain-electric filed varies linearly;
- The piezoelectric confidents are constant within the linear zone; thus, they cannot be electrically turned with a bias field;
- The electric field is assumed to be constant across each lamina; and
- The piezoelectric actuators are polarized through thickness; therefore, the electrical discharge through thickness Φ_z is considered in this study ($\Phi_x = \Phi_y = o$).

$$u(x,y,z) = u_0(x,y) - z\frac{\partial w_0}{\partial x} \tag{1.a}$$

$$v(x,y,z) = v_0(x,y) - z\frac{\partial w_0}{\partial y} \tag{1.b}$$

$$w(x,y,z) = w_0(x,y) \tag{1.c}$$

u_0, v_0, and w_0 are the mid-plane displacements along x, y, and z directions, respectively on the xy-plane[53]. z is the vertical distance from the mid-plane to the k^{th} layer which is located between $z = h_k$ and $z = h_{k+1}$ through laminate thickness, as shown in Fig.2. After obtaining the mid-plane displacements, the displacements of any arbitrary point, x, y, and z in 3D space can be determined. The linear strain-displacement relation is stated in Eqs.2a-c[54]. It is assumed that all strain components change linearly in the entire laminate independent from changes in material properties through layup thickness.

$$\begin{bmatrix}\varepsilon_{xx} & \varepsilon_{yy} & \gamma_{xy}\end{bmatrix}^T = \begin{bmatrix}\frac{\partial u}{\partial x} & \frac{\partial v}{\partial y} & \frac{\partial u}{\partial y}+\frac{\partial v}{\partial x}\end{bmatrix}^T = \begin{bmatrix}\varepsilon_{xx}^0 & \varepsilon_{yy}^0 & \tau_{xy}^0\end{bmatrix}^T + z\begin{bmatrix}\varepsilon_{xx}^f & \varepsilon_{yy}^f & \tau_{xy}^f\end{bmatrix}^T \tag{2a}$$

where,

$$\begin{bmatrix}\varepsilon_{xx}^o & \varepsilon_{yy}^o & \gamma_{xy}^o\end{bmatrix}^T = \begin{bmatrix}\frac{\partial u_o}{\partial x} & \frac{\partial v_o}{\partial y} & \frac{\partial u_o}{\partial y}+\frac{\partial v_o}{\partial x}\end{bmatrix}^T \tag{2b}$$

$$\begin{bmatrix}\varepsilon_{xx}^f & \varepsilon_{yy}^f & \gamma_{xy}^f\end{bmatrix}^T = \begin{bmatrix}-\frac{\partial^2 w_0}{\partial x^2} & -\frac{\partial^2 w_0}{\partial y^2} & -2\frac{\partial^2 w_0}{\partial x \partial y}\end{bmatrix}^T \tag{2c}$$

ε_{xx}^{o}, ε_{yy}^{o}, and γ_{xy}^{o} are the laminate's mid-plane strains, $\varepsilon_{xx}^{f}, \varepsilon_{yy}^{f}$, and γ_{xy}^{f} are the flexural (bending) strains and w_o is the transverse deflection of a composite laminate's mid-plane. The bending strains are typically caused by laminate's stacking sequence asymmetric or external electro-mechanical bending and twisting loads. Since the flexural shape control of the lateral displacements is considered in this study, the effect of laminate's mid-plane strains can be neglected and the effect of flexural strains are taken into account. Considering the plane stress assumption and neglecting the through-thickness stresses, the simplified 2D electro-mechanical plate equations are derived from the 3D equations of theory of elasticity and three charged equilibrium equations of piezoelectric medium, as stated in Eq.3a[55]. The electrical field potential relationships for an orthotropic static piezoelectric lamina is stated in Eg.3b[56].

$$\begin{bmatrix}\sigma_{11}\\ \sigma_{22}\\ 0\\ 0\\ 0\\ \tau_{12}\end{bmatrix}^{k} = \begin{bmatrix} C_{1111} & C_{1122} & C_{1133} & 0 & 0 & 0 \\ C_{1122} & C_{2222} & C_{2233} & 0 & 0 & 0 \\ C_{1133} & C_{2233} & C_{3333} & 0 & 0 & 0 \\ 0 & 0 & 0 & C_{2323} & 0 & 0 \\ 0 & 0 & 0 & 0 & C_{3131} & 0 \\ 0 & 0 & 0 & 0 & 0 & C_{1212} \end{bmatrix}^{k} \begin{bmatrix}\varepsilon_{11}\\ \varepsilon_{22}\\ \varepsilon_{33}\\ \gamma_{23}\\ \gamma_{31}\\ \gamma_{12}\end{bmatrix}^{k} - \begin{bmatrix} 0 & 0 & e_{311} \\ 0 & 0 & e_{322} \\ 0 & 0 & e_{333} \\ 0 & e_{223} & 0 \\ e_{113} & 0 & 0 \\ 0 & 0 & 0 \end{bmatrix}^{k} \begin{bmatrix}\Phi_1\\ \Phi_2\\ \Phi_3\end{bmatrix}^{k} \tag{3a}$$

$$\begin{bmatrix}\rho_1\\ \rho_2\\ \rho_3\end{bmatrix}^{k} = \begin{bmatrix} 0 & 0 & 0 & 0 & e_{113} & 0 \\ 0 & 0 & 0 & e_{223} & 0 & 0 \\ e_{311} & e_{322} & e_{333} & 0 & 0 & 0 \end{bmatrix}^{k} \begin{bmatrix}\varepsilon_{11}\\ \varepsilon_{22}\\ \varepsilon_{33}\\ \gamma_{23}\\ \gamma_{31}\\ \gamma_{12}\end{bmatrix}^{k} + \begin{bmatrix} \zeta_{11} & 0 & 0 \\ 0 & \zeta_{22} & 0 \\ 0 & 0 & \zeta_{33} \end{bmatrix}^{k} \begin{bmatrix}\Phi_1\\ \Phi_2\\ \Phi_3\end{bmatrix}^{k} \tag{3b}$$

$\sigma_{ij}, \varepsilon_{ij}, C_{ijkl}, e_{ijk}$, and Φ_i are the stresses, the strains, the elastic stiffness, the piezoelectric coefficients, and the components of the electric fields, respectively in the orthotropic material orientation. p_i and ζ_{ij} are the electric displacement and the piezoelectric dielectric constants, respectively. The Kirchhoff assumption adapted for plate theory stipulates that $\gamma_{23} = \gamma_{31} = 0$. In addition, only a through-thickness electric field is considered. Therefore, Eqs.3a-b are reduced to Eq.4a. Global stresses (Eq.4b) in the k^{th} ply along *xyz* direction can be calculated by transforming 2D stresses in the material direction through transformation matrix [*T*] (Eq.4c)[57].

$$\begin{bmatrix}\sigma_{11}\\ \sigma_{22}\\ \tau_{12}\\ \rho_3\end{bmatrix}^{k} = \begin{bmatrix} Q_{11} & Q_{12} & 0 \\ Q_{12} & Q_{22} & 0 \\ 0 & 0 & Q_{66} \\ e_{31} & e_{32} & 0 \end{bmatrix}^{k} \begin{bmatrix}\varepsilon_{11}\\ \varepsilon_{22}\\ \gamma_{12}\end{bmatrix}^{k} - \begin{bmatrix}e_{31}\\ e_{32}\\ 0\\ \zeta_{33}\end{bmatrix}^{k} \Phi_3^k \tag{4a}$$

$$\left[\sigma\right]_k^{Global} = \left[T\right]^{-1}\left[\sigma\right]_k^{Local} \tag{4b}$$

$$[T]=\begin{bmatrix} c^2 & s^2 & 2cs \\ s^2 & c^2 & -2cs \\ -cs & cs & \left(c^2-s^2\right) \end{bmatrix} \tag{4c}$$

c is $cos(\beta)$ and s is $sin(\beta)$.β is the winding angle between fibres and x axis. Q_{ij} and e_{ij} are the reduced elastic stiffness and the piezoelectric modules, respectively, as given in Eqs.5e-f, respectively.

$$Q_{11}=C_{1111}-\frac{C_{1133}^2}{C_{3333}}=\frac{E_1}{1-\nu_{12}\nu_{21}} \tag{5a}$$

$$Q_{22}=C_{2222}-\frac{C_{2233}^2}{C_{3333}}=\frac{E_2}{1-\nu_{12}\nu_{21}} \tag{5b}$$

$$Q_{12}=C_{1122}-\frac{C_{1133}C_{2233}}{C_{3333}}=\frac{\nu_{12}E_2}{1-\nu_{12}\nu_{21}} \tag{5c}$$

$$Q_{66}=C_{1212}=G_{12} \tag{5d}$$

$$e_{31}=e_{311}-\frac{C_{1133}}{C_{3333}}e_{333}=Q_{11}d_{31}-Q_{12}d_{32} \tag{5e}$$

$$e_{32}=e_{322}-\frac{C_{2233}}{C_{3333}}e_{333}=Q_{12}d_{31}-Q_{22}d_{32} \tag{5f}$$

E_1, E_2, ν_{12}, and G_{12} are in-plane local elasticity modules of an orthotropic layer in the local material coordinate system. d_{ij} is the piezoelectric dielectric constant. The in-plane stress-strain relationship for the k^{th} smart orthotropic piezo-composite plate is shown in Eq.6a [38]. For the beam type laminates, the plane stress assumption is adapted and the width along y direction is assumed to be stress free. Therefore, Eq.6a is reduced to Eq.6b and only the transformed piezoelectric coefficient along x axis is considered[12].

$$\begin{bmatrix} \sigma_{xx} \\ \sigma_{yy} \\ \tau_{xy} \\ \rho_z \end{bmatrix}^k=\begin{bmatrix} \overline{Q}_{11} & \overline{Q}_{12} & \overline{Q}_{16} \\ \overline{Q}_{12} & \overline{Q}_{22} & \overline{Q}_{26} \\ \overline{Q}_{16} & \overline{Q}_{26} & \overline{Q}_{66} \\ \overline{e}_{31} & \overline{e}_{32} & \overline{e}_{36} \end{bmatrix}^k\begin{bmatrix} \varepsilon_{xx} \\ \varepsilon_{yy} \\ \gamma_{xy} \end{bmatrix}^k-\begin{bmatrix} \overline{e}_{31} \\ \overline{e}_{32} \\ \overline{e}_{36} \\ \zeta_{33} \end{bmatrix}^k\Phi_3^k \tag{6a}$$

$$\begin{bmatrix} \sigma_{xx} \\ \tau_{xy} \\ \rho_z \end{bmatrix}^k=\begin{bmatrix} \overline{Q}_{11} & \overline{Q}_{16} \\ \overline{Q}_{16} & \overline{Q}_{66} \\ \overline{e}_{31} & \overline{e}_{36} \end{bmatrix}^k\begin{bmatrix} \varepsilon_{xx} \\ \gamma_{xy} \end{bmatrix}^k-\begin{bmatrix} \overline{e}_{31} \\ \overline{e}_{36} \\ \zeta_{33} \end{bmatrix}^k\Phi_3^k \tag{6b}$$

$\overline{Q}_{ij}^k$ and $\overline{e}_{ij}^k$ are the transformed reduced stiffness matrix and transformed piezoelectric modules in the k^{th} orthotropic layer, respectively. In Eqs.6a-b, σ_{ij}^k and ε_{ij}^k are the in-plane stress, strain, and electrical field components of the k^{th} orthotropic layer in xyz coordinate system, respectively. The elements of transformed reduced stiffness matrix are described in Eqs.7a-f, respectively[52].

$$\overline{Q}_{11} = Q_{11}c^4 + 2(Q_{12} + 2Q_{66})c^2s^2 + Q_{22}s \quad (7a)$$
$$\overline{Q}_{12} = (Q_{11} + Q_{22} - 4Q_{66})c^2s^2 + Q_{12}(c^4 + s^4) \quad (7b)$$
$$\overline{Q}_{22} = Q_{11}s^4 + 2(Q_{12} + 2Q_{66})c^2s^2 + Q_{22}c^4 \quad (7c)$$
$$\overline{Q}_{16} = -Q_{22}cs^3 + Q_{11}c^3s - (Q_{12} + 2Q_{66})(c^2 - s^2)cs \quad (7d)$$
$$\overline{Q}_{26} = -Q_{22}c^3s + Q_{11}cs^3 - (Q_{12} + 2Q_{66})(c^2 - s^2)cs \quad (7e)$$
$$\overline{Q}_{66} = (Q_{11} + Q_{22} - 2Q_{12})c^2s^2 + Q_{66}(c^2 - s^2)^2 \quad (7f)$$

The transformed piezoelectric modules are described in Eqs.8a-c, respectively [52].

$$\overline{e}_{31} = \overline{Q}_{11}\overline{d}_{31} + \overline{Q}_{12}\overline{d}_{32} = \overline{Q}_{11}\left(d_{31}\Gamma^2 + d_{32}\Gamma'^2\right) + \overline{Q}_{12}\left(d_{31}\Gamma'^2 + d_{32}\Gamma^2\right) \quad (8a)$$
$$\overline{e}_{32} = \overline{Q}_{12}\overline{d}_{31} + \overline{Q}_{22}\overline{d}_{32} = \overline{Q}_{12}\left(d_{31}\Gamma^2 + d_{32}\Gamma'^2\right) + \overline{Q}_{22}\left(d_{31}\Gamma'^2 + d_{32}\Gamma^2\right) \quad (8b)$$
$$\overline{e}_{36} = \overline{Q}_{66}\overline{d}_{36} = 2\overline{Q}_{66}(d_{31} - d_{32})\Gamma\Gamma' \quad (8c)$$

$\overline{d}_{ij}^{\,k}$ are the transformed piezoelectric dielectric constants in the k^{th} orthotropic layer. Γ and Γ' stand for $\cos(\theta)$ and $\sin(\theta)$, respectively. θ is the inclination angle between the piezoelectric actuators and x axis, as shown in Figs.1-2. The relationship between stress resultants and flexural-twisting moments for the mid-plane in a composite laminate is described in Eq.9 [58]. First, Eq.2a is substituted into Eq.6a. Subsequently, by substituting Eq.6a into Eq.9, Eq.10 is derived.

$$\left[M_{xx} \quad M_{yy} \quad M_{xy}\right]^T = \int_{-H/2}^{H/2} z\left(\sigma_{xx}, \sigma_{yy}, \tau_{xy}\right)dz - \left[M_{xx}^P \quad M_{yy}^P \quad M_{xy}^P\right]^T \quad (9)$$

$$\begin{bmatrix} M_{xx} \\ M_{yy} \\ M_{xy} \end{bmatrix} = \begin{bmatrix} B_{11} & B_{12} & B_{16} \\ B_{12} & B_{22} & B_{26} \\ B_{16} & B_{26} & B_{66} \end{bmatrix} \begin{bmatrix} \dfrac{\partial u_o}{\partial x} \\ \dfrac{\partial v_o}{\partial y} \\ \dfrac{\partial u_o}{\partial y} + \dfrac{\partial v_o}{\partial x} \end{bmatrix} + \begin{bmatrix} D_{11} & D_{12} & D_{16} \\ D_{12} & D_{22} & D_{26} \\ D_{16} & D_{26} & D_{66} \end{bmatrix} \begin{bmatrix} -\dfrac{\partial^2 w_0}{\partial x^2} \\ -\dfrac{\partial^2 w_0}{\partial y^2} \\ -2\dfrac{\partial^2 w_0}{\partial x \partial y} \end{bmatrix} - \begin{bmatrix} M_{xx} \\ M_{yy} \\ M_{xy} \end{bmatrix}^P \quad (10)$$

$[M_{xx}]^P$, $[M_{yy}]^P$, and $[M_{xy}]^P$ are bending and twisting moments induced by electrical loads, respectively[59]. It is assumed that the electric positional fields vary linearly through laminate thickness. Therefore, the linear interpolation functions can be used to simplify the electrical gradients, as shown in Eq.11 (Note: $\Phi_3 = \Phi_z$).

$$\Phi_z(x, y, z) = \Phi_a^k(x, y, z)\omega_1^k(z) + \Phi_b^k(x, y, z)\omega_2^k(z) \quad (11)$$

ω_i^k, i={1,2} shown in Eq.12 represents the linear interpolation function of the k^{th} orthotropic layer in a smart piezo-composite laminate.

$$\omega_1^k = \frac{h_{k+1} - h}{t_k} = \frac{h_{k+1} - h}{P_n t_a + N t_p}, \omega_2^k = \frac{h - h_k}{t_k} = \frac{h - h_k}{P_n t_a + N t_p}, h_k \le h \le h_{k+1} \quad (12)$$

P_n, t_a, and t_p in Eq.12 are the number of inclined piezoelectric actuators, and actuator thickness, and host structure (composite laminate) thickness, respectively (See Fig.1). Governing partial differential equation relating the transverse bending and twisting moments

to mid-plane displacements and electro-mechanical loads in a smart laminated piezo composite plate is stated in Eq.13[38]. In this study, thin symmetrical cross-ply laminates are considered. Thus, the effects of bending-stretching coupling matrix ($[B_{ij}]=0$) and bending-twisting elements of flexural stiffness matrix ($D_{16}=D_{26}=0$) in Eq.6 are neglected. However, due to inclination angle between the inclined piezoelectric actuators and composite laminate with respect to x axis, the effect of electrical twisting moment should not be neglected.

In the next step, the linear interpolation of the electrical functions stated in Eq.11 is substituted into Eq.10. Finally, by applying the initial conditions to Eq.10, it can be simplified to Eq.14. By substituting Eq.14 into Eq.13, Eqs.15a-d is derived.

$$\frac{\partial^2 (M_{xx}^{total} - M_{xx}^{P})}{\partial x^2} + 2\frac{\partial^2 (M_{xy}^{total} - M_{xy}^{P})}{\partial x \partial y} + \frac{\partial^2 (M_{yy}^{total} - M_{yy}^{P})}{\partial y^2} = P_m(x, y) \tag{13}$$

$$\begin{bmatrix} M_{xx} \\ M_{yy} \\ M_{xy} \end{bmatrix} = \begin{bmatrix} D_{11} & D_{12} & 0 \\ D_{12} & D_{22} & 0 \\ 0 & 0 & D_{66} \end{bmatrix} \begin{bmatrix} -\dfrac{\partial^2 w_0}{\partial x^2} \\ -\dfrac{\partial^2 w_0}{\partial y^2} \\ -2\dfrac{\partial^2 w_0}{\partial x \partial y} \end{bmatrix} - \begin{bmatrix} M_{xx}^{P} \\ M_{yy}^{P} \\ M_{xy}^{P} \end{bmatrix} \tag{14}$$

$$D_{11}\frac{\partial^4 w_0}{\partial x^4} + 2(D_{12} + 2D_{66})\frac{\partial^4 w_0}{\partial x^2 \partial y^2} + D_{22}\frac{\partial^4 w_0}{\partial y^4} = P_m(x, y) + \frac{\partial^2 M_{xx}^{P}}{\partial x^2} + \frac{\partial^2 M_{yy}^{T}}{\partial y^2} + 2\frac{\partial^2 M_{xy}^{P}}{\partial x \partial y} \tag{15a}$$

where,

$$P_e(x, y) = \frac{\partial^2 M_{xx}^{P}}{\partial x^2} + \frac{\partial^2 M_{yy}^{T}}{\partial y^2} + 2\frac{\partial^2 M_{xy}^{P}}{\partial x \partial y} \tag{15b}$$

$$\left[M_i^{P}\right] = \sum_{k=1}^{N} \int_{h_k}^{h_{k+1}} \left[\overline{Q}_{ij}\right]^k \left[\overline{d}_{3j}\right]^k E_z^k z dz = \frac{1}{6}\sum_{k=1}^{N} \sum_{j=1,2,6} \left[\overline{Q}_{ij}\right]^k \left[\overline{d}_{3j}\right]^k \left\{E_1^k(h_k + 3z_k) + E_2^k(2h_k + 3z_k)\right\} h_k \tag{15c}$$

$$D_{ij} = \frac{1}{3}\sum_{K=1}^{N} \sum_{j=1,2,6} \left[\overline{Q}_{ij}\right]_k (h_K^3 - h_{K-1}^3) \tag{15d}$$

$i=j=\{1,2,6\}$, D_{11} and D_{22} are flexural stiffness about x and y axis, respectively, D_{12} and D_{66} stand for effective torsional rigidity. $P_m(x,y)$ and $P_e(x,y)$ are mechanical and electrical loads applied to the smart piezo composite laminate, respectively. $[M]^{total}$ is the combination of electrical and mechanical moments. The schematic of coordinate system and geometry of the smart laminated cantilever piezo composite plate with incorporated piezoelectric actuators and actuators size and placements is illustrated in Fig.2. Activated inclined piezoelectric actuators are capable of inducing bending and twisting moments which can be expressed in terms of 2D unit step functions[38][60]. In this study, mechanical load and electrical moments are expressed in the form of multivariable unit step functions according to Eqs.16a-b, respectively.

$$\left[M_i\right]^{P} = \frac{1}{6}\sum_{L=1}^{Pn} \sum_{k=1}^{N} \sum_{j=1,2,6} \left[\overline{Q}_{ij}\right]^k \left[\overline{d}_{3j}\right]^k \left\{E_1^k(h_k + 3z_k) + E_2^k(2h_k + 3z_k)\right\} h_k \left[U_k^L(x - x_{1P}) - U_k^L(x - x_{2P})\right]\left[U_k^L(y - y_{1P}) - U_k^L(y - y_{2P})\right] \tag{16a}$$

$$P_m = \sum_{L=1}^{Mn} P_m(x, y)\left[U_k^L(x - x_{1M}) - U_k^L(x - x_{2M})\right]\left[U_k^L(y - y_{1M}) - U_k^L(y - y_{2M})\right] \tag{16b}$$

$i=j=\{1,2,6\}$ and $U_k^L(x,y)$ presents the unit step function expressed for effective areas at which the electrical bending and twisting moments are applied at the L^{th} location and in the k^{th} ply. M_n and P_n are the number of effective areas at which the mechanical and electrical loads are applied, respectively (see Fig.2). The general electro-mechanical load resultants applied to a plate element are expressed in Eqs.17a-g.

$$M_{xx}^{total} = -\left[D_{11}\frac{\partial^2 w_0}{\partial x^2} + D_{12}\frac{\partial^2 w_0}{\partial y^2} \right] \tag{17a}$$

$$M_{yy}^{total} = -\left[D_{22}\frac{\partial^2 w_0}{\partial y^2} + D_{12}\frac{\partial^2 w_0}{\partial x^2} \right] \tag{17b}$$

$$M_{xy}^{total} = -2D_{66}\frac{\partial^2 w_0}{\partial x \partial y} \tag{17c}$$

$$Q_{xx}^{total} = -\frac{\partial}{\partial x}\left[D_{11}\frac{\partial^2 w_0}{\partial x^2} + 2(D_{12}+D_{66})\frac{\partial^2 w_0}{\partial y^2} \right] \tag{17d}$$

$$Q_{yy}^{total} = -\frac{\partial}{\partial y}\left[D_{22}\frac{\partial^2 w_0}{\partial y^2} + 2(D_{12}+D_{66})\frac{\partial^2 w_0}{\partial x^2} \right] \tag{17e}$$

$$V_{xx}^{total} = -\frac{\partial}{\partial x}\left[D_{11}\frac{\partial^2 w_0}{\partial x^2} + 2(D_{12}+D_{66})\frac{\partial^2 w_0}{\partial y^2} \right] - 2D_{66}\frac{\partial}{\partial y}\left[\frac{\partial^2 w_0}{\partial x \partial y} \right] \tag{17f}$$

$$V_{yy}^{total} = -\frac{\partial}{\partial y}\left[D_{22}\frac{\partial^2 w_0}{\partial y^2} + 2(D_{12}+D_{66})\frac{\partial^2 w_0}{\partial x^2} \right] - 2D_{66}\frac{\partial}{\partial x}\left[\frac{\partial^2 w_0}{\partial x \partial y} \right] \tag{17g}$$

M_{xx}, M_{yy}, M_{xy}, Q_{xx}, Q_{yy}, V_{xx}, and V_{yy} are bending moment resultants, torsional moment resultants, shear force resultants, and the total shear force resultants per unit length, respectively [58]. The boundary conditions for a cantilever plate are prescribed as stated in Eqs.18a-j.

$$w_0(0,y) = 0 \tag{18a}$$

$$\frac{\partial w_o}{\partial x}(0,y) = 0 \tag{18b}$$

$$M_{xx}(a,y) = 0 \tag{18c}$$

$$M_{yy}(x,0) = 0 \tag{18d}$$

$$M_{yy}(x,b) = 0 \tag{18e}$$

$$V_{xx}(a,y) = 0 \tag{18f}$$

$$V_{yy}(x,0) = 0 \tag{18g}$$

$$V_{yy}(x,b) = 0 \tag{18h}$$

$$M_{xy}(a,0) = 0 \tag{18i}$$

$$M_{xy}(a,b) = 0 \tag{18j}$$

The double finite integral transformation of the mid-plane vertical displacement of function $w_o(x,y)$ is shown in Eq.19.

$$w_{mn} = \int_0^a \int_0^a w_0(x,y)\sin(\frac{\alpha_m}{2}x)\cos(\beta_n y)dxdy \quad (m=1,3,5,\ldots)(n=0,1,2,\ldots) \tag{19}$$

Eq.19 is then inversed to represent the exact mid-plane vertical displacement of function $w_o(x,y)$ as stated in Eq.20.

$$w_0(x,y)=\frac{4}{ab}\sum_{m=1,3,5,\ldots}^{\infty}\sum_{n=0,1,2,\ldots}^{\infty} w_{mn}\lambda_n \sin(\frac{\alpha_m}{2}x)\cos(\beta_n y) \tag{20}$$

where,

$$\alpha_m=\frac{m\pi}{a},\ \beta_n=\frac{n\pi}{b}\ \text{and}\ \lambda_n=\begin{cases}0.5\rightarrow(n=0)\\1\rightarrow(n=1,2,3,\ldots)\end{cases}$$

In Eq.20, a and b stand for the plate's length and width, respectively (see Fig.1). The double integral transformation of higher-order partial derivatives of the multivariable function $w_o(x,y)$ over Eq.15a results in Eqs.21a-f:

$$\begin{aligned}&\int_0^a\int_0^b\left[D_{11}\frac{\partial^4 w_0}{\partial x^4}+2(D_{12}+2D_{66})\frac{\partial^4 w_0}{\partial x^2\partial y^2}+D_{22}\frac{\partial^4 w_0}{\partial y^4}\right]\sin(\frac{\alpha_m}{2}x)\cos(\beta_n y)dxdy=\\&\int_0^a\int_0^b\left[P_m(x,y)+\frac{\partial^2 M_{xx}^P}{\partial x^2}+2\frac{\partial^2 M_{xy}^P}{\partial x\partial y}+\frac{\partial^2 M_{yy}^P}{\partial y^2}\right]\sin(\frac{\alpha_m}{2}x)\cos(\beta_n y)dxdy\end{aligned} \tag{21a}$$

where,

$$I_1=\int_0^a\int_0^b\frac{\partial^4 w_0}{\partial x^4}\sin(\frac{\alpha_m}{2}x)\cos(\beta_n y)dxdy \tag{21b}$$

$$I_2=\int_0^a\int_0^b\frac{\partial^4 w_0}{\partial y^4}\sin(\frac{\alpha_m}{2}x)\cos(\beta_n y)dxdy \tag{21c}$$

$$I_3=\int_0^a\int_0^b\frac{\partial^4 w_0}{\partial x^2\partial y^2}\sin(\frac{\alpha_m}{2}x)\cos(\beta_n y)dxdy \tag{21d}$$

$$I_4=\int_0^a\int_0^b P_m(x,y)\sin(\frac{\alpha_m}{2}x)\cos(\beta_n y)dxdy \tag{21e}$$

$$I_5=\int_0^a\int_0^b\left(\frac{\partial^2 M_{xx}^P}{\partial x^2}+2\frac{\partial^2 M_{xy}^P}{\partial x\partial y}+\frac{\partial^2 M_{yy}^P}{\partial y^2}\right)\sin(\frac{\alpha_m}{2}x)\cos(\beta_n y)dxdy \tag{21f}$$

Considering the integral by parts principle and applying the boundary conditions in Eqs.18a,b,i,j to I_1, I_2, and I_3, the double integral transformations of higher-order partial derivatives of the function $w_o(x,y)$ over Eqs.21b-e result in Eqs.22a-e, respectively.

$$\begin{aligned}&I_1=\int_0^a\int_0^b\frac{\partial^4 w_0}{\partial x^4}\sin(\frac{\alpha_m}{2}x)\cos(\beta_n y)dxdy=\\&\int_0^b\left[(-1)^{\frac{m-1}{2}}\left(\frac{\partial^3 w_0}{\partial x^3}\middle|x=a\right)+\frac{\alpha_m}{2}\left(\frac{\partial^2 w_0}{\partial x^2}\middle|x=0\right)-(-1)^{\frac{m-1}{2}}\frac{\alpha_m^2}{4}\left(\frac{\partial w_0}{\partial x}\middle|x=a\right)-\frac{\alpha_m^3}{8}\left(w_0\middle|x=0\right)\right]\cos(\beta_n y)dy\\&+\frac{\alpha_m^4}{16}w_{mn}=\int_0^b\left[(-1)^{\frac{m-1}{2}}\left(\frac{\partial^3 w_0}{\partial x^3}\middle|x=a\right)+\frac{\alpha_m}{2}\left(\frac{\partial^2 w_0}{\partial x^2}\middle|x=0\right)-(-1)^{\frac{m-1}{2}}\frac{\alpha_m^2}{4}\left(\frac{\partial w_0}{\partial x}\middle|x=a\right)\right]\cos(\beta_n y)dy\\&+\frac{\alpha_m^4}{16}w_{mn}\end{aligned} \tag{22a}$$

$$I_2 = \int_0^a \int_0^b \frac{\partial^4 w_0}{\partial y^4} \sin(\frac{\alpha_m}{2} x) \cos(\beta_n y) dx dy =$$

$$\int_0^a \left[(-1)^n \left(\frac{\partial^3 w_0}{\partial y^3} \middle| y = b \right) - \left(\frac{\partial^3 w_0}{\partial y^3} \middle| y = 0 \right) - (-1)^n \beta_n^2 \left(\frac{\partial w_0}{\partial y} \middle| y = b \right) + \beta_n^2 \left(\frac{\partial w_0}{\partial y} \middle| y = 0 \right) \right] \sin(\frac{\alpha_m}{2} x) dx \quad (22b)$$

$$+ \beta_n^4 w_{mn}$$

$$I_3 = \int_0^a \int_0^b \frac{\partial^4 w_0}{\partial x^2 \partial y^2} \sin(\frac{\alpha_m}{2} x) \cos(\beta_n y) dx dy =$$

$$(-1)^n (-1)^{\frac{m-1}{2}} \left(\frac{\partial^2 w_0}{\partial x \partial y} \middle| \begin{matrix} x = a \\ y = b \end{matrix} \right) - (-1)^{\frac{m-1}{2}} \left(\frac{\partial^2 w_0}{\partial x \partial y} \middle| \begin{matrix} x = a \\ y = 0 \end{matrix} \right) + (-1)^n \frac{\alpha_m}{2} \left(\frac{\partial w_0}{\partial y} \middle| \begin{matrix} x = 0 \\ y = b \end{matrix} \right) - \frac{\alpha_m}{2} \left(\frac{\partial w_0}{\partial y} \middle| \begin{matrix} x = 0 \\ y = 0 \end{matrix} \right)$$

$$+ \frac{\alpha_m^2 \beta_n^2}{4} w_{mn} - \frac{\alpha_m^2}{4} \int_0^a \left[(-1)^n \left(\frac{\partial w_0}{\partial y} \middle| y = b \right) - \left(\frac{\partial w_0}{\partial y} \middle| y = 0 \right) \right] \sin(\frac{\alpha_m}{2} x) dx - \beta_n^2 \int_0^b \left[(-1)^{\frac{m-1}{2}} \left(\frac{\partial w_0}{\partial x} \middle| x = a \right) \right. \quad (22c)$$

$$\left. + \frac{\alpha_m}{2} \left(w_0 \middle| x = 0 \right) \right] \cos(\beta_n y) dy = -\frac{\alpha_m^2}{4} \int_0^a \left[(-1)^n \left(\frac{\partial w_0}{\partial y} \middle| y = b \right) - \left(\frac{\partial w_0}{\partial y} \middle| y = 0 \right) \right] \sin(\frac{\alpha_m}{2} x) dx$$

$$- (-1)^{\frac{m-1}{2}} \beta_n^2 \int_0^b \left[\left(\frac{\partial w_0}{\partial x} \middle| x = a \right) \right] \cos(\beta_n y) dy + \frac{\alpha_m^2 \beta_n^2}{4} w_{mn}$$

Let $P_m(x, y) = P_o$ be defined as uniform distributed pressure or patch loading magnitude, hence:

$$I_4 = \int_0^a \int_0^b \sum_{L=1}^{Mn} P_o \left[U_k^L (x - x_{1M}) - U_k^L (x - x_{2M}) \right] \left[U_k^L (y - y_{1M}) - U_k^L (y - y_{2M}) \right] \sin(\frac{\alpha_m}{2} x) \cos(\beta_n y) dx dy$$

If n={0}, m={1,3,5…}, then,

$$I_4 = \sum_{L=1}^{Mn} \left(\frac{-2P_o}{\alpha_m} \right) \left(y_{1M} - y_{2M} \right)_L \left(\cos(\frac{\alpha_m}{2} x_{1M}) - \cos(\frac{\alpha_m}{2} x_{2M}) \right)_L \quad (22d)$$

and if n={1,2,3,…}, m={1,3,5,…}, then,

$$I_4 = \sum_{L=1}^{Mn} \left(\frac{-2P_o}{\alpha_m \beta_n} \right) \left(\cos(\frac{\alpha_m}{2} x_{1M}) - \cos(\frac{\alpha_m}{2} x_{2M}) \right)_L \left(\sin(\beta_n y_{1M}) - \sin(\beta_n y_{2M}) \right)_L \quad (22e)$$

The second derivatives of partial differential 2D unit step function equations of electrical bending and twisting moments (Eq.21f) acting on a smart laminated cantilever piezo composite plate with respect to x and y are expanded in Eqs.23a-f, respectively.

$$\frac{\partial^2 M_{xx}^P}{\partial x^2} = \frac{1}{6} \sum_{L=1}^{Tn} \sum_{k=1}^{N} \sum_{j=1,2,6} \left[\overline{Q}_{1j} \right]^k \left[\overline{d}_{3j} \right]^k h_k \left\{ E_1^k (h_k + 3z_k) + E_2^k (2h_k + 3z_k) \right\} \frac{\partial^2}{\partial x^2} \left(\left[U_k^L (x - x_{1P}) - U_k^L (x - x_{2P}) \right] \right.$$

$$\left. \left[U_k^L (y - y_{1P}) - U_k^L (y - y_{2P}) \right] \right) = \frac{1}{6} \sum_{L=1}^{Tn} \sum_{k=1}^{N} \sum_{j=1,2,6} \left[\overline{Q}_{1j} \right]^k \left[\overline{d}_{3j} \right]^k h_k \left\{ E_1^k (h_k + 3z_k) + E_2^k (2h_k + 3z_k) \right\} \left[U_k^L (y - y_{1P}) \right. \quad (23a)$$

$$\left. - U_k^L (y - y_{2P}) \right] \left[\delta_k^{'L} (x - x_{1P}) - \delta_k^{'L} (x - x_{2P}) \right]$$

$$\frac{\partial^2 M_{yy}^{P}}{\partial y^2}=\tfrac{1}{6}\sum_{L=1}^{Tn}\sum_{k=1}^{N}\sum_{j=1,2,6}\left[\overline{Q}_{2j}\right]^k\left[\overline{d}_{3j}\right]^k h_k\left\{E_1^k(h_k+3z_k)+E_2^k(2h_k+3z_k)\right\}\frac{\partial^2}{\partial y^2}\left(\left[U_k^L(x-x_{1P})-U_k^L(x-x_{2P})\right]\right.$$

$$\left.\left[U_k^L(y-y_{1P})-U_k^L(y-y_{2P})\right]\right)=\tfrac{1}{6}\sum_{L=1}^{Tn}\sum_{k=1}^{N}\sum_{j=1,2,6}\left[\overline{Q}_{2j}\right]^k\left[\overline{d}_{3j}\right]^k h_k\left\{E_1^k(h_k+3z_k)+E_2^k(2h_k+3z_k)\right\}\left[U_k^L(x-x_{1P})\right. \quad (23b)$$

$$\left.-U_k^L(x-x_{2P})\right]\left[\delta_k^{'L}(y-y_{1P})-\delta_k^{'L}(y-y_{2P})\right]$$

$$\frac{\partial^2 M_{xy}^{P}}{\partial x\partial y}=\tfrac{1}{6}\sum_{L=1}^{Tn}\sum_{k=1}^{N}\sum_{j=1,2,6}\left[\overline{Q}_{6j}\right]^k\left[\overline{d}_{3j}\right]^k h_k\left\{E_1^k(h_k+3z_k)+E_2^k(2h_k+3z_k)\right\}\frac{\partial^2}{\partial x^2}\left(\left[U_k^L(x-x_{1P})-U_k^L(x-x_{2P})\right]\right.$$

$$\left.\frac{\partial}{\partial y}\left[U_k^L(y-y_{1P})-U_k^L(y-y_{2P})\right]\right)=\tfrac{1}{6}\sum_{L=1}^{Tn}\sum_{k=1}^{N}\sum_{j=1,2,6}\left[\overline{Q}_{6j}\right]^k\left[\overline{d}_{3j}\right]^k h_k\left\{E_1^k(h_k+3z_k)+E_2^k(2h_k+3z_k)\right\}\left[\delta_k^L(x-x_{1P})\right. \quad (23c)$$

$$\left.-\delta_k^L(x-x_{2P})\right]\left[\delta_k^L(y-y_{1P})-\delta_k^L(y-y_{2P})\right]$$

$$I_5^A=\int_0^a\int_0^b\left(\frac{\partial^2 M_{xx}^{P}}{\partial x^2}\right)\sin(\frac{\alpha_m}{2}x)\cos(\beta_n y)dxdy=\tfrac{1}{6}\int_0^a\int_0^b\sum_{L=1}^{Tn}\sum_{k=1}^{N}\sum_{j=1,2,6}\left[\overline{Q}_{1j}\right]^k\left[\overline{d}_{3j}\right]^k h_k\left\{E_1^k(h_k+3z_k)+E_2^k\right.$$

$$\left.(2h_k+3z_k)\right\}\left[U_k^L(y-y_{1P})-U_k^L(y-y_{2P})\right]\left[\delta_k^{'L}(x-x_{1P})-\delta_k^{'L}(x-x_{2P})\right]\sin(\frac{\alpha_m}{2}x)\cos(\beta_n y)dxdy \quad (23d)$$

$$=\tfrac{1}{6}\sum_{L=1}^{Tn}\sum_{k=1}^{N}\sum_{j=1,2,6}\frac{\alpha_m}{2\beta_n}\left[\overline{Q}_{1j}\right]^k\left[\overline{d}_{3j}\right]^k h_k\left\{E_1^k(h_k+3z_k)+E_2^k(2h_k+3z_k)\right\}\left(\cos(\frac{\alpha_m}{2}x_{1T})-\cos(\frac{\alpha_m}{2}x_{2T})\right)_L$$

$$\left(\sin(\beta_n y_{1T})-\sin(\beta_n y_{2T})\right)_L$$

$$I_5^B=\int_0^a\int_0^b\left(\frac{\partial^2 M_{yy}^{P}}{\partial y^2}\right)\sin(\frac{\alpha_m}{2}x)\cos(\beta_n y)dxdy=\tfrac{1}{6}\int_0^a\int_0^b\sum_{L=1}^{Tn}\sum_{k=1}^{N}\sum_{j=1,2,6}\left[\overline{Q}_{2j}\right]^k\left[\overline{d}_{3j}\right]^k h_k\left\{E_1^k(h_k+3z_k)+E_2^k\right.$$

$$\left.(2h_k+3z_k)\right\}\left[U_k^L(x-x_{1P})-U_k^L(x-x_{2P})\right]\left[\delta_k^{'L}(y-y_{1P})-\delta_k^{'L}(y-y_{2P})\right]\sin(\frac{\alpha_m}{2}x)\cos(\beta_n y)dxdy \quad (23e)$$

$$=\tfrac{1}{6}\sum_{L=1}^{Tn}\sum_{k=1}^{N}\sum_{j=1,2,6}\frac{2\beta_n}{\alpha_m}\left[\overline{Q}_{2j}\right]^k\left[\overline{d}_{3j}\right]^k h_k\left\{E_1^k(h_k+3z_k)+E_2^k(2h_k+3z_k)\right\}\left(\cos(\frac{\alpha_m}{2}x_{1P})-\cos(\frac{\alpha_m}{2}x_{2P})\right)_L$$

$$\left(\sin(\beta_n y_{1P})-\sin(\beta_n y_{2P})\right)_L$$

$$I_5^C=\int_0^a\int_0^b\left(2\frac{\partial^2 M_{xy}^{P}}{\partial x\partial y}\right)\sin(\frac{\alpha_m}{2}x)\cos(\beta_n y)dxdy=\tfrac{1}{3}\int_0^a\int_0^b\sum_{L=1}^{Tn}\sum_{k=1}^{N}\sum_{j=1,2,6}\left[\overline{Q}_{6j}\right]^k\left[\overline{d}_{3j}\right]^k h_k\left\{E_1^k(h_k+3z_k)+E_2^k\right.$$

$$\left.(2h_k+3z_k)\right\}\left[\delta_k^L(x-x_{1P})-\delta_k^L(x-x_{2P})\right]\left[\delta_k^L(y-y_{1P})-\delta_k^L(y-y_{2P})\right]\sin(\frac{\alpha_m}{2}x)\cos(\beta_n y)dxdy \quad (23f)$$

$$=\tfrac{1}{3}\sum_{L=1}^{Tn}\sum_{k=1}^{N}\sum_{j=1,2,6}\left[\overline{Q}_{6j}\right]^k\left[\overline{d}_{3j}\right]^k h_k\left\{E_1^k(h_k+3z_k)+E_2^k(2h_k+3z_k)\right\}\left(\sin(\frac{\alpha_m}{2}x_{1P})-\sin(\frac{\alpha_m}{2}x_{2P})\right)_L$$

$$\left(\cos(\beta_n y_{1P})-\cos(\beta_n y_{2P})\right)_L$$

Hence, the effect of twisting-bending moments acting on a smart laminated cantilever piezo composite plate is stated in Eqs24a-f. According to Eq.24f, it is assumed that the electrical intensity field (E_z) varies linearly through piezoelectric actuators thickness.

If n={0}, m={1,3,5…}, then,

$$I_5 = \sum_{L=1}^{Tn}\left[\frac{\alpha_m\left[M_x^P\right]^{\Theta}}{2}\right]\left(\cos(\frac{\alpha_m}{2}x_{1P})-\cos(\frac{\alpha_m}{2}x_{2P})\right)_L\left(y_{1P}-y_{2P}\right)_L \tag{24a}$$

and if n={1,2,3,…}, m={1,3,5,…}, then,

$$I_5 = \sum_{L=1}^{Tn}\left[\left\{\frac{\left[M_x^P\right]^{\Theta}\alpha_m^2+4\left[M_y^P\right]^{\Theta}\beta_n^2}{2\alpha_m\beta_n}\left(\cos(\frac{\alpha_m}{2}x_{1P})-\cos(\frac{\alpha_m}{2}x_{2P})\right)_L\left(\sin(\beta_n y_{1P})-\sin(\beta_n y_{2P})\right)_L\right\}\right. \tag{24b}$$
$$\left.+\left\{\left[M_{xy}^P\right]^{\Theta}\left(\sin(\frac{\alpha_m}{2}x_{1P})-\sin(\frac{\alpha_m}{2}x_{2P})\right)_L\left(\cos(\beta_n y_{1P})-\cos(\beta_n y_{2P})\right)_L\right\}\right]$$

where,

$$\left[M_x^P\right]^{\Theta} = \tfrac{1}{6}\sum_{k=1}^{N}\sum_{j=1,2,6}\left[\overline{Q}_{1j}\right]^k\left[\overline{d}_{3j}\right]^k\left\{E_1^k(h_k+3z_k)+E_2^k(2h_k+3z_k)\right\}h_k \tag{24c}$$

$$\left[M_y^P\right]^{\Theta} = \tfrac{1}{6}\sum_{k=1}^{N}\sum_{j=1,2,6}\left[\overline{Q}_{2j}\right]^k\left[\overline{d}_{3j}\right]^k\left\{E_1^k(h_k+3z_k)+E_2^k(2h_k+3z_k)\right\}h_k \tag{24d}$$

$$\left[M_{xy}^P\right]^{\Theta} = \tfrac{1}{3}\sum_{k=1}^{N}\sum_{j=1,2,6}\left[\overline{Q}_{6j}\right]^k\left[\overline{d}_{3j}\right]^k\left\{E_1^k(h_k+3z_k)+E_2^k(2h_k+3z_k)\right\}h_k \tag{24e}$$

$$E_z{}^k = \frac{V_a^k}{t_a^k} \tag{24f}$$

The values x_{1M}, x_{2M}, x_{1P}, x_{2P}, y_{1M}, y_{2M}, y_{1P}, and y_{2P} are the placements of effective mechanical and electrical loads along x and y axis, respectively. $V_a{}^k$ stands for the applied electrical voltage through the k^{th} layer's thickness and $t_a{}^k$ presents the thickness of the piezoelectric actuators in the k^{th} layer. E_x=E_y=0 is based on the fact that for the shell/plate type piezoelectric materials, only the transverse electric field component E_z is dominant when the electrical voltage V_a is only applied to the actuators through thickness [61][62]. In the next step, parameters I_1, I_2,…, I_5 are substituted into Eq.21a, resulting in Eq.25. Simplifying and rearranging both sides of Eqs.25 leads to Eqs.26a-d. x_{1P}, x_{2P}, y_{1P}, and y_{2P} can be obtained using Eqs.24g-j, respectively.

$$x_{1p} = O_x - \tfrac{1}{2}\sqrt{L_a^2+W_a^2}\cos\left(\arctan(\tfrac{W_a}{L_a})\right) \tag{24g}$$

$$x_{2p} = O_x + L_a - \tfrac{1}{2}\sqrt{L_a^2+W_a^2}\cos\left(\arctan(\tfrac{W_a}{L_a})\right) \tag{24h}$$

$$y_{1p} = O_y + \tfrac{1}{2}\sqrt{L_a^2+W_a^2}\sin\left(\arctan(\tfrac{W_a}{L_a})\right) \tag{24i}$$

$$y_{2p} = O_y + W_a + \tfrac{1}{2}\sqrt{L_a^2+W_a^2}\sin\left(\arctan(\tfrac{W_a}{L_a})\right) \tag{24j}$$

O_x and O_y are the x and y coordinates of the inclined piezoelectric actuators, respectively (see Fig.2).

$$D_{11}\int_0^b\left[(-1)^{\frac{m-1}{2}}\left(\frac{\partial^3 w_0}{\partial x^3}\Big|x=a\right)+\frac{\alpha_m}{2}\left(\frac{\partial^2 w_0}{\partial x^2}\Big|x=0\right)-(-1)^{\frac{m-1}{2}}\frac{\alpha_m^2}{4}\left(\frac{\partial w_0}{\partial x}\Big|x=a\right)\right]\cos(\beta_n y)dy+D_{11}\frac{\alpha_m^4}{16}w_{mn}$$

$$D_{22}\int_0^a\left[(-1)^n\left(\frac{\partial^3 w_0}{\partial y^3}\Big|y=b\right)-\left(\frac{\partial^3 w_0}{\partial y^3}\Big|y=0\right)-(-1)^n\beta_n^2\left(\frac{\partial w_0}{\partial y}\Big|y=b\right)+\beta_n^2\left(\frac{\partial w_0}{\partial y}\Big|y=0\right)\right]\sin(\frac{\alpha_m}{2}x)dx+$$

$$D_{22}\beta_n^4 w_{mn}+(D_{12}+2D_{66})\frac{\alpha_m^2\beta_n^2}{2}w_{mn}-(D_{12}+2D_{66})\frac{\alpha_m^2}{2}\int_0^a\left[(-1)^n\left(\frac{\partial w_0}{\partial y}\Big|y=b\right)-\left(\frac{\partial w_0}{\partial y}\Big|y=0\right)\right]\sin(\frac{\alpha_m}{2}x)dx$$

$$-2(D_{12}+2D_{66})(-1)^{\frac{m-1}{2}}\beta_n^2\int_0^b\left[\left(\frac{\partial w_0}{\partial x}\Big|x=a\right)\right]\cos(\beta_n y)dy=\sum_{L=1}^{Mn}C_{mn}^1\left(\frac{-2P_0}{\alpha_m\beta_n}\right)\left(\cos(\frac{\alpha_m}{2}x_{1M})-\cos(\frac{\alpha_m}{2}x_{2M})\right)_L \tag{25}$$

$$\left(\sin(\beta_n y_{1M})-\sin(\beta_n y_{2M})\right)_L+\sum_{L=1}^{Pn}C_{mn}^2\left[\frac{\left[M_x^P\right]^{\Theta}\alpha_m^2+4\left[M_y^P\right]^{\Theta}\beta_n^2}{2\alpha_m\beta_n}\right]\left(\cos(\frac{\alpha_m}{2}x_{1P})-\cos(\frac{\alpha_m}{2}x_{2P})\right)_L$$

$$\left(\sin(\beta_n y_{1P})-\sin(\beta_n y_{2P})\right)_L+\sum_{L=1}^{Pn}C_{mn}^3\left[M_{xy}^P\right]^{\Theta}\left(\sin(\frac{\alpha_m}{2}x_{1P})-\sin(\frac{\alpha_m}{2}x_{2P})\right)_L\left(\cos(\beta_n y_{1P})-\cos(\beta_n y_{2P})\right)_L$$

$$D_{11}(-1)^{\frac{m-1}{2}}\int_0^b\left(\frac{\partial^3 w_0}{\partial x^3}\Big|x=a\right)\cos(\beta_n y)dy+D_{22}(-1)^n\int_0^a\left(\frac{\partial^3 w_0}{\partial y^3}\Big|y=b\right)\sin(\frac{\alpha_m}{2}x)dx-(-1)^n\Big(D_{22}\beta_n^2$$

$$+\frac{(D_{12}+2D_{66})\alpha_m^2}{2}\Big)\int_0^a\left(\frac{\partial w_0}{\partial y}\Big|y=b\right)\sin(\frac{\alpha_m}{2}x)dx-D_{22}\int_0^a\left(\frac{\partial^3 w_0}{\partial y^3}\Big|y=0\right)\sin(\frac{\alpha_m}{2}x)dx+\Big(D_{22}\beta_n^2+$$

$$\frac{(D_{12}+2D_{66})\alpha_m^2}{2}\Big)\int_0^a\left(\frac{\partial w_0}{\partial y}\Big|y=0\right)\sin(\frac{\alpha_m}{2}x)dx-(-1)^{\frac{m-1}{2}}\left(\frac{D_{11}\alpha_m^2}{4}+2(D_{12}+2D_{66})\beta_n^2\right)\int_0^b\left(\frac{\partial w_0}{\partial x}\Big|x=a\right)$$

$$\cos(\beta_n y)dy+\left(\frac{D_{11}\alpha_m}{2}\right)\int_0^b\left(\frac{\partial^2 w_0}{\partial x^2}\Big|x=0\right)\cos(\beta_n y)dy+\left(\frac{D_{11}\alpha_m^4}{16}+\frac{(D_{12}+2D_{66})\alpha_m^2\beta_n^2}{2}+D_{22}\beta_n^4\right)w_{mn}$$

$$=\sum_{L=1}^{Mn}C_{mn}^1\left(\frac{-2P_0}{\alpha_m\beta_n}\right)\left(\cos(\frac{\alpha_m}{2}x_{1M})-\cos(\frac{\alpha_m}{2}x_{2M})\right)_L\left(\sin(\beta_n y_{1M})-\sin(\beta_n y_{2M})\right)_L$$

$$+\sum_{L=1}^{Pn}C_{mn}^2\left[\frac{\left[M_x^P\right]^{\Theta}\alpha_m^2+4\left[M_y^P\right]^{\Theta}\beta_n^2}{2\alpha_m\beta_n}\right]\left(\cos(\frac{\alpha_m}{2}x_{1P})-\cos(\frac{\alpha_m}{2}x_{2P})\right)_L\left(\sin(\beta_n y_{1P})-\sin(\beta_n y_{2P})\right)_L$$

$$+\sum_{L=1}^{Pn}C_{mn}^3\left[M_{xy}^P\right]^{\Theta}\left(\sin(\frac{\alpha_m}{2}x_{1P})-\sin(\frac{\alpha_m}{2}x_{2P})\right)_L\left(\cos(\beta_n y_{1P})-\cos(\beta_n y_{2P})\right)_L \tag{26a}$$

where,

$$C_{mn}^1=\begin{cases}n=0,m=1,3,5,\ldots\rightarrow 1\\ n=1,2,3,\ldots,m=1,3,5,\ldots\rightarrow\beta_n\left[\dfrac{y_{1M}-y_{2M}}{\sin(\beta_n y_{1M})-\sin(\beta_n y_{2M})}\right]_L\end{cases} \tag{26b}$$

$$C_{mn}^{2}=\begin{cases} n=0,m=1,3,5,...\rightarrow \dfrac{\left[M_x^P\right]^{\Theta}\alpha_m^2\beta_n}{\left[M_x^P\right]^{\Theta}\alpha_m^2+4\left[M_y^P\right]^{\Theta}\beta_n^2}\left[\dfrac{y_{1P}-y_{2P}}{\sin(\beta_n y_{1P})-\sin(\beta_n y_{2P})}\right]_L \\ \\ n=1,2,3,...,m=1,3,5,..\rightarrow 1 \end{cases} \tag{26c}$$

$$C_{mn}^{3}=\begin{cases} n=0,m=1,3,5,...\rightarrow 0 \\ \\ n=1,2,3,...,m=1,3,5,..\rightarrow 1 \end{cases} \tag{26d}$$

$C_{mn}{}^{1}$, $C_{mn}{}^{2}$, and $C_{mn}{}^{3}$ can be defined as effective mechanical and electrical bending and electrical twisting coefficients in the smart laminated cantilever piezo composite plate, respectively. The boundary conditions in Eqs.18f,g,h are expanded as shown in Eqs.27a-c and then substituted into Eq.26a. Rearranging Eq.26a results in Eq.28. For simplicity purposes, unknown variables Δ_m, Ω_m, Π_n, and Ψ_n are defined as shown in Eqs.29a-d, respectively.

$$D_{11}\int_0^b\left(\frac{\partial^3 w_0}{\partial x^3}\Big|x=a\right)\cos(\beta_n y)dy=(3D_{12}+2D_{66})\beta_n^2\int_0^b\left(\frac{\partial w_0}{\partial x}\Big|x=a\right)\cos(\beta_n y)dy \tag{27a}$$

$$D_{22}\int_0^a\left(\frac{\partial^3 w_0}{\partial y^3}\Big|y=0\right)\sin(\frac{\alpha_m}{2}x)dx=\frac{1}{4}(3D_{12}+2D_{66})\alpha_m^2\int_0^a\left(\frac{\partial w_0}{\partial y}\Big|y=0\right)\sin(\frac{\alpha_m}{2}x)dx \tag{27b}$$

$$D_{22}\int_0^a\left(\frac{\partial^3 w_0}{\partial y^3}\Big|y=b\right)\sin(\frac{\alpha_m}{2}x)dx=\frac{1}{4}(3D_{12}+2D_{66})\alpha_m^2\int_0^a\left(\frac{\partial w_0}{\partial y}\Big|y=b\right)\sin(\frac{\alpha_m}{2}x)dx \tag{27c}$$

$$\begin{aligned} &-(-1)^n\left[D_{22}\beta_n^2+D_{12}\frac{\alpha_m^2}{4}\right]\int_0^a\left(\frac{\partial w_0}{\partial y}\Big|y=b\right)\sin(\frac{\alpha_m}{2}x)dx+\left[D_{22}\beta_n^2+D_{12}\frac{\alpha_m^2}{4}\right]\int_0^a\left(\frac{\partial w_0}{\partial y}\Big|y=0\right)\sin(\frac{\alpha_m}{2}x)dx \\ &-(-1)^{\frac{m-1}{2}}\left[D_{12}\beta_n^2+D_{11}\frac{\alpha_m^2}{4}\right]\int_0^b\left(\frac{\partial w_0}{\partial x}\Big|x=a\right)\cos(\beta_n y)dy+D_{11}\frac{\alpha_m}{2}\int_0^b\left(\frac{\partial^2 w_0}{\partial x^2}\Big|x=0\right)\cos(\beta_n y)dy+ \\ &\left[\frac{D_{11}\alpha_m^4}{16}+\frac{(D_{12}+2D_{66})\alpha_m^2\beta_n^2}{2}+D_{22}\beta_n^4\right]w_{mn}=\sum_{L=1}^{Mn}C_{mn}^{1}\left(\frac{-2P_0}{\alpha_m\beta_n}\right)\left(\cos(\frac{\alpha_m}{2}x_{1M})-\cos(\frac{\alpha_m}{2}x_{2M})\right)_L \\ &\left(\sin(\beta_n y_{1M})-\sin(\beta_n y_{2M})\right)_L+\sum_{L=1}^{Pn}C_{mn}^{2}\left[\frac{\left[M_x^P\right]^{\Theta}\alpha_m^2+4\left[M_y^P\right]^{\Theta}\beta_n^2}{2\alpha_m\beta_n}\right]\left(\cos(\frac{\alpha_m}{2}x_{1P})-\cos(\frac{\alpha_m}{2}x_{2P})\right)_L \\ &\left(\sin(\beta_n y_{1P})-\sin(\beta_n y_{2P})\right)_L+\sum_{L=1}^{Pn}C_{mn}^{3}\left[M_{xy}^P\right]^{\Theta}\left(\sin(\frac{\alpha_m}{2}x_{1P})-\sin(\frac{\alpha_m}{2}x_{2P})\right)_L\left(\cos(\beta_n y_{1P})-\cos(\beta_n y_{2P})\right)_L \end{aligned} \tag{28}$$

$$\Delta_m=\int_0^a\left(\frac{\partial w_0}{\partial y}\Big|y=b\right)\sin(\frac{\alpha_m}{2}x)dx \tag{29a}$$

$$\Omega_m=\int_0^a\left(\frac{\partial w_0}{\partial y}\Big|y=0\right)\sin(\frac{\alpha_m}{2}x)dx \tag{29b}$$

$$\Pi_n = \int_0^b \left(\frac{\partial w_0}{\partial x} \middle| x = a \right) \cos(\beta_n y) dy \tag{29c}$$

$$\Psi_n = \int_0^b \left(\frac{\partial^2 w_0}{\partial x^2} \middle| x = 0 \right) \cos(\beta_n y) dy \tag{29d}$$

Substituting Eqs.29a-d into Eq.28 and then rearranging Eq.28 yields Eq.30, which satisfies the boundary conditions in Eq.18. Eq.30 represents the double finite integral transformation of the mid-plane vertical displacement of function $w_o(x,y)$ in the smart laminated cantilever piezo composite plate incorporated with arbitrarily positioned inclined piezoelectric actuators and under electro-mechanical loads, which can be expressed in terms of function w_{mn}. In the next attempt, the remaining boundary conditions in Eqs.18c,d,e are substituted in the first and second partial derivatives of the double Fourier series $w_o(x,y)$ in Eqs.31a-d[60]. Simplifying and rearranging Eqs.31a-d results in Eqs.32a-d.

$$\begin{aligned} w_{mn} = & \left[\frac{D_{11}\alpha_m^4}{16} + \frac{(D_{12}+2D_{66})\alpha_m^2\beta_n^2}{2} + D_{22}\beta_n^4 \right]^{-1} \left\{ \sum_{L=1}^{Mn} C_{mn}^1 \left(\frac{-2P_0}{\alpha_m \beta_n} \right) \left(\cos(\frac{\alpha_m}{2} x_{1M}) - \cos(\frac{\alpha_m}{2} x_{2M}) \right)_L \right. \\ & \left(\sin(\beta_n y_{1M}) - \sin(\beta_n y_{2M}) \right)_L + \sum_{L=1}^{Pn} C_{mn}^2 \left[\frac{\left[M_x^P \right]^{\Theta} \alpha_m^2 + 4\left[M_y^P \right]^{\Theta} \beta_n^2}{2\alpha_m \beta_n} \right] \left(\cos(\frac{\alpha_m}{2} x_{1P}) - \cos(\frac{\alpha_m}{2} x_{2P}) \right)_L \\ & \left(\sin(\beta_n y_{1P}) - \sin(\beta_n y_{2P}) \right)_L + \sum_{L=1}^{Pn} C_{mn}^3 \left[M_{xy}^P \right]^{\Theta} \left(\sin(\frac{\alpha_m}{2} x_{1P}) - \sin(\frac{\alpha_m}{2} x_{2P}) \right)_L \left(\cos(\beta_n y_{1P}) - \cos(\beta_n y_{2P}) \right)_L \\ & \left. + (-1)^n \left[D_{22}\beta_n^2 + D_{12}\frac{\alpha_m^2}{4} \right] \Delta_m - \left[D_{22}\beta_n^2 + D_{12}\frac{\alpha_m^2}{4} \right] \Omega_m + (-1)^{\frac{m-1}{2}} \left[D_{12}\beta_n^2 + D_{11}\frac{\alpha_m^2}{4} \right] \Pi_n - \left[\frac{D_{11}\alpha_m}{2} \right] \Psi_n \right\} \end{aligned} \tag{30}$$

$$\begin{aligned} & \frac{\partial w_0(x,y)}{\partial x} = \frac{4}{ab} \sum_{m=1,3,5,\ldots}^{\infty} \sum_{n=0,1,2,\ldots}^{\infty} \lambda_n \lambda^* \cos(\frac{\alpha_m}{2} x) \cos(\beta_n y) = \\ & \frac{4}{ab} \sum_{m=1,3,5,\ldots}^{\infty} \sum_{n=0,1,2,\ldots}^{\infty} \lambda_n \left[\frac{\alpha_m}{2} w_{mn} \right] \cos(\frac{\alpha_m}{2} x) \cos(\beta_n y) \end{aligned} \tag{31a}$$

$$\begin{aligned} & \frac{\partial^2 w_0(x,y)}{\partial x^2} = \frac{4}{ab} \sum_{m=1,3,5,\ldots}^{\infty} \sum_{n=0,1,2,\ldots}^{\infty} \lambda_n \lambda^{**} \sin(\frac{\alpha_m}{2} x) \cos(\beta_n y) = \\ & \frac{4}{ab} \sum_{m=1,3,5,\ldots}^{\infty} \sum_{n=0,1,2,\ldots}^{\infty} \lambda_n \left[(-1)^{\frac{m-1}{2}} \int_0^b \left(\frac{\partial w_0(x,y)}{\partial x} \middle| (x=a) \right) \cos(\beta_n y) dy - \frac{\alpha_m^2}{4} w_{mn} \right] \sin(\frac{\alpha_m}{2} x) \cos(\beta_n y) \end{aligned} \tag{31b}$$

$$\begin{aligned} & \frac{\partial w_0(x,y)}{\partial y} = \frac{4}{ab} \sum_{m=1,3,5,\ldots}^{\infty} \sum_{n=1,2,3,\ldots}^{\infty} \lambda_n \lambda^* \sin(\frac{\alpha_m}{2} x) \sin(\beta_n y) = \\ & \frac{4}{ab} \sum_{m=1,3,5,\ldots}^{\infty} \sum_{n=1,2,3,\ldots}^{\infty} \lambda_n \left[-\beta_n w_{mn} \right] \sin(\frac{\alpha_m}{2} x) \sin(\beta_n y) \end{aligned} \tag{31c}$$

$$\frac{\partial^2 w_0(x,y)}{\partial y^2}=\frac{4}{ab}\sum_{m=1,3,5,\ldots}^{\infty}\sum_{n=0,1,2,\ldots}^{\infty}\lambda_n\lambda^{**}\sin(\frac{\alpha_m}{2}x)\cos(\beta_n y)=$$

$$\frac{4}{ab}\sum_{m=1,3,5,\ldots}^{\infty}\sum_{n=0,1,2,\ldots}^{\infty}\lambda_n\left[(-1)^n\int_0^a\left(\frac{\partial w_0(x,y)}{\partial y}\Big|(y=b)\right)\sin(\frac{\alpha_m}{2}x)dx-\int_0^a\left(\frac{\partial w_0(x,y)}{\partial y}\Big|(y=0)\right)\sin(\frac{\alpha_m}{2}x)dx\right. \quad (31d)$$

$$\left.-\left(\frac{\alpha_m^2}{4}+\beta_n^2\right)w_{mn}\right]\sin(\frac{\alpha_m}{2}x)\cos(\beta_n y)$$

$$\sum_{m=1,3,5,\ldots}^{\infty}\sum_{n=0,1,2,\ldots}^{\infty}\alpha_m w_{mn}\cos(\beta_n y)=0 \quad (32a)$$

$$\sum_{m=1,3,5,\ldots}^{\infty}\sum_{n=0,1,2,\ldots}^{\infty}(-1)^{\frac{m-1}{2}}\left[D_{12}(-1)^n\Delta_m-D_{12}\Omega_m+D_{11}(-1)^{\frac{m-1}{2}}\Pi_n-\left[D_{12}\beta_n^2+\frac{D_{11}\alpha_m^2}{4}\right]w_{mn}\right]\cos(\beta_n y)=0 \quad (32b)$$

$$\sum_{m=1,3,5,\ldots}^{\infty}\sum_{n=0,1,2,\ldots}^{\infty}\lambda_n\left[D_{22}(-1)^n\Delta_m-D_{22}\Omega_m+D_{12}(-1)^{\frac{m-1}{2}}\Pi_n-\left[D_{22}\beta_n^2+\frac{D_{12}\alpha_m^2}{4}\right]w_{mn}\right]\sin(\frac{\alpha_m}{2}x)=0 \quad (32c)$$

$$\sum_{m=1,3,5,\ldots}^{\infty}\sum_{n=0,1,2,\ldots}^{\infty}\lambda_n\left[D_{22}\Delta_m-D_{22}(-1)^n\Omega_m+D_{12}(-1)^n(-1)^{\frac{m-1}{2}}\Pi_n-(-1)^n\left[D_{22}\beta_n^2+\frac{D_{12}\alpha_m^2}{4}\right]w_{mn}\right]\sin(\frac{\alpha_m}{2}x)=0 \quad (32d)$$

The double finite integral transformation CI_n and SI_m are performed over Eqs.32a-b and Eqs.32c-d, respectively. The CI_n and SI_m are stated in Eqs.33a-b, respectively. Performing integration over the specified domains results in Eqs.34a-d, respectively.

$$CI_n=\int_0^b\cos(\beta_n y)dy \quad (33a)$$

$$SI_m=\int_0^a\sin(\frac{\alpha_m}{2}x)dx \quad (33b)$$

$$\sum_{m=1,3,5,\ldots}^{\infty}\sum_{n=0,1,2,\ldots}^{\infty}\alpha_m w_{mn}=0 \quad (34a)$$

$$\sum_{m=1,3,5,\ldots}^{\infty}\sum_{n=0,1,2,\ldots}^{\infty}(-1)^{\frac{m-1}{2}}\left[D_{12}(-1)^n\Delta_m-D_{12}\Omega_m+D_{11}(-1)^{\frac{m-1}{2}}\Pi_n-\left[D_{12}\beta_n^2+\frac{D_{11}\alpha_m^2}{4}\right]w_{mn}\right]=0 \quad (34b)$$

$$\sum_{m=1,3,5,\ldots}^{\infty}\sum_{n=0,1,2,\ldots}^{\infty}\lambda_n\left[D_{22}(-1)^n\Delta_m-D_{22}\Omega_m-D_{12}(-1)^{\frac{m-1}{2}}\Pi_n-\left[D_{22}\beta_n^2+\frac{D_{12}\alpha_m^2}{4}\right]w_{mn}\right]=0 \quad (34c)$$

$$\sum_{m=1,3,5,\ldots}^{\infty}\sum_{n=0,1,2,\ldots}^{\infty}\lambda_n\left[D_{22}\Delta_m-D_{22}(-1)^n\Omega_m+D_{12}(-1)^n(-1)^{\frac{m-1}{2}}\Pi_n-(-1)^n\left[D_{22}\beta_n^2+\frac{D_{12}\alpha_m^2}{4}\right]w_{mn}\right]=0 \quad (34d)$$

Finally, Eq.30 is substituted into Eqs.34a-d to obtain the four finite systems of linear simultaneous multivariable equations, as stated in Eqs.35a-d, respectively. The sufficient finite terms of m and n in each set of multivariable equations are considered in order to accurately compute the constant values of unknown variables Δ_m, Ω_m, Π_n, and Ψ_n.

$$\sum_{m=1,3,5,\ldots}^{\infty}\sum_{n=0,1,2,\ldots}^{\infty} S^{1}_{mn}\Delta_m + \sum_{m=1,3,5,\ldots}^{\infty}\sum_{n=0,1,2,\ldots}^{\infty} S^{2}_{mn}\Omega_m + \sum_{m=1,3,5,\ldots}^{\infty}\sum_{n=0,1,2,\ldots}^{\infty} S^{3}_{mn}\Pi_n + \sum_{m=1,3,5,\ldots}^{\infty}\sum_{n=0,1,2,\ldots}^{\infty} S^{4}_{mn}\Psi_n = \sum_{m=1,3,5,\ldots}^{\infty}\sum_{n=0,1,2,\ldots}^{\infty} S^{5}_{mn} \quad (35a)$$

$$\sum_{m=1,3,5,\ldots}^{\infty}\sum_{n=0,1,2,\ldots}^{\infty} S^{6}_{mn}\Delta_m + \sum_{m=1,3,5,\ldots}^{\infty}\sum_{n=0,1,2,\ldots}^{\infty} S^{7}_{mn}\Omega_m + \sum_{m=1,3,5,\ldots}^{\infty}\sum_{n=0,1,2,\ldots}^{\infty} S^{8}_{mn}\Pi_n + \sum_{m=1,3,5,\ldots}^{\infty}\sum_{n=0,1,2,\ldots}^{\infty} S^{9}_{mn}\Psi_n = \sum_{m=1,3,5,\ldots}^{\infty}\sum_{n=0,1,2,\ldots}^{\infty} S^{10}_{mn} \quad (35b)$$

$$\sum_{m=1,3,5,\ldots}^{\infty}\sum_{n=0,1,2,\ldots}^{\infty} S^{11}_{mn}\Delta_m + \sum_{m=1,3,5,\ldots}^{\infty}\sum_{n=0,1,2,\ldots}^{\infty} S^{12}_{mn}\Omega_m + \sum_{m=1,3,5,\ldots}^{\infty}\sum_{n=0,1,2,\ldots}^{\infty} S^{13}_{mn}\Pi_n + \sum_{m=1,3,5,\ldots}^{\infty}\sum_{n=0,1,2,\ldots}^{\infty} S^{14}_{mn}\Psi_n = \sum_{m=1,3,5,\ldots}^{\infty}\sum_{n=0,1,2,\ldots}^{\infty} S^{15}_{mn} \quad (35c)$$

$$\sum_{m=1,3,5,\ldots}^{\infty}\sum_{n=0,1,2,\ldots}^{\infty} S^{16}_{mn}\Delta_m + \sum_{m=1,3,5,\ldots}^{\infty}\sum_{n=0,1,2,\ldots}^{\infty} S^{17}_{mn}\Omega_m + \sum_{m=1,3,5,\ldots}^{\infty}\sum_{n=0,1,2,\ldots}^{\infty} S^{18}_{mn}\Pi_n + \sum_{m=1,3,5,\ldots}^{\infty}\sum_{n=0,1,2,\ldots}^{\infty} S^{19}_{mn}\Psi_n = \sum_{m=1,3,5,\ldots}^{\infty}\sum_{n=0,1,2,\ldots}^{\infty} S^{20}_{mn} \quad (35d)$$

Computation of S^{i}_{mn}, $i=\{1,2,..,20\}$ as shown in Appendix.1 leads to obtaining the unknown constants in Eqs.35a-d as four finite systems of linear simultaneous multivariable equations, which are later substituted into Eq.30 to calculate the double finite integral transformation of the mid-plane vertical displacement of function $w_o(x,y)$. Once the w_{mn} is found, it is substituted into Eq.20 to calculate the exact mid-plane twisting-bending displacements of the function $w_o(x,y)$ in the smart laminated cantilever piezo composite plates induced by electro-mechanical loads.

3. Numerical simulation: finite element method (FEM)

The electro-mechanical coupled FE simulation of smart cantilever piezo composite plates and beams induced by electro-mechanical twisting-bending loads was implemented using FE software package ABAQUS/CEA 6.13-1. The smart piezo composite structure consists of the host structure (fibre-reinforced composite laminate) and the piezoelectric actuator patches. First, each part is sketched, the dimensions and material properties are assigned, and material coordinate systems are defined to composite laminate and piezoelectric actuators separately (see Fig.3a). Since the piezoelectric actuators are polarized through thickness, only the piezoelectric coefficients d_{31} and d_{32} for plate/piezo and d_{31} for beam/piezo systems are considered, respectively. The host structure consists of multiple cross-ply fibre-reinforced composite plies in which each ply is defined through partitioning. The host structure and the piezoelectric actuators are considered passive and active parts, respectively, which will be later assembled together in the assembly module, and subsequently the boundary conditions, piezoelectric actuators groundings, and electro-mechanical loads are applied (see Fig.3b). For a cantilever plate/beam, the displacements and angel of rotations are equal to zero at the fixed end as seen in Fig.3b. In ABAQYS software, U_1, U_2, and U_3 are defined as the displacements and UR_1, UR_2, and UR_3 as the rotational angels along x,y, and z directions, respectively. The inclination angle between the piezoelectric actuator patches and host structure is created during the assembly. To intensify the effect of electrical twisting-bending moments and greater actuation result, the piezoelectric actuators were symmetrically bounded with respect to the mid-plane under the same amount of constant electrical voltage but different polarization direction. In general, for an upward displacement, the upper and lower actuator patches require a negative and positive voltage, respectively and vice versa[63]. After assembling and defining the boundary conditions and loads, the Structured Hex Element Shape was set as the finite

element mesh control in the smart piezo composite structure. An 8-node quadrilateral in-plane general-purpose continuum shell, reduced integration with hourglass control, finite membrane strains (SC8R) was defined as the element type in the host structure while a 20-node quadratic piezoelectric brick, reduced integration (C3D20RE) was used to define the piezoelectric actuator patches element type (see Fig.3c). Finally, after submitting the model through the job module for the full analysis, in order to obtain the displacements in the arbitrarily selected element nodes, a path is defined along a specific direction in the smart piezo composite laminate's mid-plane (see Fig.3d). The displacement values (U_3) in each path is compared with the proposed explicit results for verification purpose. It must be noted that the U_3 in the visualization module 3D contour plot stands for the vertical displacement of the mid-plane.

In order to prevent the low accuracy in computational results of twisting-bending type problems known as Locking phenomenon, the solid element in FEM linear approximations should be prevented whereas it shows the twisting-bending behaviour much stiffer in comparison with explicit analytical solution. Locking is higher if the solid element looks like shell (thickness is smaller than two other sizes). However, it can be resolved by selecting an appropriate FE with quadratic shape functions such as continuum shell element (SC8R). Since the Locking phenomena may still be found for FE quadratic shape functions, taking many elements for the thickness, therefore, leads to higher accuracy of the results, despite increasing the computational time as a disadvantage. Considering the element type in the piezoelectric actuator patches, a 20-node quadratic piezoelectric brick, reduced integration (C3D20RE) has more accuracy over an 8-node linear piezoelectric brick (C3D8E).

4. Results and discussions

In this section, various examples are intended to demonstrate and evaluate the accuracy of the proposed method for twisting-bending deformation analysis and shape control task of smart laminated cantilever piezo composite plates and beams induced electro-mechanically. The results are verified with the ones obtained from numerical simulations. In the first example, the effect of electrical twisting-bending coupling is taken into account. In the last example, a serious of bounded piezoelectric patches with various inclination angles are intended to control the twisting-bending deformation of a smart laminated cantilever fibre-reinforced composite beam induced by asymmetrical concentrated load at the free end corner. Generally, the effect of various parameters including electro-mechanical twisting coupling, layup thickness, piezoelectric actuators size, placement, and inclination angle, electrical potential intensity, stacking sequence, and geometrical dimension are considered using the proposed exact solution and FEM. Material properties of piezoelectric actuators and fibre-reinforced composite laminates used in the following examples are summarised in Table.1[61][63][64].

4.1. Example.1: *Effect of single inclined actuators pair on twisting deformation of the smart cantilever laminated piezo composite plates*

As shown in Fig.4a, a smart elastic cantilever composite plate (a=0.2 [m], b=0.04 [m]) with thickness t_p=1 [mm] and made of unidirectional T300/976 GFRP is incorporated with KYNAR piezoelectric actuator patches (t_a=0.2 [mm], L_a=0.1 [m], w_a=0.05 [m]). The host structure is a fourth-layered cross-ply laminate with stacking sequence of $[0/90]_s$. Each composite ply is assumed to have the same thickness. Inclined piezoelectric actuators pair, as shown in Fig.4a, are bounded to the plate and then polarized with opposite directions (upper patch:300 [V] and lower patch: -300 [V]). The inclination angle created in the piezoelectric actuators with respect to x axis causes the plate to twist due to existence of electrical twisting moment [M_{xy}^{P}]. The

mechanical twisting-bending deformation created in the smart cantilever composite plate as a result of electro-mechanical coupling is analysed against various inclination angles, {0,30,45,60,90} degrees, through new proposed explicit solution and FEM (see Figs.5-9). Good agreement between the results is observed. It can be noticed from the results obtained from both approaches that when the inclination angle is equal to 0 (see Fig.5) and 90 (see Fig.9) degrees, no twisting deformation occurs in the plate while the effect of longitudinal and transverse piezoelectric coefficients is switched when inclination angle is 90 degrees ($d_{31}\rightarrow d_{32}$ and $d_{32}\rightarrow d_{31}$). Moreover, according to Figs.6-8, as the inclination angle increases, the electrical twisting moment effectiveness reduces. Thus, 30 degrees results in the most twisting deformation while 60 degrees the lowest.

4.2. Example.2: *Effect of double inclined actuators pairs on twisting deformation of the smart cantilever laminated piezo composite plates*

A combination of the multiple bounded inclined actuator groups (t_a=0.2 [mm], L_a=0.05 [m], w_a=0.025 [m]) positioned at ① and ② in the smart elastic cantilever composite plate (t_p=1 [mm], a=0.2 [m], b=0.04 [m]) is considered in this example (see Fig.4b). The amount of applied electrical voltage, piezoelectric actuators polarization direction, actuator and composite plate material properties, and plate stacking sequence are the same as the ones used in Example.1. It can be easily seen that the combination of actuator groups can result in significantly higher twisting deformation in the composite plate. Thus, for twisting-bending shape control purposes, more energy can be saved to achieve the same results by applying lower electrical voltage than is it achieved when using single actuators pair. Again, the mechanical twisting-bending deformation created in the smart cantilever composite plate with multiple bounded actuators pairs is analysed against various inclination angles, {0,30,45,60,90} degrees, through new proposed explicit solution and FEM (see Figs.10-14). Good agreement between the results is observed. The effect of inclination angle variation on shape deformation in composite plates under either multiple or single actuator pairs seems to be constant. However, since a higher electrical voltage and electrical filed intensity are required for shape deformation task, therefor, the use of multiple actuator patches would be more beneficial and optimal compared with a single actuator patch.

4.3. Example.3: *Effect of stacking sequence selection on shape deformation of smart laminated cantilever piezo composite plates*

In this example, the effect of various stacking sequence on shape deformation of smart cantilever piezo composite laminate is investigated. The relationship between the stacking sequence and the composite laminates stiffness can result in shape deformation varying considerably. Thus, it is important to choose the suitable layup to control the structural shape deformation of composite laminates to our advantage. A combination of the double bounded inclined actuator groups positioned at ① and ② is considered in this example (see Fig.4c). The piezoelectric actuators polarization direction, actuator and composite plate properties, thickness and dimensions are the same as the ones used in Example.2. In order to observe the sole effect of stacking sequence on electro-mechanical twisting-bending coupling, same amount of electrical voltage is applied to each sample regardless of the stacking sequence configuration. However, 400 [V] and 300 [V] are applied to the bounded actuators pairs positioned at ① and ②, respectively. Upper and lower actuator patches are subjected to positive and negative voltage, respectively. Samples stacking sequence configurations are selected as $[\text{Piezo}/0/0]_s$, $[\text{Piezo}/90/90]_s$, $[\text{Piezo}/0/90]_s$, $[\text{Piezo}/90/0]_s$. The inclination angle is also kept constant for all actuators in each sample at 45 degrees. The results are then obtained using the

proposed explicit solution and the numerical simulation. Figs.15a-b represents the vertical displacements of mid-plane points along $w_o(x,b)$ and $w_o(a,y)$ along x and y directions, respectively, in a smart laminated cantilever piezo composite plate with various stacking sequence configurations. According to the results, the configuration $[\text{Piezo}/0/90]_s$ and $[\text{Piezo}/90/90]_s$ has the highest and lowest twisting-bending stiffness when subjected to electrical voltage, respectively. However, no major difference in results between the configurations $[\text{Piezo}/0/90]_s$ and $[\text{Piezo}/0/0]_s$ are observed. The results from both approaches show a good agreement. Subsequently, the $w_o(x,y)$ for each configuration are obtained. The 3D shape deformations obtained using the explicit solution (see Fig.16) and the numerical simulation (see Fig.17) show the same twisting-bending deformation trend.

4.4. Example.4: *Effect of electrical voltage intensity on shape deformation of smart laminated cantilever piezo composite plates*

In this example, the effect of electrical voltage intensity on a laminated cantilever piezo composite square plate (a=b=0.2 [m]) is investigated numerically and analytically. The piezoelectric actuators and composite plate properties, thickness and stacking sequence are same as the ones used in Example.1, while opposite polarization direction is selected to polarize bounded piezoelectric actuator patches groups (L_a=0.1 [m], w_a=0.02 [m]; upper and lower actuator patches are subjected to negative and positive voltage, respectively). To observe the sole effect of electrical voltage on twisting-bending deformation of the cantilevered composite plates, a series of various electrical voltages, {100,250,350,500} [V], are applied to the bounded piezoelectric patches and the results are presented in Figs.18-20, respectively. According to results, any increase in the amount of electrical voltage results in higher twisting-bending deformation in the composite plates. The results from both approaches shows a good agreement. In addition, it is noticed that the twisting curvature increases as the electrical voltage is raised.

4.5. Example.5: *Effect of single inclined actuators pair on twisting deformation of the smart cantilever laminated piezo composite beams*

As shown in Fig.21a, a smart fourth-layered cross-ply cantilever composite beam (t_p=1 [mm], a=0.2 [m], b=0.03 [m]), made of unidirectional T300/976 GFRP, and with the stacking sequence of $[0/90]_s$, is incorporated with the bounded PZTG1195 piezoelectric actuator patches (t_a=1 [mm], L_a=0.05 [m], w_a=0.03 [m]). Inclined piezoelectric actuators pair are polarized with opposite directions (upper patch: -300 [V] and lower patch: 300 [V]). The mechanical twisting-bending deformation created in the smart cantilever composite beam as a result of electro-mechanical coupling is analysed against various inclination angles, {0,30,45,60,90} degrees, through new proposed explicit solution and FEM (see Figs.22-24). Good agreement between the results is observed. As discussed in the results and discussion section, for beam type laminates, it is assumed that the width along y direction is stress free while considering the plane stress assumption. Thus, only the longitudinal piezoelectric coefficient d_{31} is taken into consideration. According to the results obtained from both approaches, any changes in inclination angle can results in the twisting-bending deformation varying considerably. In addition, as predicated by the explicit solution, no twisting deformation occurred for inclination angles 0 and 90 degrees.

4.6. Example 6: twisting-bending *control of the smart piezo composite beams under asymmetrical point load*

In the final example, the effectiveness of the piezoelectric actuators for the shape control of laminated composite structures under combination of twisting and bending deformations is investigated. As seen in Fig.21b, a combination of the multiple bounded PZTG1195 actuator groups (t_a=0.2 [*mm*], L_a= w_a=0.05 [*m*]), positioned at ① and ②, is considered. The host structure is a laminated cantilever composite beam (t_p=1 [*mm*], *a*=0.2 [*m*], *b*=0.05 [*m*]) made of unidirectional T300/976 GFRP. The composite beam is subjected to a point load *F*=-1 [*N*] as seen in Fig.21b. Since the concentrated load is unsymmetrically applied to the composite beam, it results in in-plane twitting deformation while deflecting downward. In order to fully suspend the twisting-bending effect, actuator ① is positioned without any indication angle and actuator ②, in contrast, with a negative inclination angle of -30 degrees with respect to the *x* axis. The actuator patches ① and ② are used in a two-level attempt to suspend the twisting and bending deformations, respectively. Upper and lower actuator patches positioned at ① and ② receive same amount of electrical voltage but negative and positive values, respectively. First, for controlling the twisting deformation, actuator patches ② are subjected to an initial electrical voltage of 100 [*V*]. As seen in Fig.25, the twisting deformation is slightly suspended and the beam starts restoring its original shape. Finally, by increasing the amount of electrical voltage applied to actuator patches ② up to the optimal level, the twisting deformation is fully suspended at 170 [*V*]. During these steps, no electrical voltage is applied to the actuator patches ①. Subsequently, in order to suspend the beam deflection, the actuator patches ① are initially subjected to the electrical voltage of 100 [*V*] and it is increased until the optimal voltage of 200 [*V*]. During the final steps, the electrical voltage applied to the actuator patches ② is kept constant at 170 [*V*]. It is observed that the beam deflection is significantly reduced as the electrical voltage increases. Therefore, by applying the optimal voltages of 200 [*V*] and 170 [*V*] to the actuator patches ① and ②, respectively, the twisting-bending deformations could be fully supressed according to the results illustrated in Fig.25.

Conclusion:

In this study, a new explicit analytical solution is presented for obtaining twisting-bending deformation and optimal shape control of smart laminated cantilever composite plates and beams using inclined piezoelectric actuators. For the first time, a mathematical relationship between the electrical and mechanical twisting moments are developed. The reliability of the proposed method is compared with the FE simulation results. The relationship between electro-mechanical twisting-bending deformation and various electro-mechanical parameters are taken into account. Generally, based on the results in the current research, the following remarks are concluded:

1. A good agreement observed between the proposed exact analytical solution and numerical simulation demonstrates the reliability of the model proposed in this paper.

2. Inclined piezoelectric actuators are capable of inducing twisting deformation in laminated composite structures through applying electrical voltage to piezoelectric actuators. The intensity of twisting shape deformation varies by changing the inclination angle. Therefore, through optimal inclination angle and applied electrical voltage, the shape control task of laminated composite structures under asymmetrical loads can be reliably implemented.

3. Piezoelectric actuator's size and placement have direct effect on twisting-bending shape deformation of laminated composite structures. Typically, considering the constant electrical voltage, inclination angle, and composite laminate's stiffness, larger ones have more power to induce twisting-bending deformation. In addition, the ones placed closed to the composite plates/beams fixed end show a better shape deformation while this effectiveness decreases as they are placed closer to the free end.

4. Six samples with various inclination angles ({0,30,45,60,90} degrees) were selected in this study. According to the numerical and analytical results, for the inclination angles $\theta \neq 0,90$ degrees, the twisting deformation reduces when the inclination angle increases. As predicted by the both approaches, when $\theta = 0,90$ degrees, no twisting deformation occurs since the transformed piezoelectric twisting coefficient is equal to zero. Moreover, when the inclination angle is equal to 90 degrees, the effect of longitudinal and transverse piezoelectric coefficients is switched ($d_{31} \rightarrow d_{32}$ and $d_{32} \rightarrow d_{31}$).

5. By increasing the applied electrical voltage and/or the number of inclined piezoelectric patches, the maximum twisting deformation in composite laminates can be achieved. Meanwhile, higher electrical voltage for shape deformation control purposes is difficult to control and may result in the piezoelectric actuators being destroyed[60]. Thus, the finding in the current research could be significant for shape control of laminated composite structures. For example, by selecting the optimal number of inclined piezoelectric patches and/or adjusting the applied electrical voltage, optimal results can be achieved.

6. Composite laminates stiffness can significantly affect the electro-mechanical twisting-bending coupling. The stiffness matrix can be induced by selecting various stacking sequence configurations. Among those with symmetrical cross-ply configuration, $[\text{Piezo}/0/90]_s$ and $[\text{Piezo}/90/90]_s$ have the highest and lowest twisting-bending stiffness when subjected to electrical voltage, respectively. However, no major differences in results between the configurations $[\text{Piezo}/0/90]_s$ and $[\text{Piezo}/0/0]_s$ are observed.

7. The shape control task in smart laminated cantilever composite plates and beams can be reliably implemented using the proposed explicit exact analytical solution. The proposed method is well suited for laminated composite structures subjected to more complex and asymmetrical loading systems whereas the characteristic and trial deflection functions are not required to be predetermined for shape control performance. According to the results, through a two-step task, twisting-bending deformation in the laminated composite structures can be suspended. For instance, piezoelectric actuators with no inclination angles could be exploited to control pure bending deformation while inclined ones can be used to suspend the pure twisting deformation.

Appendix.1:

The coefficients S^i_{mn}, $i=\{1,2,..,20\}$, in the four finite systems of the linear simultaneous multivariable Eqs.35a-d, can be computed as follows:

$$S_{mn}^{1}=(-1)^{n}\left(\frac{\alpha_m\left(\frac{(D_{12})\alpha_m^2}{4}+D_{22}\beta_n^2\right)}{\frac{D_{11}\alpha_m^4}{16}+\frac{(D_{12}+2D_{66})\alpha_m^2\beta_n^2}{2}+D_{22}\beta_n^4}\right)$$

$$S_{mn}^{2}=-\left(\frac{\alpha_m\left(\frac{(D_{12})\alpha_m^2}{4}+D_{22}\beta_n^2\right)}{\frac{D_{11}\alpha_m^4}{16}+\frac{(D_{12}+2D_{66})\alpha_m^2\beta_n^2}{2}+D_{22}\beta_n^4}\right)$$

$$S_{mn}^{3}=(-1)^{\frac{m-1}{2}}\left(\frac{\alpha_m\left(\frac{D_{11}\alpha_m^2}{4}+D_{12}\beta_n^2\right)}{\frac{D_{11}\alpha_m^4}{16}+\frac{(D_{12}+2D_{66})\alpha_m^2\beta_n^2}{2}+D_{22}\beta_n^4}\right)$$

$$S_{mn}^{4}=-\frac{D_{11}}{2}\left(\frac{\alpha_m^2}{\frac{D_{11}\alpha_m^4}{16}+\frac{(D_{12}+2D_{66})\alpha_m^2\beta_n^2}{2}+D_{22}\beta_n^4}\right)$$

$$S_{mn}^{5}=\left(\frac{-\alpha_m}{\frac{D_{11}\alpha_m^4}{16}+\frac{(D_{12}+2D_{66})\alpha_m^2\beta_n^2}{2}+D_{22}\beta_n^4}\right)\left\{\sum_{L=1}^{Mn}C_{mn}^{1}\left(\frac{-2P_0}{\alpha_m\beta_n}\right)\left(\cos(\frac{\alpha_m}{2}x_{1M})-\cos(\frac{\alpha_m}{2}x_{2M})\right)_L\right.$$

$$\left(\sin(\beta_n y_{1M})-\sin(\beta_n y_{2M})\right)_L+\sum_{L=1}^{Pn}C_{mn}^{2}\left[\frac{\left[M_x^P\right]^{\Theta}\alpha_m^2+4\left[M_y^P\right]^{\Theta}\beta_n^2}{2\alpha_m\beta_n}\right]\left(\cos(\frac{\alpha_m}{2}x_{1P})-\cos(\frac{\alpha_m}{2}x_{2P})\right)_L$$

$$\left.\left(\sin(\beta_n y_{1P})-\sin(\beta_n y_{2P})\right)_L+\sum_{L=1}^{Pn}C_{mn}^{3}\left[M_{xy}^P\right]^{\Theta}\left(\sin(\frac{\alpha_m}{2}x_{1P})-\sin(\frac{\alpha_m}{2}x_{2P})\right)_L\left(\cos(\beta_n y_{1P})-\cos(\beta_n y_{2P})\right)_L\right\}$$

$$S_{mn}^{6}=(-1)^{n}(-1)^{\frac{m-1}{2}}\left[D_{12}-\frac{\left(D_{22}\beta_n^2+\frac{D_{12}\alpha_m^2}{4}\right)\left(\frac{D_{11}\alpha_m^2}{4}+D_{12}\beta_n^2\right)}{\frac{D_{11}\alpha_m^4}{16}+\frac{(D_{12}+2D_{66})\alpha_m^2\beta_n^2}{2}+D_{22}\beta_n^4}\right]$$

$$S_{mn}^{7}=-(-1)^{\frac{m-1}{2}}\left[D_{12}-\frac{\left(D_{22}\beta_n^2+\frac{D_{12}\alpha_m^2}{4}\right)\left(\frac{D_{11}\alpha_m^2}{4}+D_{12}\beta_n^2\right)}{\frac{D_{11}\alpha_m^4}{16}+\frac{(D_{12}+2D_{66})\alpha_m^2\beta_n^2}{2}+D_{22}\beta_n^4}\right]$$

$$S_{mn}^{8}=(-1)^{m-1}\left(D_{11}-\frac{\left(\frac{D_{11}\alpha_m^2}{4}+D_{12}\beta_n^2\right)^2}{\frac{D_{11}\alpha_m^4}{16}+\frac{(D_{12}+2D_{66})\alpha_m^2\beta_n^2}{2}+D_{22}\beta_n^4}\right)$$

$$S_{mn}^{9}=\frac{D_{11}}{2}(-1)^{\frac{m-1}{2}}\left(\frac{\alpha_m\left(\frac{D_{11}\alpha_m^2}{4}+D_{12}\beta_n^2\right)}{\frac{D_{11}\alpha_m^4}{16}+\frac{(D_{12}+2D_{66})\alpha_m^2\beta_n^2}{2}+D_{22}\beta_n^4}\right)$$

$$S_{mn}^{10}=(-1)^{\frac{m-1}{2}}\left[\frac{D_{11}\alpha_m^4}{16}+\frac{(D_{12}+2D_{66})\alpha_m^2\beta_n^2}{2}+D_{22}\beta_n^4\right]^{-1}\left(\frac{D_{11}\alpha_m^2}{4}+D_{12}\beta_n^2\right)\left\{\sum_{L=1}^{Mn}C_{mn}^{1}\left(\frac{-2P_0}{\alpha_m\beta_n}\right)\right.$$
$$\left(\cos(\frac{\alpha_m}{2}x_{1M})-\cos(\frac{\alpha_m}{2}x_{2M})\right)_L\left(\sin(\beta_n y_{1M})-\sin(\beta_n y_{2M})\right)_L+\sum_{L=1}^{Pn}C_{mn}^{2}\left[\frac{\left[M_x^P\right]^{\Theta}\alpha_m^2+4\left[M_y^P\right]^{\Theta}\beta_n^2}{2\alpha_m\beta_n}\right]$$
$$\left(\cos(\frac{\alpha_m}{2}x_{1P})-\cos(\frac{\alpha_m}{2}x_{2P})\right)_L\left(\sin(\beta_n y_{1P})-\sin(\beta_n y_{2P})\right)_L+\sum_{L=1}^{Pn}C_{mn}^{3}\left[M_{xy}^P\right]^{\Theta}\left(\sin(\frac{\alpha_m}{2}x_{1P})-\sin(\frac{\alpha_m}{2}x_{2P})\right)_L$$
$$\left.\left(\cos(\beta_n y_{1P})-\cos(\beta_n y_{2P})\right)_L\right\}$$

$$S_{mn}^{11}=\lambda_n(-1)^{n}\left[D_{22}-\frac{\left(\frac{D_{12}\alpha_m^2}{4}+D_{22}\beta_n^2\right)^2}{\frac{D_{11}\alpha_m^4}{16}+\frac{(D_{12}+2D_{66})\alpha_m^2\beta_n^2}{2}+D_{22}\beta_n^4}\right]$$

$$S_{mn}^{12}=-\lambda_n\left[D_{22}-\frac{\left(\frac{D_{12}\alpha_m^2}{4}+D_{22}\beta_n^2\right)^2}{\frac{D_{11}\alpha_m^4}{16}+\frac{(D_{12}+2D_{66})\alpha_m^2\beta_n^2}{2}+D_{22}\beta_n^4}\right]$$

$$S_{mn}^{13}=\lambda_n(-1)^{\frac{m-1}{2}}\left[D_{12}-\frac{\left(\frac{D_{12}\alpha_m^2}{4}+D_{22}\beta_n^2\right)\left(\frac{D_{11}\alpha_m^2}{4}+D_{12}\beta_n^2\right)}{\frac{D_{11}\alpha_m^4}{16}+\frac{(D_{12}+2D_{66})\alpha_m^2\beta_n^2}{2}+D_{22}\beta_n^4}\right]$$

$$S_{mn}^{14}=\frac{D_{11}}{2}\lambda_n\left[\frac{\alpha_m\left(\frac{D_{12}\alpha_m^2}{4}+D_{22}\beta_n^2\right)}{\frac{D_{11}\alpha_m^4}{16}+\frac{(D_{12}+2D_{66})\alpha_m^2\beta_n^2}{2}+D_{22}\beta_n^4}\right]$$

$$S_{mn}^{15}=\lambda_n\left[\frac{D_{11}\alpha_m^4}{16}+\frac{(D_{12}+2D_{66})\alpha_m^2\beta_n^2}{2}+D_{22}\beta_n^4\right]^{-1}\left(\frac{D_{12}\alpha_m^2}{4}+D_{22}\beta_n^2\right)\left\{\sum_{L=1}^{Mn}C_{mn}^1\left(\frac{-2P_0}{\alpha_m\beta_n}\right)\right.$$
$$\left(\cos(\frac{\alpha_m}{2}x_{1M})-\cos(\frac{\alpha_m}{2}x_{2M})\right)_L\left(\sin(\beta_n y_{1M})-\sin(\beta_n y_{2M})\right)_L+\sum_{L=1}^{Pn}C_{mn}^2\left[\frac{\left[M_x^P\right]^{\Theta}\alpha_m^2+4\left[M_y^P\right]^{\Theta}\beta_n^2}{2\alpha_m\beta_n}\right]$$
$$\left(\cos(\frac{\alpha_m}{2}x_{1P})-\cos(\frac{\alpha_m}{2}x_{2P})\right)_L\left(\sin(\beta_n y_{1P})-\sin(\beta_n y_{2P})\right)_L+\sum_{L=1}^{Pn}C_{mn}^3\left[M_{xy}^P\right]^{\Theta}\left(\sin(\frac{\alpha_m}{2}x_{1P})-\sin(\frac{\alpha_m}{2}x_{2P})\right)_L$$
$$\left.\left(\cos(\beta_n y_{1P})-\cos(\beta_n y_{2P})\right)_L\right\}$$

$$S_{mn}^{16}=\lambda_n\left[D_{22}-\frac{\left(\frac{D_{12}\alpha_m^2}{4}+D_{22}\beta_n^2\right)^2}{\frac{D_{11}\alpha_m^4}{16}+\frac{(D_{12}+2D_{66})\alpha_m^2\beta_n^2}{2}+D_{22}\beta_n^4}\right]$$

$$S_{mn}^{17}=-\lambda_n(-1)^n\left[D_{22}-\frac{\left(\frac{D_{12}\alpha_m^2}{4}+D_{22}\beta_n^2\right)^2}{\frac{D_{11}\alpha_m^4}{16}+\frac{(D_{12}+2D_{66})\alpha_m^2\beta_n^2}{2}+D_{22}\beta_n^4}\right]$$

$$S_{mn}^{18}=\lambda_n(-1)^n(-1)^{\frac{m-1}{2}}\left[D_{12}-\frac{\left(\frac{D_{12}\alpha_m^2}{4}+D_{22}\beta_n^2\right)\left(\frac{D_{11}\alpha_m^2}{4}+D_{12}\beta_n^2\right)}{\frac{D_{11}\alpha_m^4}{16}+\frac{(D_{12}+2D_{66})\alpha_m^2\beta_n^2}{2}+D_{22}\beta_n^4}\right]$$

$$S_{mn}^{19}=\lambda_n\frac{D_{11}}{2}(-1)^n\left[\frac{\alpha_m\left(\frac{D_{12}\alpha_m^2}{4}+D_{22}\beta_n^2\right)}{\frac{D_{11}\alpha_m^4}{16}+\frac{(D_{12}+2D_{66})\alpha_m^2\beta_n^2}{2}+D_{22}\beta_n^4}\right]$$

$$S_{mn}^{20}=\lambda_n(-1)^n\left[\frac{D_{11}\alpha_m^4}{16}+\frac{(D_{12}+2D_{66})\alpha_m^2\beta_n^2}{2}+D_{22}\beta_n^4\right]^{-1}\left(\frac{D_{12}\alpha_m^2}{4}+D_{22}\beta_n^2\right)\left\{\sum_{L=1}^{Mn}C_{mn}^1\left(\frac{-2P_0}{\alpha_m\beta_n}\right)\right.$$
$$\left(\cos(\frac{\alpha_m}{2}x_{1M})-\cos(\frac{\alpha_m}{2}x_{2M})\right)_L\left(\sin(\beta_n y_{1M})-\sin(\beta_n y_{2M})\right)_L+\sum_{L=1}^{Pn}C_{mn}^2\left[\frac{\left[M_x^P\right]^{\Theta}\alpha_m^2+4\left[M_y^P\right]^{\Theta}\beta_n^2}{2\alpha_m\beta_n}\right]$$
$$\left(\cos(\frac{\alpha_m}{2}x_{1P})-\cos(\frac{\alpha_m}{2}x_{2P})\right)_L\left(\sin(\beta_n y_{1P})-\sin(\beta_n y_{2P})\right)_L+\sum_{L=1}^{Pn}C_{mn}^3\left[M_{xy}^P\right]^{\Theta}\left(\sin(\frac{\alpha_m}{2}x_{1P})-\sin(\frac{\alpha_m}{2}x_{2P})\right)_L$$
$$\left.\left(\cos(\beta_n y_{1P})-\cos(\beta_n y_{2P})\right)_L\right\}$$

Acknowledgements:

Soheil Gohari would like to thank the College of Engineering and Science at Victoria University, Melbourne for offering the Victoria University International Postgraduate Research scholarship (VUIPRS) to undertake his Ph.D. study. This financial support is gratefully acknowledged.

References:

[1] S. Gohari, S. Sharifi, Z. Vrcelj, and M. Y. Yahya, "First-ply failure prediction of an unsymmetrical laminated ellipsoidal woven GFRP composite shell with incorporated surface-bounded sensors and internally pressurized," *Compos. Part B Eng.*, vol. 77, pp. 502–518, 2015.

[2] S. Sharifi, S. Gohari, M. Sharifiteshnizi, and Z. Vrcelj, "Numerical and experimental study on mechanical strength of internally pressurized laminated woven composite shells incorporated with surface-bounded sensors," *Compos. Part B Eng.*, vol. 94, pp. 224–237, 2016.

[3] G. Sharifishourabi, A. Ayob, S. Gohari, M. Y. B. Yahya, S. Sharifi, and Z. Vrcelj, "Flexural behavior of functionally graded slender beams with complex cross-section," *J. Mech. Mater. Struct.*, vol. 10, no. 1, pp. 1–16, 2015.

[4] H. B. Coda, "Continuous inter-laminar stresses for regular and inverse geometrically non linear dynamic and static analyses of laminated plates and shells," *Compos. Struct.*, vol. 132, pp. 406–422, 2015.

[5] Q. Liu, "Analytical sensitivity analysis of eigenvalues and lightweight design of composite laminated beams," *Compos. Struct.*, vol. 134, pp. 918–926, 2015.

[6] J. E. Sader and L. White, "Theoretical analysis of the static deflection of plates for atomic force microscope applications," *J. Appl. Phys.*, vol. 74, no. 1, pp. 1–9, 1993.

[7] M. J. Lachut and J. E. Sader, "Buckling of a cantilever plate uniformly loaded in its plane with applications to surface stress and thermal loads," *J. Appl. Phys.*, vol. 113, no. 2, pp. 1–11, 2013.

[8] D. K. Shin and J. J. Lee, "Theoretical analysis of the deflection of a cantilever plate for wirebonding on overhang applications," *IEEE Trans. Components, Packag. Manuf. Technol.*, vol. 2, no. 6, pp. 916–924, 2012.

[9] S. C. Kattimani and M. C. Ray, "Smart damping of geometrically nonlinear vibrations of magneto-electro-elastic plates," *Compos. Struct.*, vol. 114, no. 1, pp. 51–63, 2014.

[10] S. Sawarkar, S. Pendhari, and Y. Desai, "Semi-analytical solutions for static analysis of piezoelectric laminates," *Compos. Struct.*, vol. 153, pp. 242–252, 2016.

[11] S. Murugan and M. I. Friswell, "Morphing wing flexible skins with curvilinear fiber composites," *Compos. Struct.*, vol. 99, pp. 69–75, 2013.

[12] M. Adnan Elshafei, A. Farid, and A. A. Omer, "Modeling of torsion actuation of beams using inclined piezoelectric actuators," *Arch. Appl. Mech.*, vol. 85, no. 2, pp. 171–189, 2014.

[13] M. Akbar and J. L. Curiel-Sosa, "Piezoelectric energy harvester composite under dynamic bending with implementation to aircraft wingbox structure," *Compos. Struct.*, vol. 153, pp. 193–203, 2016.

[14] M. Kerboua, A. Megnounif, M. Benguediab, K. H. Benrahou, and F. Kaoulala,

"Vibration control beam using piezoelectric-based smart materials," *Compos. Struct.*, vol. 123, pp. 430–442, 2015.

[15] H. Brito-Santana, R. de Medeiros, R. Rodriguez-Ramos, and V. Tita, "Different interface models for calculating the effective properties in piezoelectric composite materials with imperfect fiber-matrix adhesion," *Compos. Struct.*, vol. 151, pp. 70–80, 2016.

[16] D. B. Koconis, L. P. Kollar, and G. S. Springer, "Shape control of composite plates and shells with embedded actuators .1. voltages specified," *J. Compos. Mater.*, vol. 28, no. 5, pp. 415–458, 1994.

[17] D. B. Koconis, L. P. Kollar, and G. S. Springer, "Shape control of composite plates and shells with embedded actuators. II. desired shape specified," *J. Compos. Mater.*, vol. 28, no. 3, pp. 459–482, 1994.

[18] A. Andakhshideh and M. Tahani, "Free-edge stress analysis of general rectangular composite laminates under bending , torsion and thermal loads," *Eur. J. Mech. / A Solids*, vol. 42, pp. 229–240, 2013.

[19] S. Gohari, S. Sharifi, G. Sharifishourabi, Z. Vrcelj, and R. Abadi, "Effect of temperature on crack initiation in gas formed structures," *J. Mech. Sci. Technol.*, vol. 27, no. 12, pp. 3745–3754, 2013.

[20] C. C. Lin, C. Y. Hsu, and H. N. Huang, "Finite element analysis on deflection control of plates with piezoelectric actuators," *Compos. Struct.*, vol. 35, no. 4, pp. 423–433, 1996.

[21] A. C. Cook and S. S. Vel, "Multiscale analysis of laminated plates with integrated piezoelectric fiber composite actuators," *Compos. Struct.*, vol. 94, no. 2, pp. 322–336, 2012.

[22] A. Milazzo, "Refined equivalent single layer formulations and finite elements for smart laminates free vibrations," *Compos. Part B Eng.*, vol. 61, pp. 238–253, 2014.

[23] M. Sartorato, R. de Medeiros, and V. Tita, "A finite element formulation for smart piezoelectric composite shells: Mathematical formulation, computational analysis and experimental evaluation," *Compos. Struct.*, vol. 127, pp. 185–198, 2015.

[24] S. Q. Zhang, Y. X. Li, and R. Schmidt, "Modeling and simulation of macro-fiber composite layered smart structures," *Compos. Struct.*, vol. 126, pp. 89–100, 2015.

[25] S. Q. Zhang and R. Schmidt, "Static and dynamic FE analysis of piezoelectric integrated thin-walled composite structures with large rotations," *Compos. Struct.*, vol. 112, pp. 345–357, 2014.

[26] J. Plattenburg, J. T. Dreyer, and R. Singh, "Active and passive damping patches on a thin rectangular plate: A refined analytical model with experimental validation," *J. Sound Vib.*, vol. 353, pp. 75–95, 2015.

[27] C. R. Bowen, R. Butler, R. Jervis, H. A. Kim, and A. I. T. Salo, "Morphing and shape control using unsymmetrical composites," *J. Intell. Mater. Struct.*, vol. 18, no. January, 2007.

[28] P. Giddings, C. R. Bowen, R. Butler, and H. A. Kim, "Characterisation of actuation properties of piezoelectric bi-stable carbon-fibre laminates," *Compos. Part A Appl. Sci. Manuf.*, vol. 39, no. 4, pp. 697–703, 2008.

[29] T. I. Thinh and L. K. Ngoc, "Static behavior and vibration control of piezoelectric cantilever composite plates and comparison with experiments," *Comput. Mater. Sci.*, vol. 49, no. 4 SUPPL., pp. S276–S280, 2010.

[30] R. P. Khandelwal, A. Chakrabarti, and P. Bhargava, "Static and dynamic control of

smart composite laminates," *AIAA J.*, vol. 52, no. 9, pp. 1896–1914, 2014.

[31] S. Gohari, A. Golshan, and A. Ayob, "Theoretical Analysis and Finite Element Simulation of Behavior of Laminated Hemispherical GRP Dome Subjected to Internal Pressure," *Int. Conf. Comput. Softw. Model.*, vol. 14, pp. 122–129, 2011.

[32] S. Gohari, A. Golshan, A. B. Nia, and M. Hashemzadeh, "Prediction of Failure in Thin-Walled Hemispherical GRP Dome Subjected to Static Internal Pressure Based on a Failure Factor," *Adv. Mater. Res.*, vol. 488–489, pp. 358–366, 2012.

[33] S. Gohari, a. Golshan, M. Mostakhdemin, F. Mozafari, and a. Momenzadeh, "Failure Strength of Thin-walled Cylindrical GFRP Composite Shell against Static Internal and External Pressure for various Volumetric Fiber Fraction," *International Journal of Applied Physics and Mathematics*, vol. 2, no. 2. pp. 111–116, 2012.

[34] S. Gohari, A. Golshan, F. Firouzabadi, and N. Hosseininezhad, "Effect of Volumetric Fiber Fraction on Failure Strength of Thin-Walled GFRP Composite Cylindrical Shell Externally Pressurized," *Adv. Mater. Res.*, vol. 488–489, pp. 530–536, 2012.

[35] S. Gohari, A. Golshan, M. Hashemzadeh, and N. Hosseininezhad, "First-Ply Strength of Thick Circular Cylindrical GRP Composite Shell Subjected to Static External Pressure via Finite Element Simulation and Analytical Approaches," *Adv. Mater. Res.*, vol. 463–464, pp. 477–483, 2012.

[36] F. Firouzabadi, A. Ayob, M. R. Arjmandi, S. Gohari, and N. Deirram, "Modeling of the impact on cylindrical composite shell as continuous patch loading," *Int. J. Mech. Mech. Eng.*, vol. 12, no. 3, pp. 8–13, 2012.

[37] S. Sharifi, T. A. D. M. S. Almula, S. Gohari, G. Sharifishourabi, Y. Saed, and M. Y. Bin Yahya, "Impact Response of Laminated Composite Cylindrical Shell: Finite Element Simulation Approach," *Appl. Mech. Mater.*, vol. 393, pp. 387–392, 2013.

[38] S. C. Her and C. S. Lin, "Deflection of cross-ply composite laminates induced by piezoelectric actuators," *Sensors*, vol. 10, no. 1, pp. 719–733, 2010.

[39] S.-C. Her and C.-S. Lin, "Vibration analysis of composite laminate plate excited by piezoelectric actuators.," *Sensors*, vol. 13, no. 3, pp. 2997–3013, 2013.

[40] Y. Sakava, S. Member, and Z. H. Luo, "Modeling and Control of Coupled Bending and Torsional Vibrations of Flexible Beams," *IEEE Trans. Autom. Control*, vol. 34, no. 9, pp. 970–977, 1989.

[41] H. D. Bureau and H. A. Limited, "Structural dynamic analysis of composite beams," *J. Sound Vib.*, vol. 143, pp. 503–519, 1990.

[42] A. P. Boresi, R. J. Schmidt, and O. M. Sidebottom, "Advanced Mechanics of Materials," *Wiley, New York*, pp. 242–249, 1978.

[43] B. V. Sankar, "A Beam Theory for Laminated Composites and Application to Torsion Problems," *J. Appl. Mech.*, vol. 60, no. 1, pp. 246–249, 1993.

[44] J. R. Banerjee and F. W. Williams, "Coupled bending-torsional dynamic stiffness matrix of an axially loaded timoshenko beam element," *Int. J. Solids Struct.*, vol. 31, no. 6, pp. 749–762, 1994.

[45] C. Park, C. Walz, and I. Chopra, "Bending and torsion models of beams with induced strain actuators," *SPIE Conf. Albuquerque, NM*, 1993.

[46] C. Park and I. Chopra, "Modeling piezoceramic actuation of beam in torsion," *Proc. 35th AIAA/ASME/ASCE/AHS Struct. Struct. Dyn. Mater. Conf. Adapt. Struct. Forum*, pp. 438–450, 1994.

[47] P. C. Chen and I. Chopra, "Induced strain actuation of composite beams and rotor

blades with embedded piezoceramic elements," *Smart Mater. Struct.*, vol. 5, pp. 35–48, 1996.

[48] T. Takawa, T. Fu kuda, and T. Takada, "Flexural–torsion coupling vibration control of fiber composite cantilevered beam by using piezo-ceramic actuators," *Smart Mater. Struct.*, vol. 6, pp. 447–484, 1997.

[49] S. R. Thirupathi, P. Seshu, and N. G. Naganathan, "A finite element static analysis of smart turbine blades," *Smart Mater. Struct.*, vol. 6, pp. 607–615, 1997.

[50] J. Kim, V. V. Varadan, V. K. Varadan, and X. Q. Bao, "Finite-element modeling of a smart cantilever plate and comparison with experiments," *Smart Materials and Structures*, vol. 5, no. 2. pp. 165–170, 1996.

[51] L. Ren, "A theoretical study on shape control of arbitrary lay-up laminates using piezoelectric actuators," *Compos. Struct.*, vol. 83, no. 1, pp. 110–118, 2008.

[52] J. N. Reddy, "On laminated composite plates with integrated sensors and actuators," *Eng. Struct.*, vol. 21, no. 7, pp. 568–593, 1999.

[53] N. Kharghani and C. Guedes Soares, "Behaviour of composite laminates with embedded delaminations," *Compos. Struct.* , vol. 150, pp. 226–239, 2016.

[54] D. Shao, F. Hu, Q. Wang, F. Pang, and S. Hu, "Transient response analysis of cross-ply composite laminated rectangular plates with general boundary restraints by the method of reverberation ray matrix," *Compos. Struct.*, vol. 152, pp. 168–182, 2016.

[55] Y. M. Yue, K. Y. Xu, and T. Chen, "A micro scale Timoshenko beam model for piezoelectricity with flexoelectricity and surface effects," *Compos. Struct.*, vol. 136, pp. 278–286, 2016.

[56] Z. Wu, C. Han, and Z. Niu, "A 3D exact analysis of the boundary layer effect of asymmetric piezoelectric laminates with electromechanical coupling," *Int. J. Solids Struct.*, vol. 72, pp. 118–129, 2015.

[57] J. Zhu, J. Wang, and L. Zu, "Influence of out-of-plane ply waviness on elastic properties of composite laminates under uniaxial loading," *Compos. Struct.*, vol. 132, pp. 440–450, 2015.

[58] P. Y. Moghadam, M. Tahani, and A. M. Naserian-Nik, "Analytical solution of piezolaminated rectangular plates with arbitrary clamped/simply-supported boundary conditions under thermo-electro-mechanical loadings," *Appl. Math. Model.*, vol. 37, no. 5, pp. 3228–3241, 2013.

[59] G. Kress and M. Winkler, "Corrugated laminate homogenization model," *Compos. Struct.*, vol. 92, no. 3, pp. 795–810, 2010.

[60] S. Gohari, S. Sharifi, and Z. Vrcelj, "New explicit solution for static shape control of smart laminated cantilever piezo-composite-hybrid plates/beams under thermo-electro-mechanical loads using piezoelectric actuators," *Compos. Struct.*, vol. 145, pp. 89–112, 2016.

[61] N. D. Duc, T. Q. Quan, and V. D. Luat, "Nonlinear dynamic analysis and vibration of shear deformable piezoelectric FGM double curved shallow shells under damping-thermo-electro-mechanical loads," *Compos. Struct.*, vol. 125, pp. 29–40, Jul. 2015.

[62] G. A. Foutsitzi, C. G. Gogos, E. P. Hadjigeorgiou, and G. E. Stavroulakis, "Actuator location and voltages optimization for shape control of smart beams using genetic algorithms," *Actuators*, vol. 2, no. 4, pp. 111–128, 2013.

[63] Y. Yu, X. N. Zhang, and S. L. Xie, "Optimal shape control of a beam using piezoelectric actuators with low control voltage," *Smart Mater. Struct.*, vol. 18, no. 9, pp. 1–15, 2009.

[64] M. S. I. Shaik Dawood, L. Iannucci, and E. S. Greenhalgh, “Three-dimensional static shape control analysis of composite plates using distributed piezoelectric actuators,” *Smart Mater. Struct.*, vol. 17, no. 2, pp. 1–10, 2008.

Tables:

Table.1. Material properties.

Material properties	KYNAR [57]	PZT G1195N [54]	T300/976 GFRP [56]
E_1 [GPa]	2	63	150
E_2 [GPa]	2	63	9
v_{12}	0.29	0.3	0.3
G_{12} [GPa]	0.77	24.2	7.1
G_{13} [GPa]	0.77	24.2	2.5
$d_{31}\left[{}^{nm}/_{V}\right]$	0.023	0.254	0
$d_{32}\left[{}^{nm}/_{V}\right]$	0.0046	0.254	0
$\rho_z\left[{}^{nF}/_{m}\right]$	0.1062	15	0

Figures:

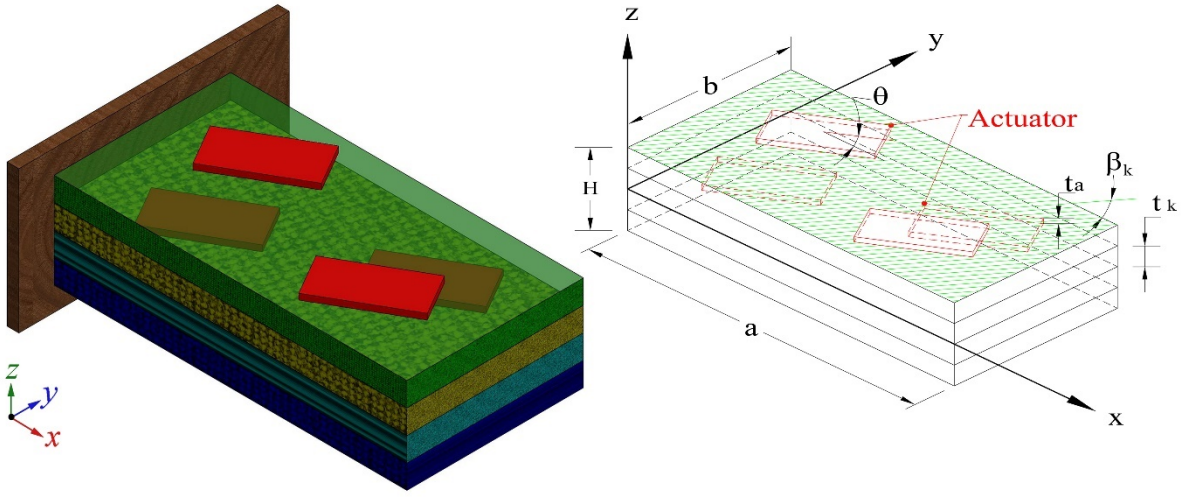

Fig.1. Schematics of smart laminated cantilever piezo composite plate integrated with arbitrarily positioned inclined piezoelectric actuators.

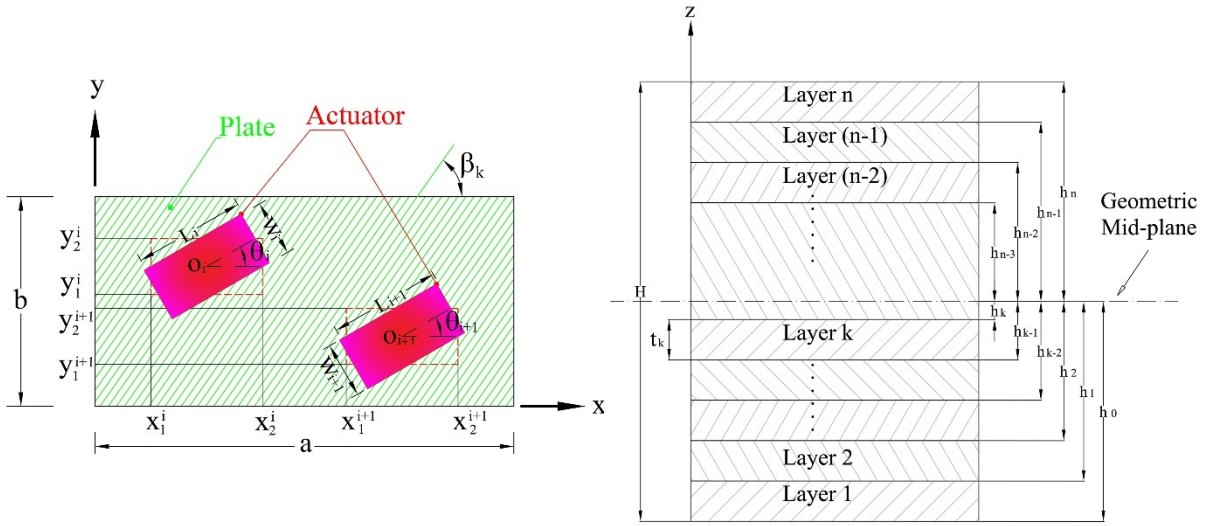

Fig.2. Schematic of placement, geometry, and inclination angles of inclined piezoelectric actuators and smart composite laminate layup cross-section.

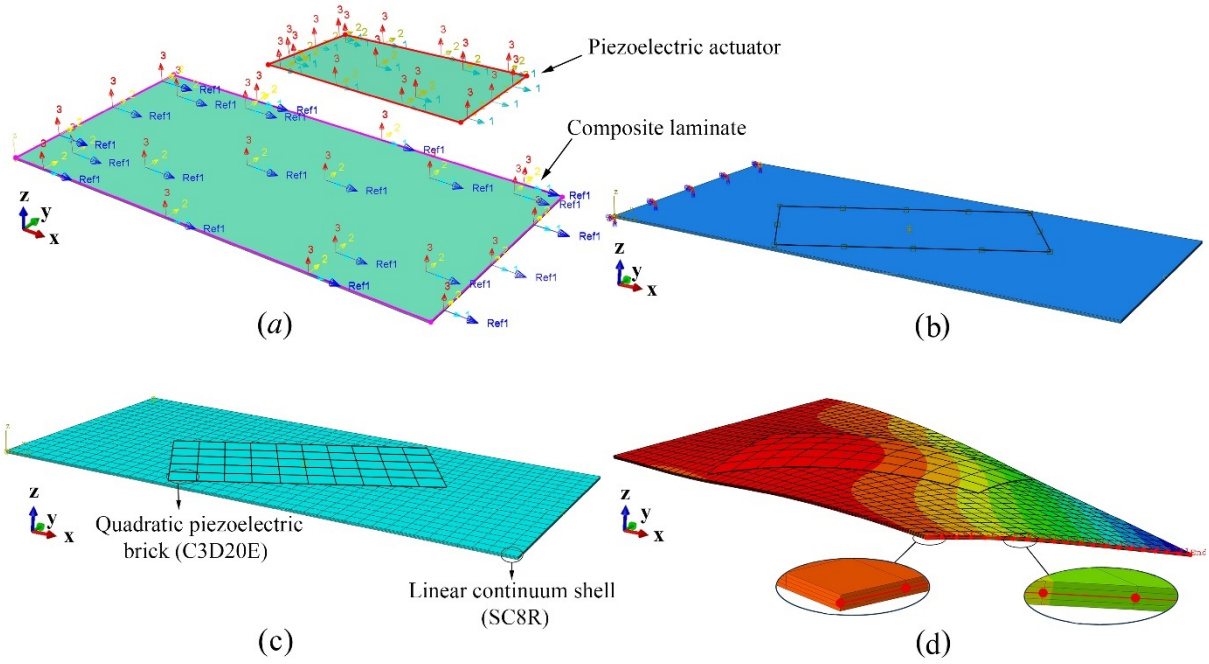

Fig.3. The schematic of FE simulation of smart cantilever piezo composite plates and beams induced by electro-mechanical twisting loads using Commercial Finite Element software ABAQUS/CEA 6.13-1: a) sketching and defining the dimensions and material properties to composite laminate and piezoelectric actuators, b) applying the electro-mechanical boundary conditions, piezoelectric actuators groundings, inclination angle and electrical surface charges, c) Applying the FE meshing to the smart cantilever piezo composite and defining the element type of host structure and piezoelectric actuators, d) defining a path/paths along a specific direction in the smart cantilever piezo composite laminate's mid-plane.

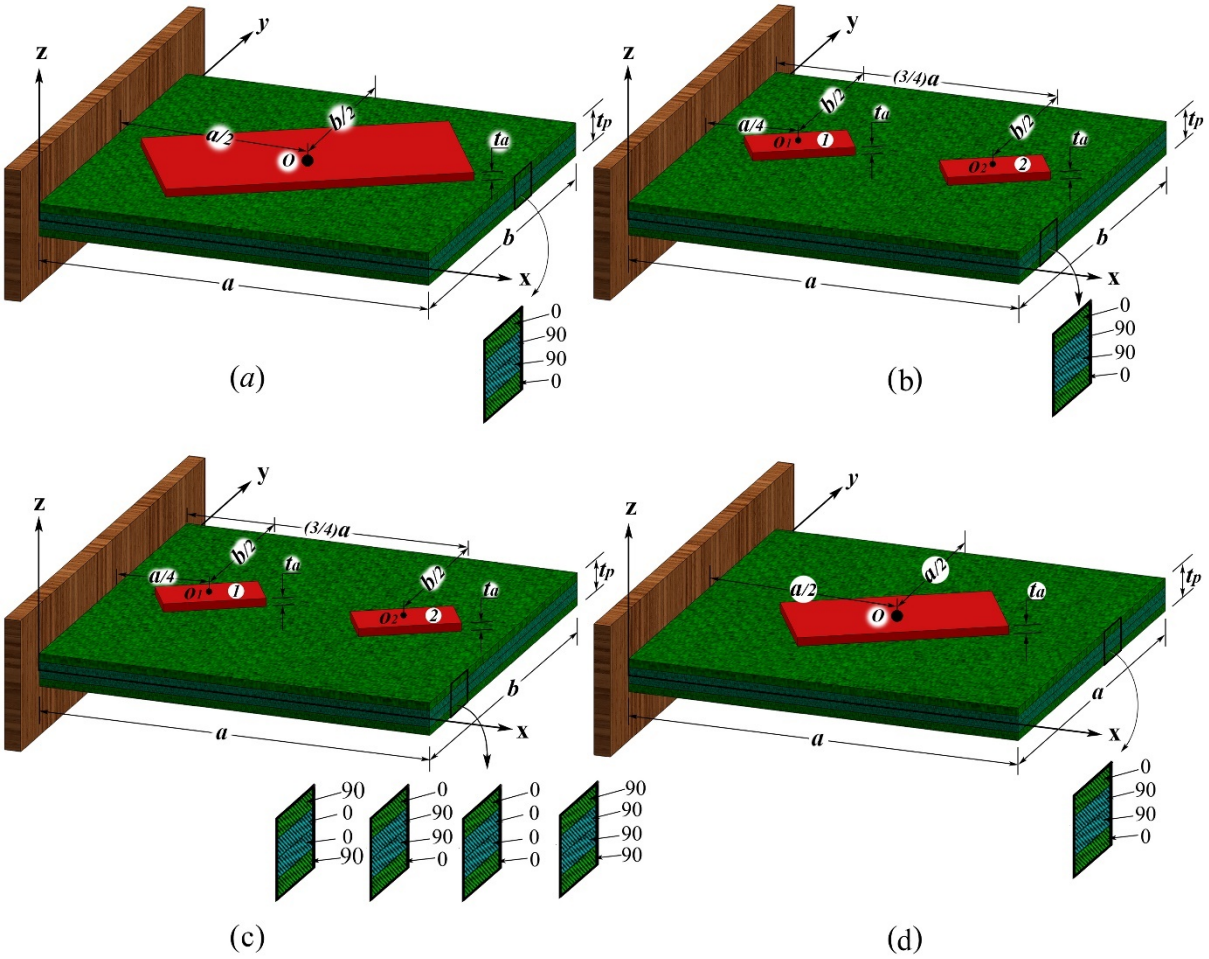

Fig.4. Schematic of the smart laminated cantilever composite plates with a) single bounded actuator pair, b) double bounded actuator pairs, c) double bounded actuator pairs and various stacking sequence configuration, d) single bounded actuator pair and under various electrical voltage.

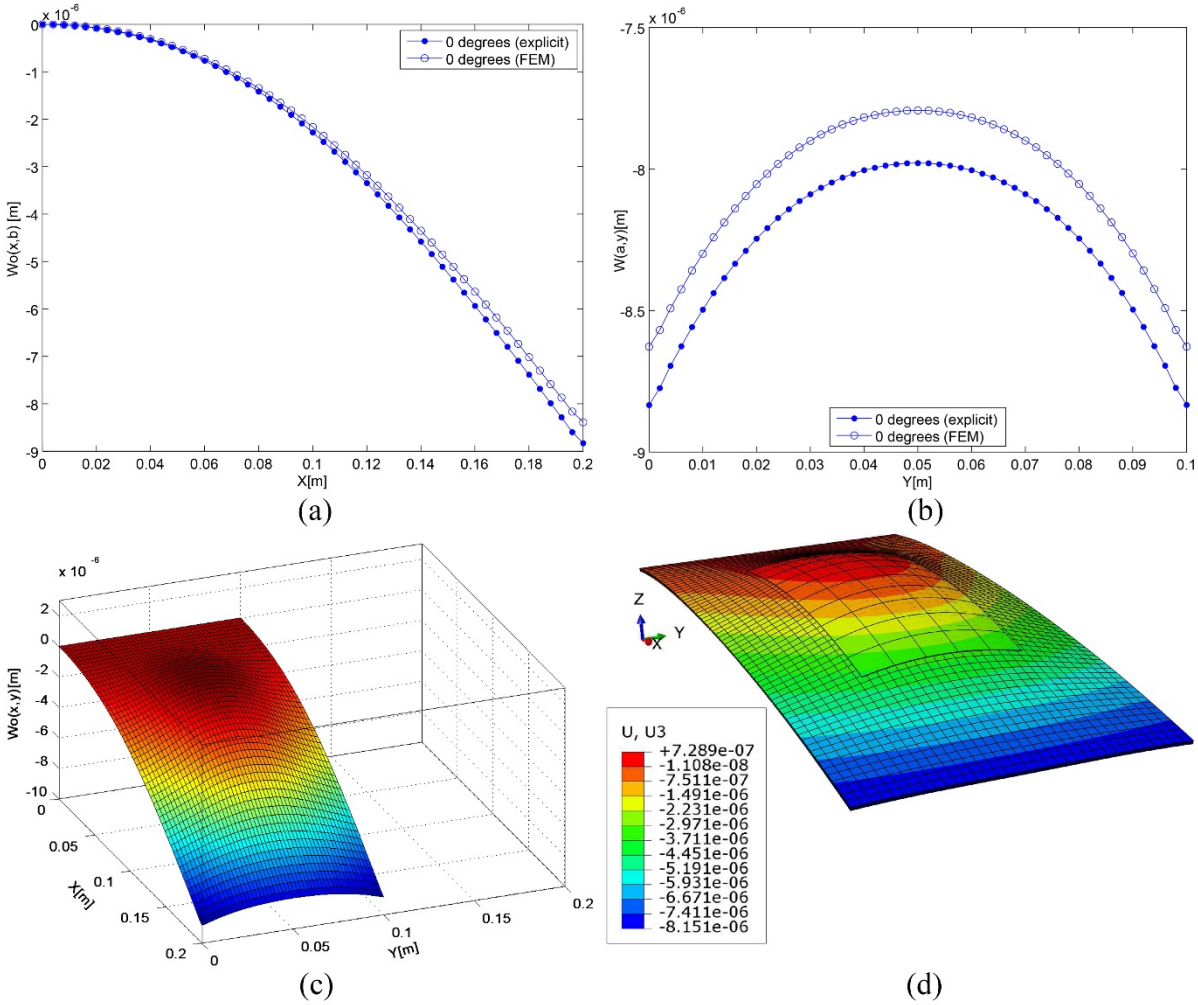

Fig.5. Explicit and numerical analysis of shape deformation in the smart cantilever composite plate integrated with single piezoelectric actuator pair when $\theta = 0^o$: a) $w_o(x,b)$, b) $w_o(a,y)$, c) $w_o(x,y)$: Explicit, d) $w_o(x,y)$: Numerical.

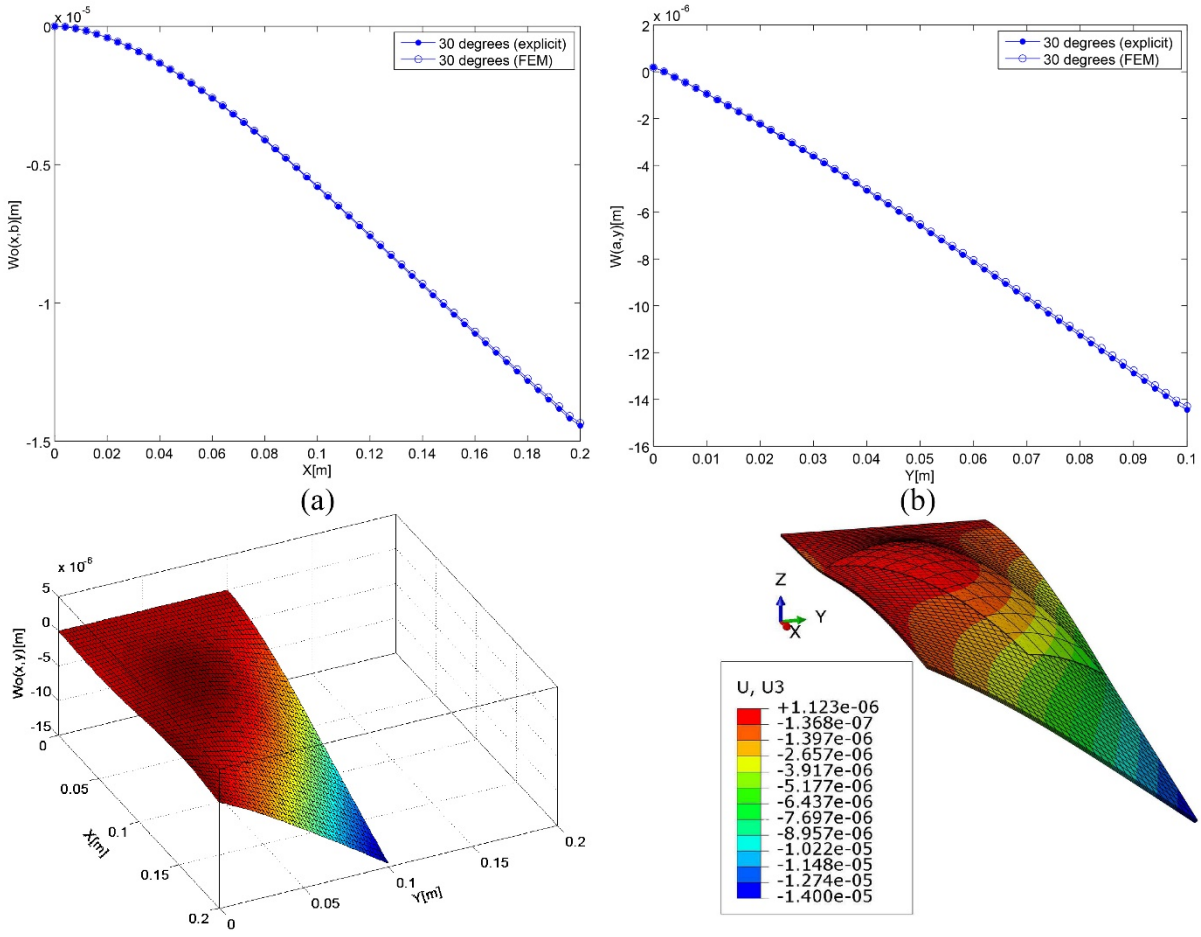

Fig.6. Explicit and numerical analysis of shape deformation in the smart cantilever composite plate integrated with inclined single piezoelectric actuator pair when $\theta = 30^o$: a) $w_o(x,b)$, b) $w_o(a,y)$, c) $w_o(x,y)$: Explicit, d) $w_o(x,y)$: Numerical.

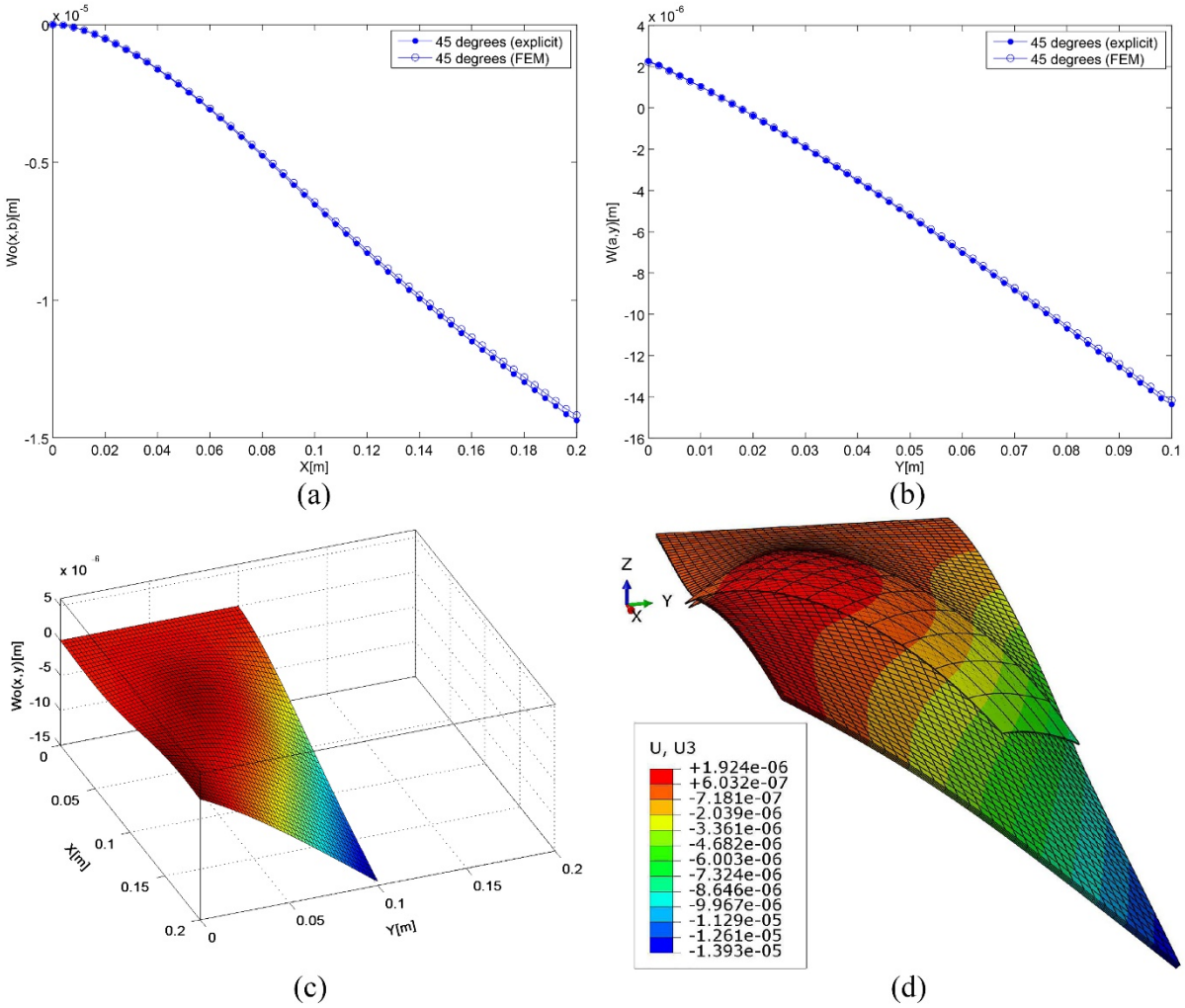

Fig.7. Explicit and numerical analysis of shape deformation in the smart cantilever composite plate integrated with inclined single piezoelectric actuator pair when $\theta = 45^o$: a) $w_o(x,b)$, b) $w_o(a,y)$, c) $w_o(x,y)$: Explicit, d) $w_o(x,y)$: Numerical.

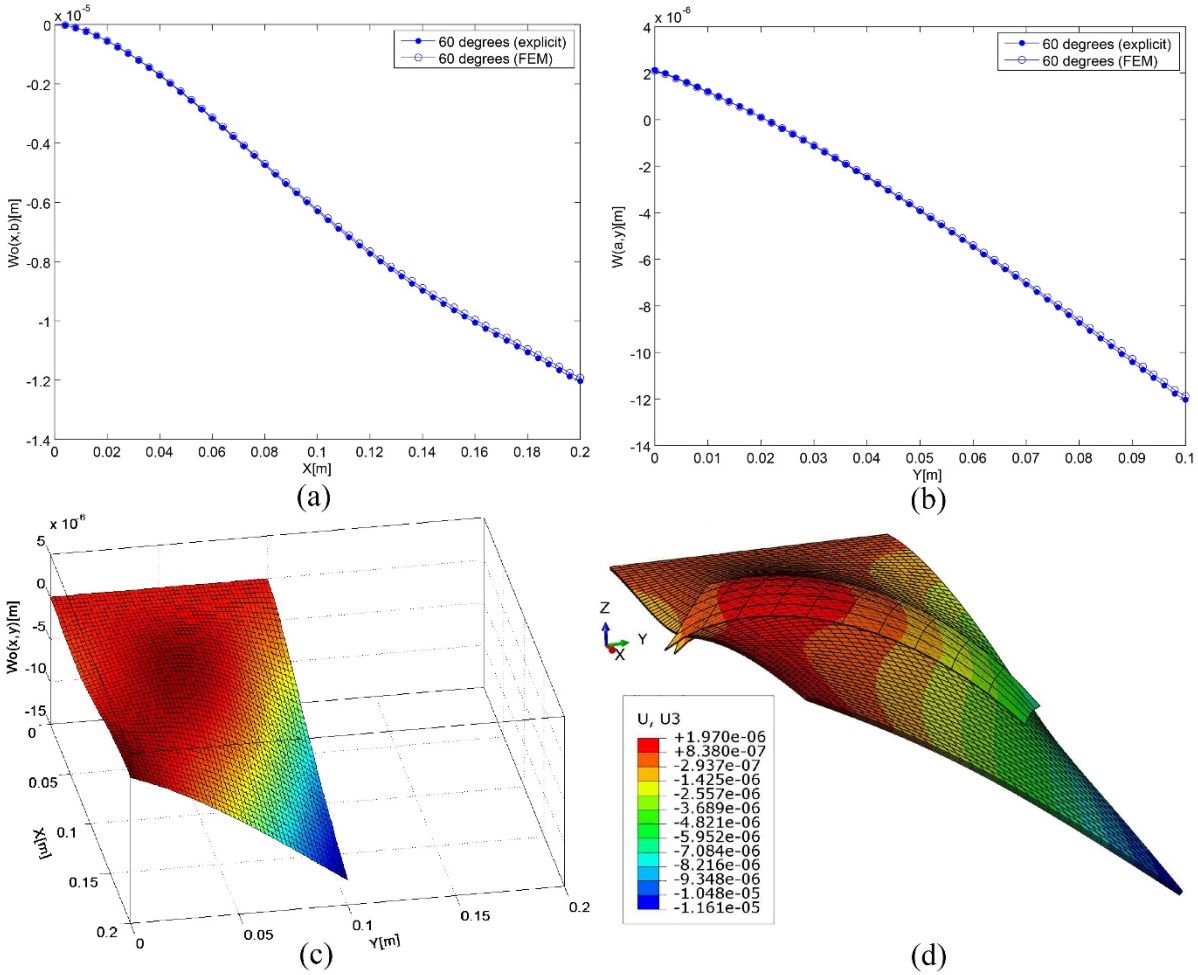

Fig.8. Explicit and numerical analysis of shape deformation in the smart cantilever composite plate integrated with inclined single piezoelectric actuator pair when $\theta = 60^o$: a) $w_o(x,b)$, b) $w_o(a,y)$, c) $w_o(x,y)$: Explicit, d) $w_o(x,y)$: Numerical.

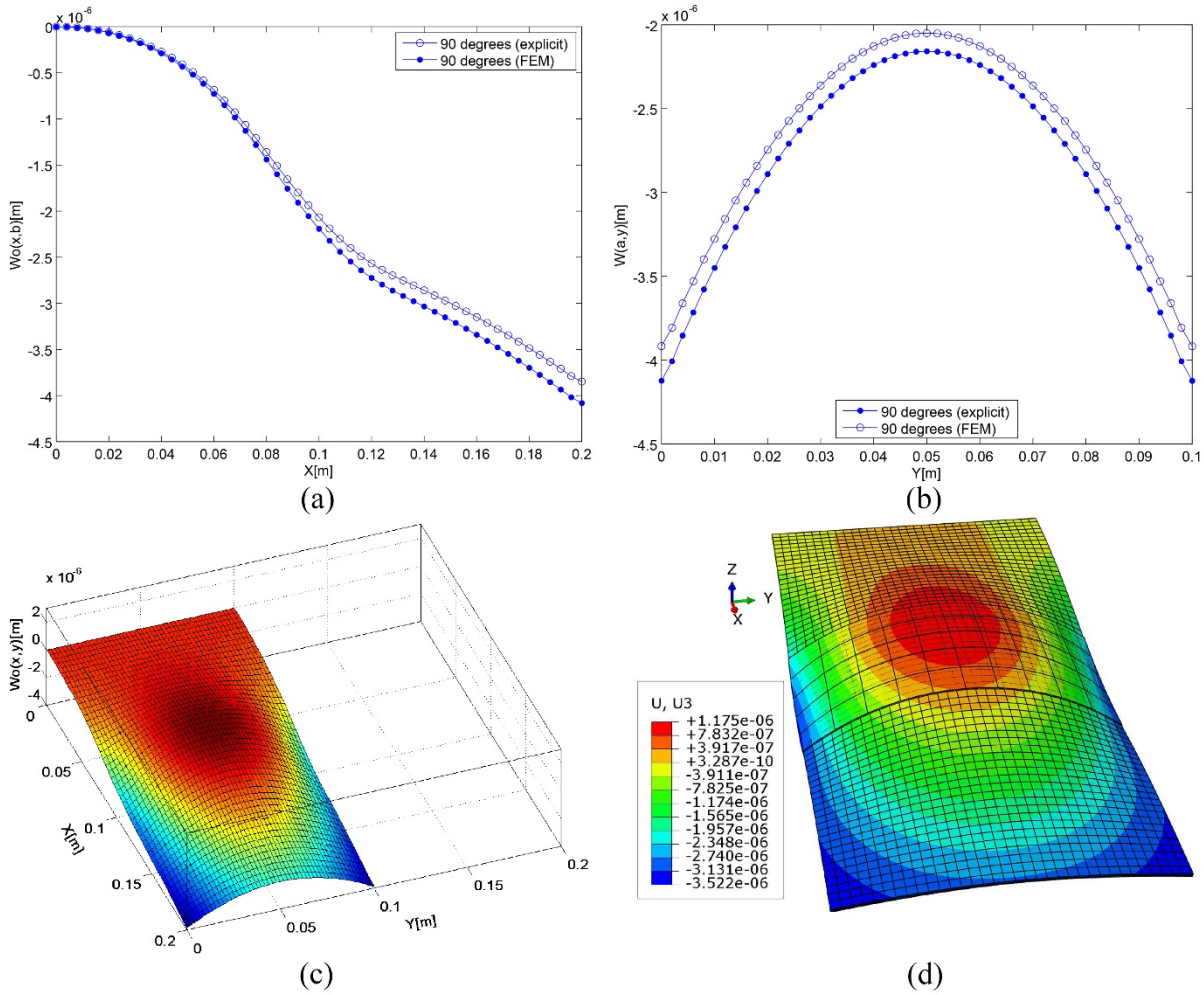

Fig.9. Explicit and numerical analysis of shape deformation in the smart cantilever composite plate integrated with inclined single piezoelectric actuator pair when $\theta = 90^o$: a) $w_o(x,b)$, b) $w_o(a,y)$, c) $w_o(x,y)$: Explicit, d) $w_o(x,y)$: Numerical.

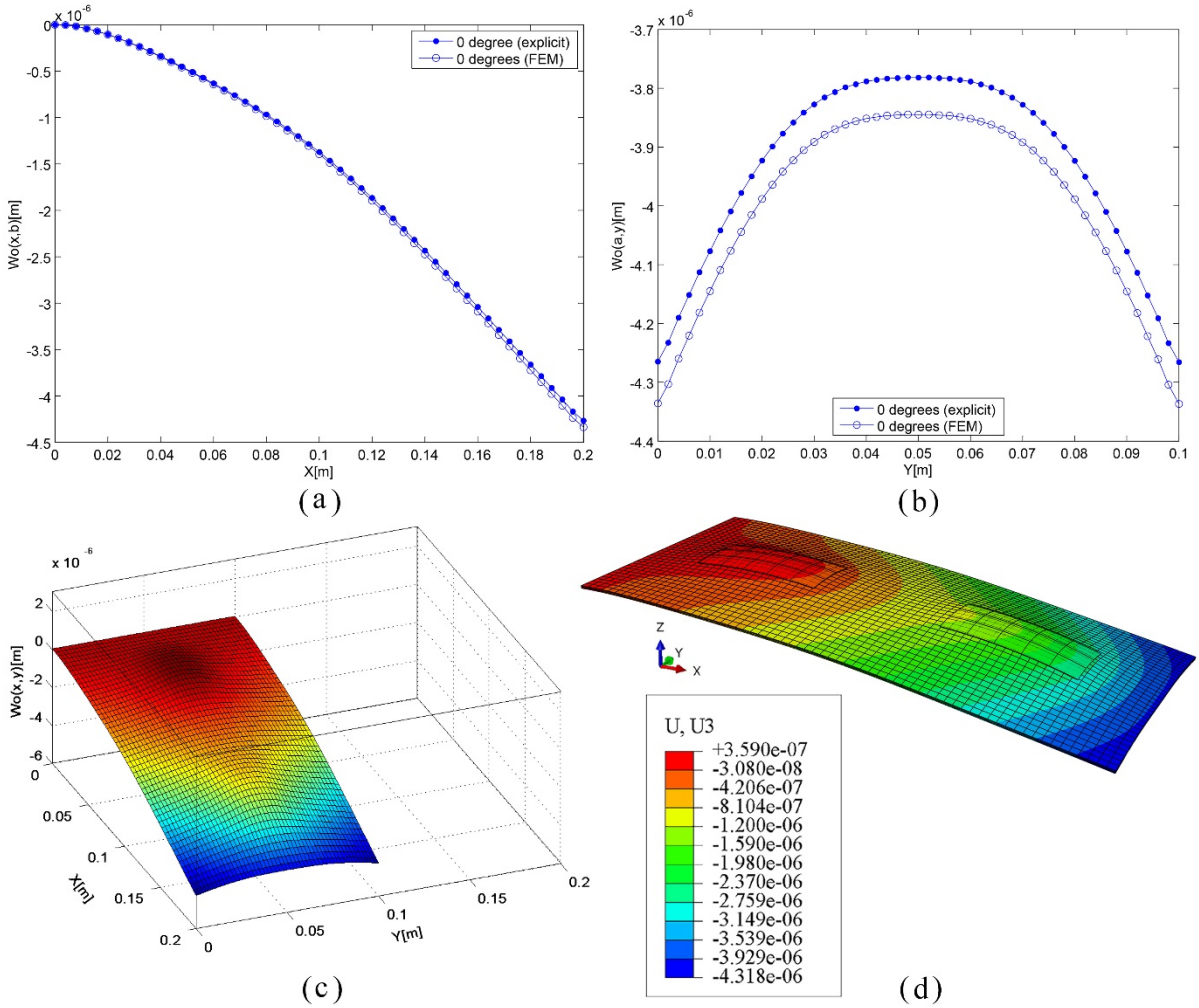

Fig.10. Explicit and numerical analysis of shape deformation in the smart cantilever composite plate integrated with double piezoelectric actuator pairs when $\theta = 0^o$: a) $w_o(x,b)$, b) $w_o(a,y)$, c) $w_o(x,y)$: Explicit, d) $w_o(x,y)$: Numerical.

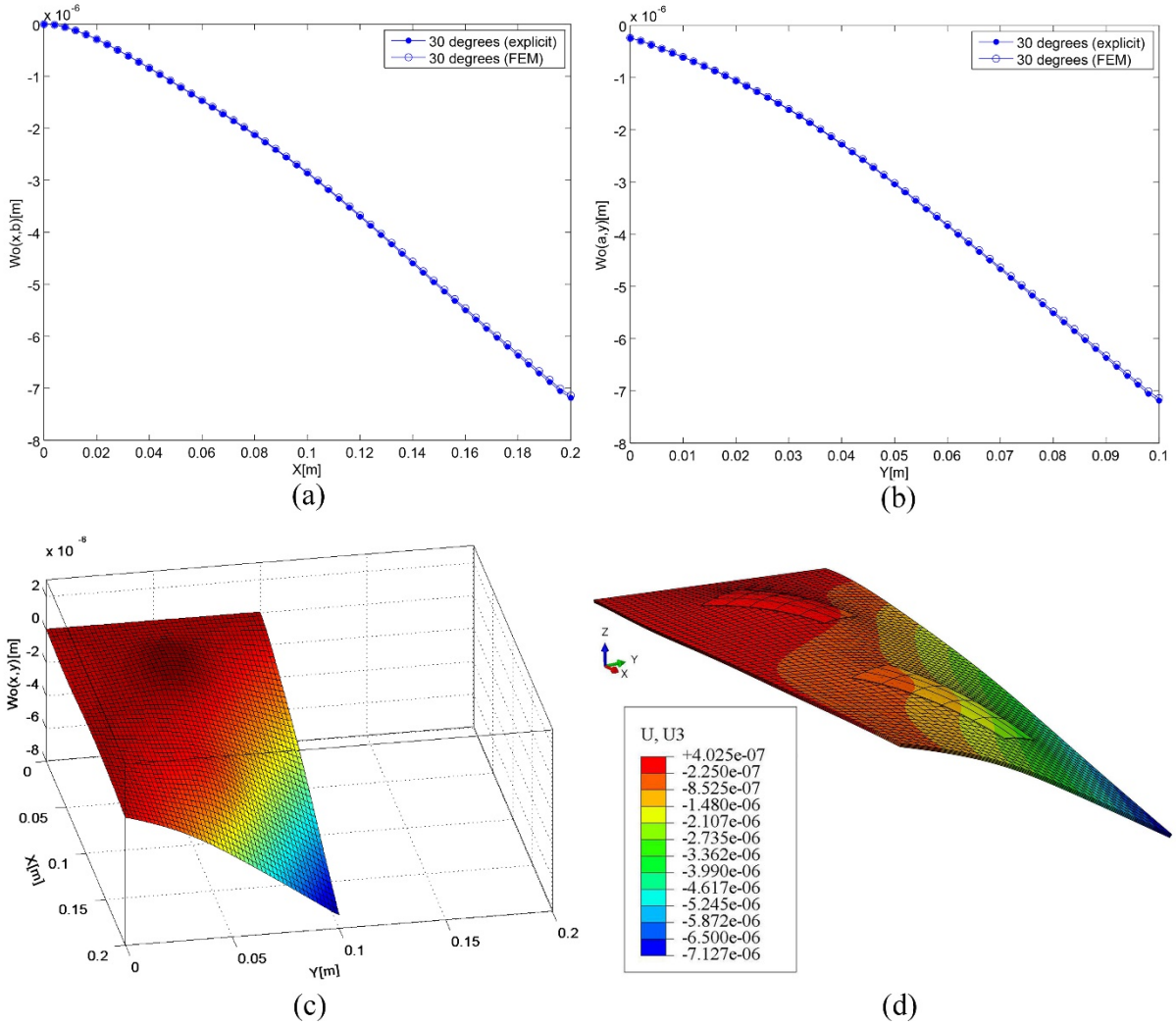

Fig.11. Explicit and numerical analysis of shape deformation in the smart cantilever composite plate integrated with inclined double piezoelectric actuator pairs when $\theta = 30^o$: a) $w_o(x,b)$, b) $w_o(a,y)$, c) $w_o(x,y)$: Explicit, d) $w_o(x,y)$: Numerical.

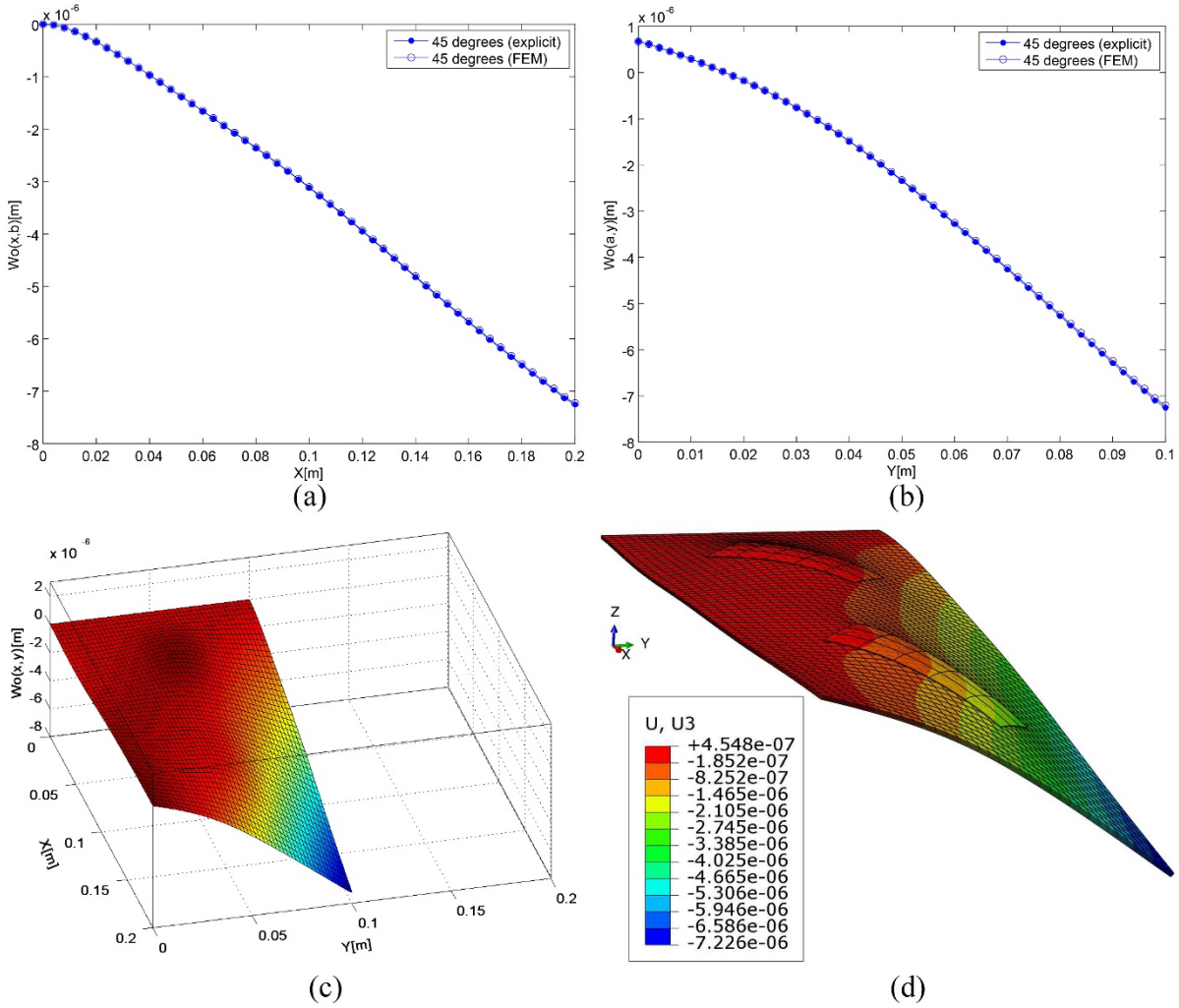

Fig.12. Explicit and numerical analysis of shape deformation in the smart cantilever composite plate integrated with inclined double piezoelectric actuator pairs when $\theta = 45^o$: a) $w_o(x,b)$, b) $w_o(a,y)$, c) $w_o(x,y)$: Explicit, d) $w_o(x,y)$: Numerical.

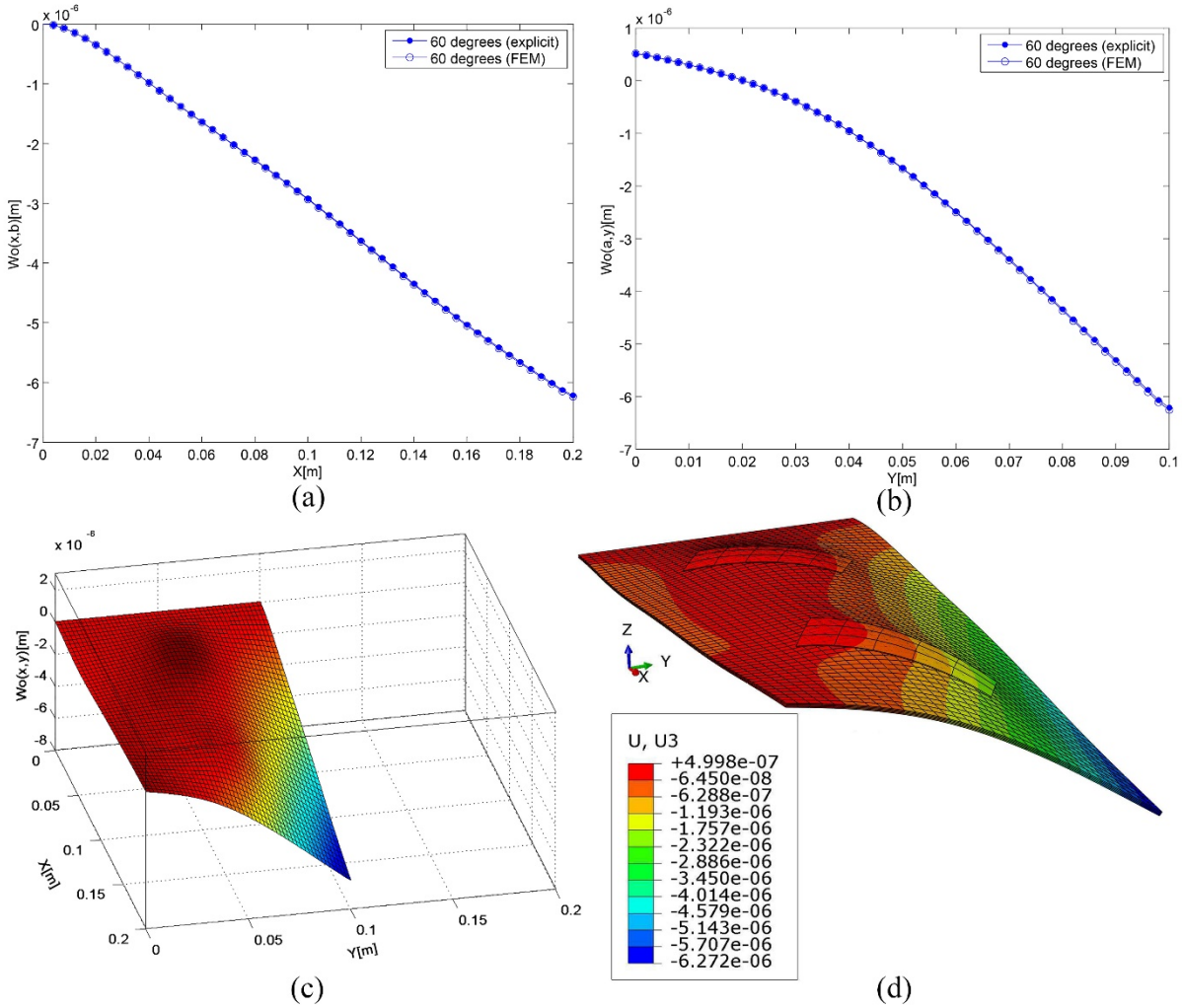

Fig.13. Explicit and numerical analysis of shape deformation in the smart cantilever composite plate integrated with inclined double piezoelectric actuator pairs when $\theta = 60^o$: a) $w_o(x,b)$, b) $w_o(a,y)$, c) $w_o(x,y)$: Explicit, d) $w_o(x,y)$: Numerical.

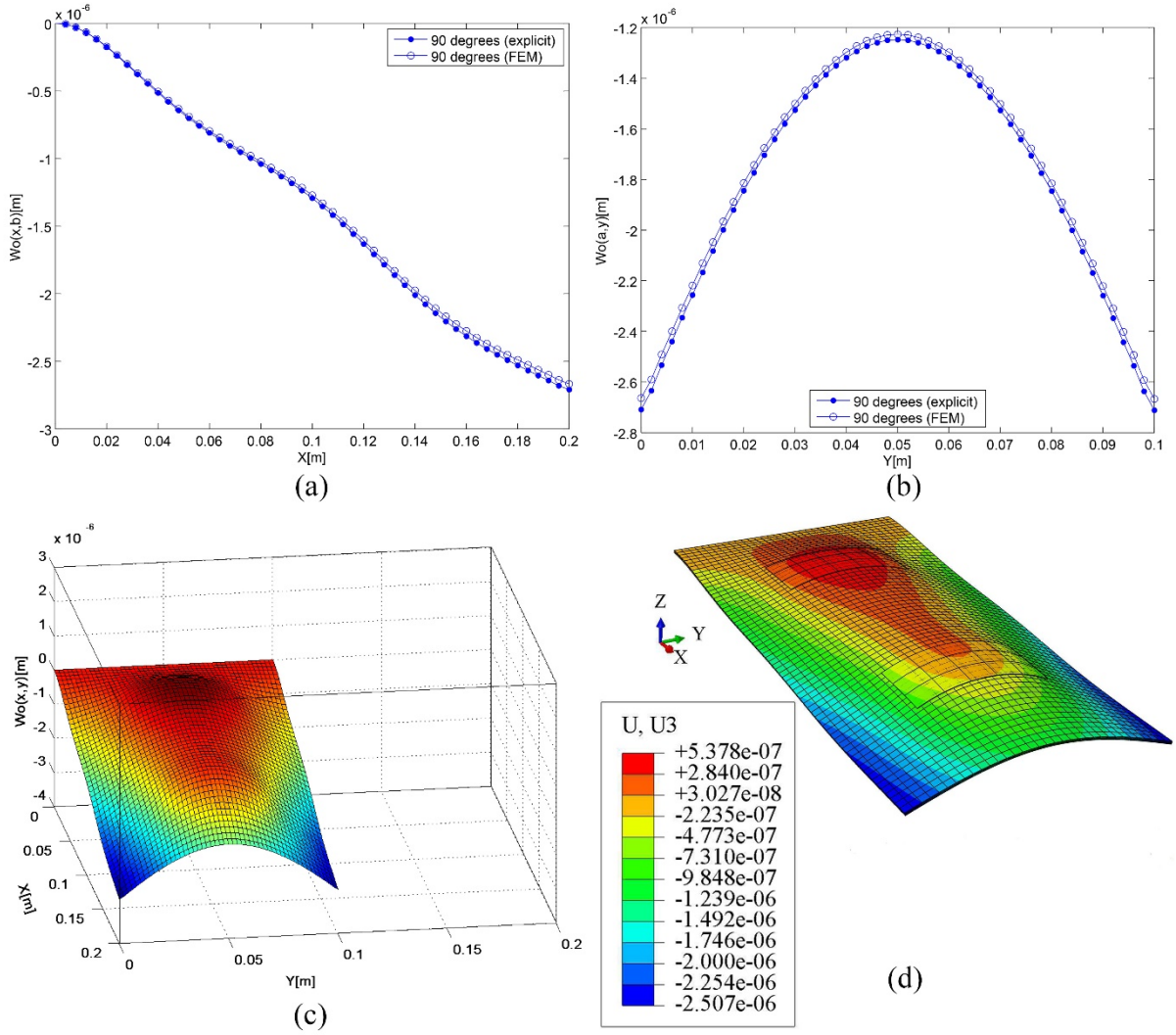

Fig.14. Explicit and numerical analysis of shape deformation in the smart cantilever composite plate integrated with inclined double piezoelectric actuator pairs when $\theta = 90^o$: a) $w_o(x,b)$, b) $w_o(a,y)$, c) $w_o(x,y)$: Explicit, d) $w_o(x,y)$: Numerical.

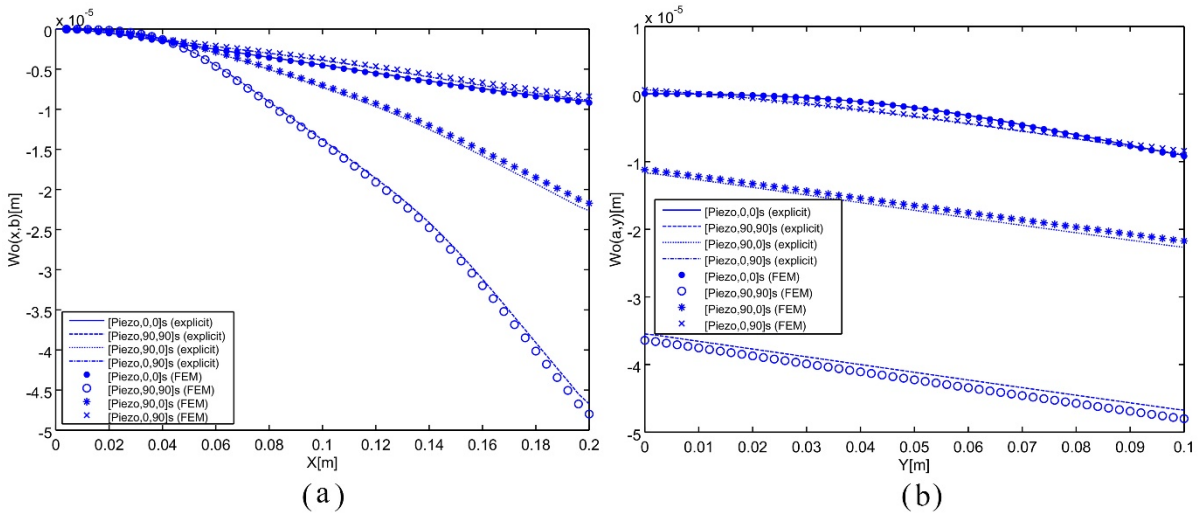

Fig.15. Explicit and numerical analysis of stacking sequence configuration effect on shape deformation in the smart cantilever composite plate integrated with inclined double piezoelectric actuator pairs: a) $w_o(x,b)$, b) $w_o(a,y)$.

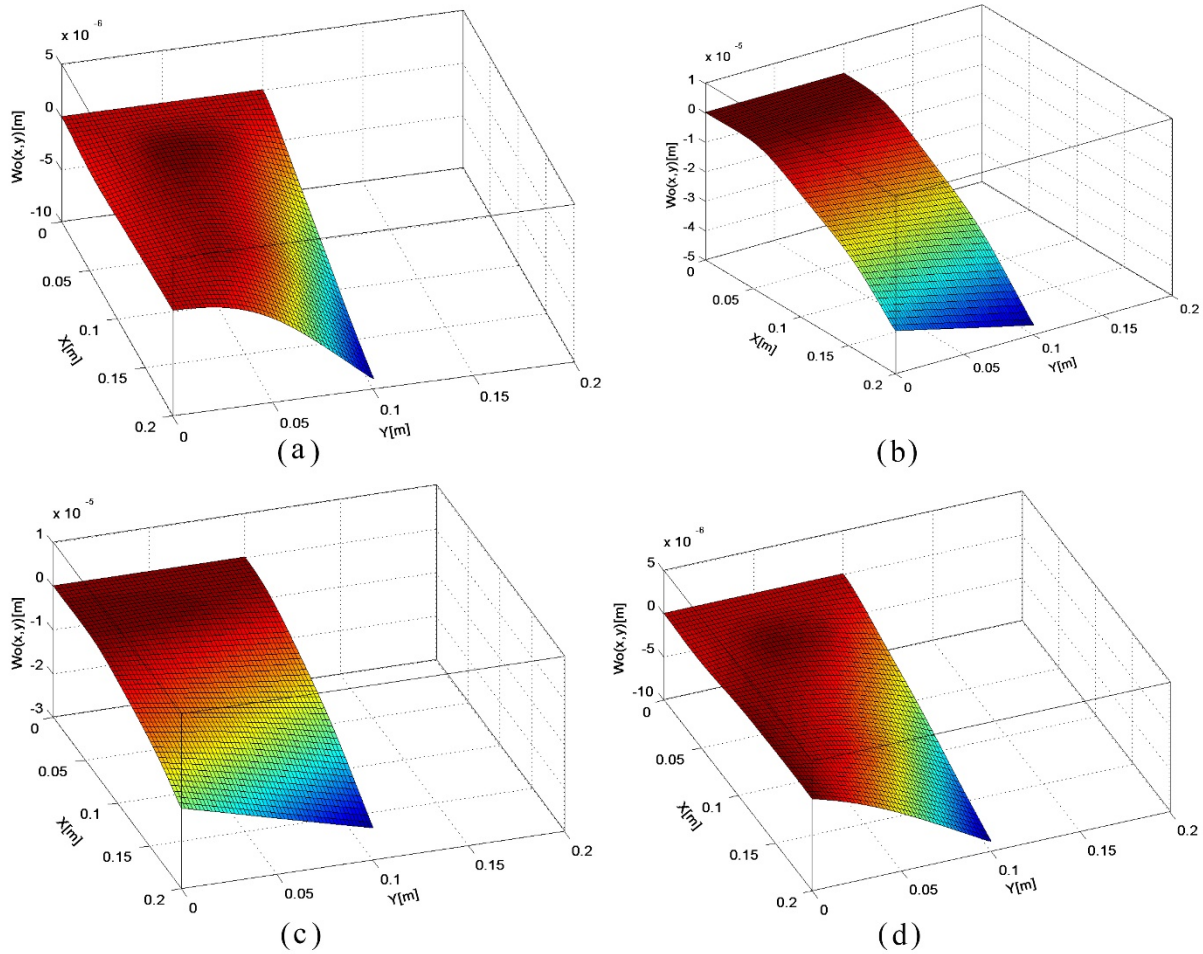

Fig.16. Explicit analysis of stacking sequence configuration effect on shape deformation in the smart cantilever composite plate integrated with inclined double piezoelectric actuator pairs: a) $[Piezo,0,0]_s$, b) $[Piezo,90,90]_s$, c) $[Piezo,90,0]_s$, d) $[Piezo,0,90]_s$.

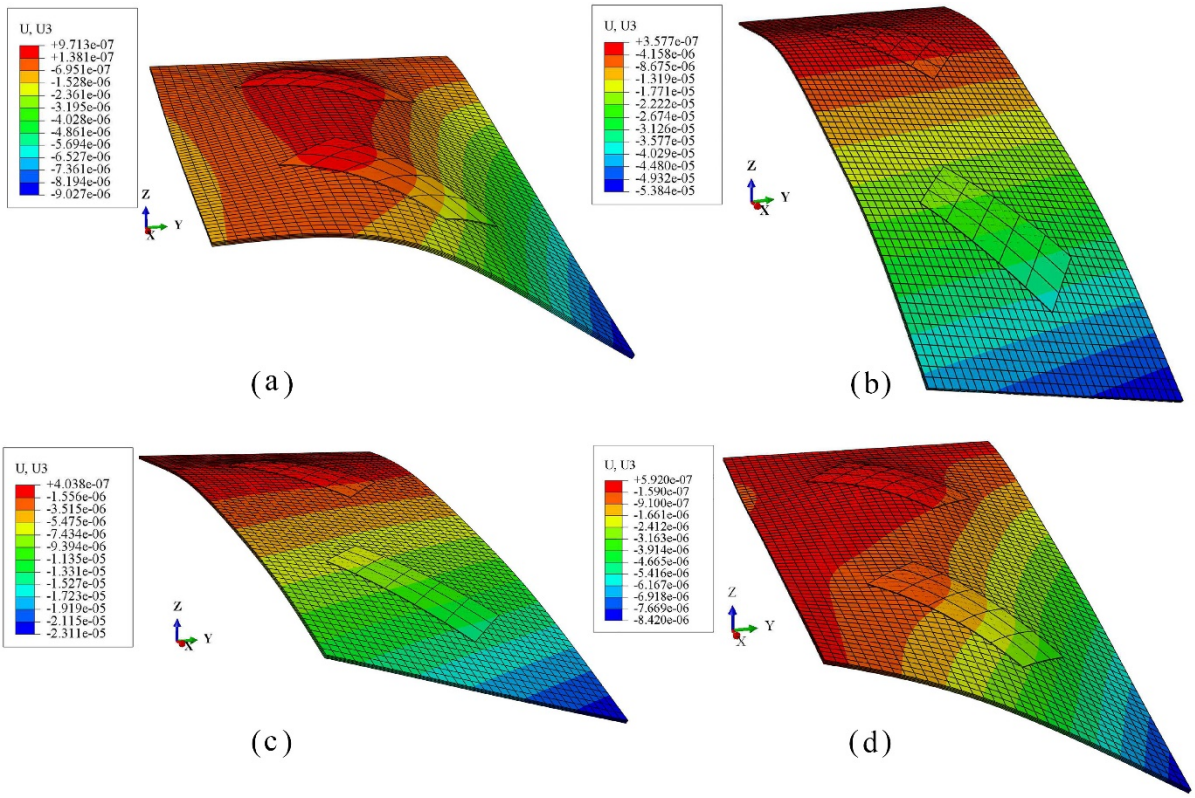

Fig.17. Numerical analysis of stacking sequence configuration effect on shape deformation in the smart cantilever composite plate integrated with inclined double piezoelectric actuator pairs: a) $[Piezo,0,0]_s$, b) $[Piezo,90,90]_s$, c) $[Piezo,90,0]_s$, d) $[Piezo,0,90]_s$.

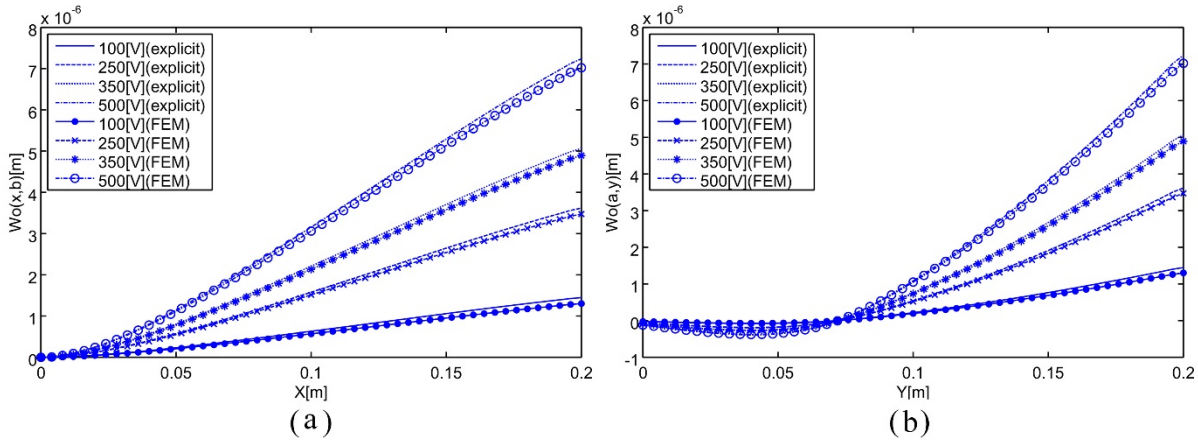

Fig.18. Explicit and numerical analysis of electrical voltage effect on shape deformation in the smart cantilever composite plate integrated with inclined double piezoelectric actuator pairs: a) $w_o(x,b)$, b) $w_o(a,y)$.

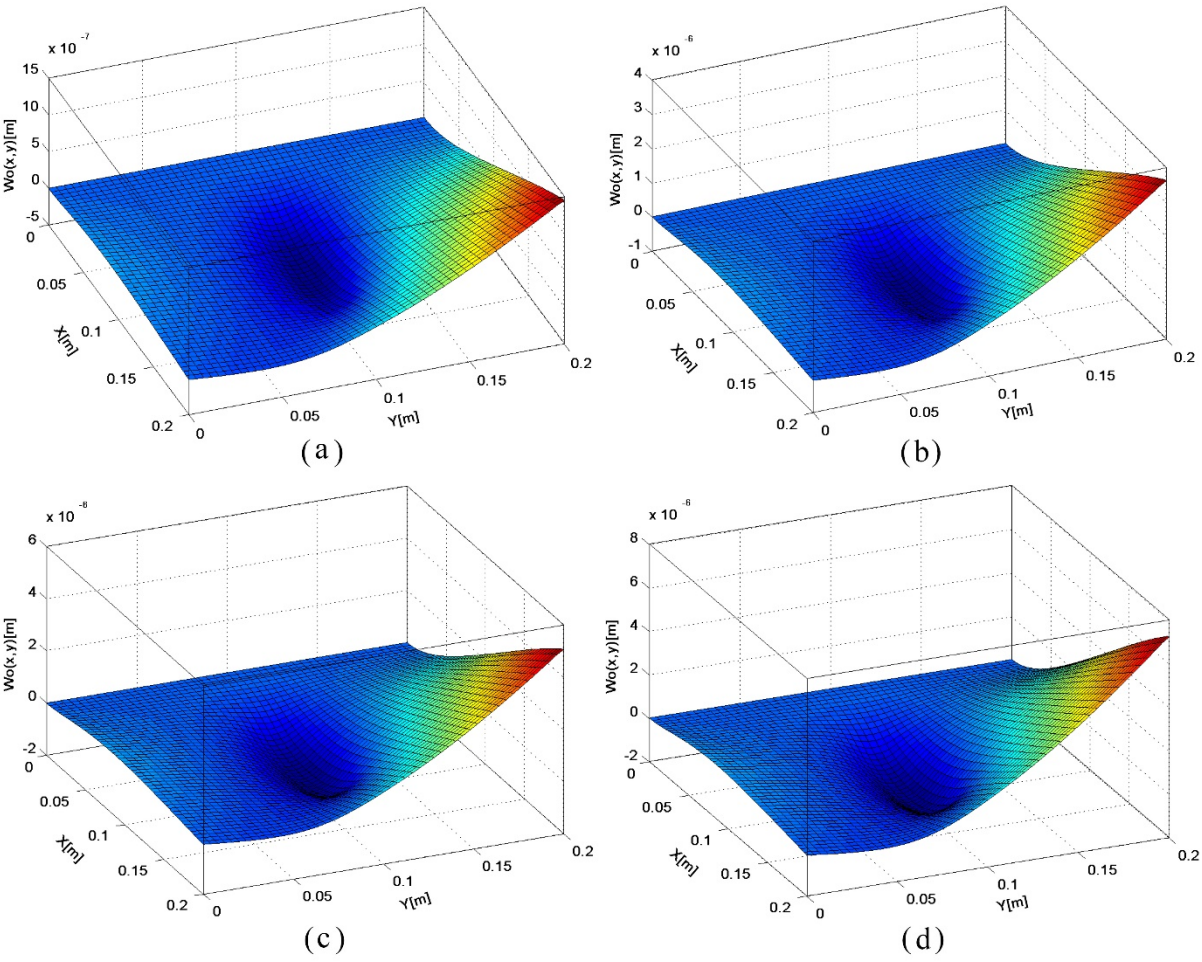

Fig.19. Explicit analysis of electrical voltage effect on shape deformation in the smart cantilever composite plate integrated with inclined double piezoelectric actuator pairs: a) 100 [*V*], b) 250 [*V*], c) 350 [*V*], d) 500 [*V*].

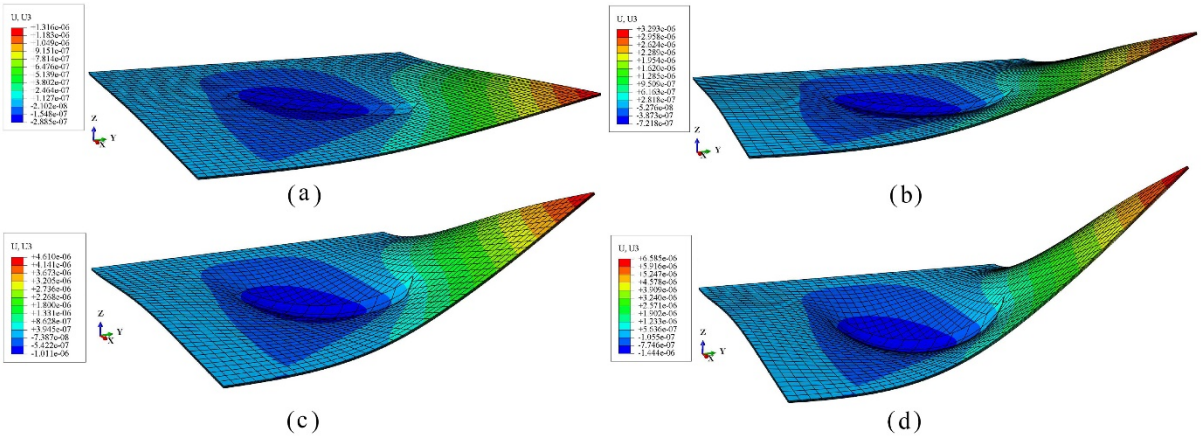

Fig.20. Numerical analysis of electrical voltage effect on shape deformation in the smart cantilever composite plate integrated with inclined double piezoelectric actuator pairs: a) 100 [*V*], b) 250 [*V*], c) 350 [*V*], d) 500 [*V*].

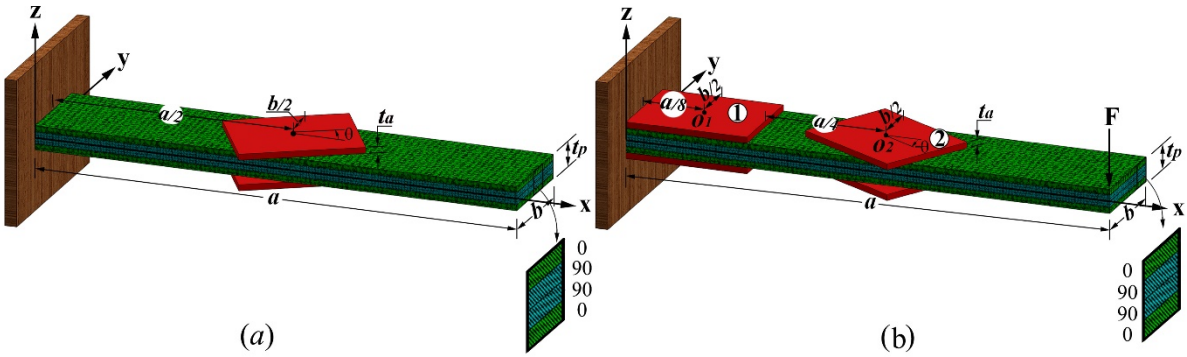

Fig.21. a) The smart laminated cantilever composite beam integrated with inclined single bounded piezoelectric actuator pair, b) shape control task of the smart composite laminate subjected to asymmetrical concentrated load using double inclined bounded piezoelectric actuator pairs.

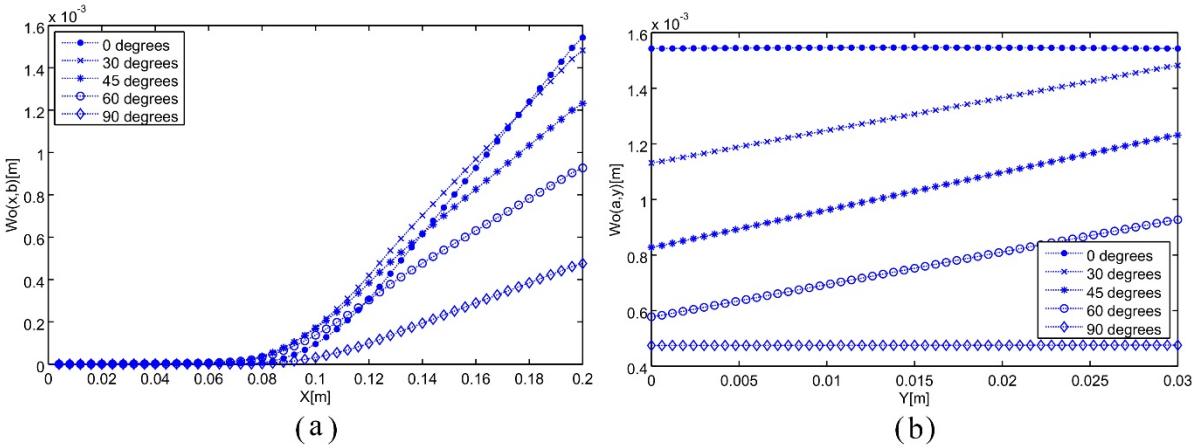

Fig.22. Explicit and numerical analysis of various inclination angle effect on shape deformation in the smart cantilever composite plate integrated with inclined double piezoelectric actuator pairs: a) $w_o(x,b)$, b) $w_o(a,y)$.

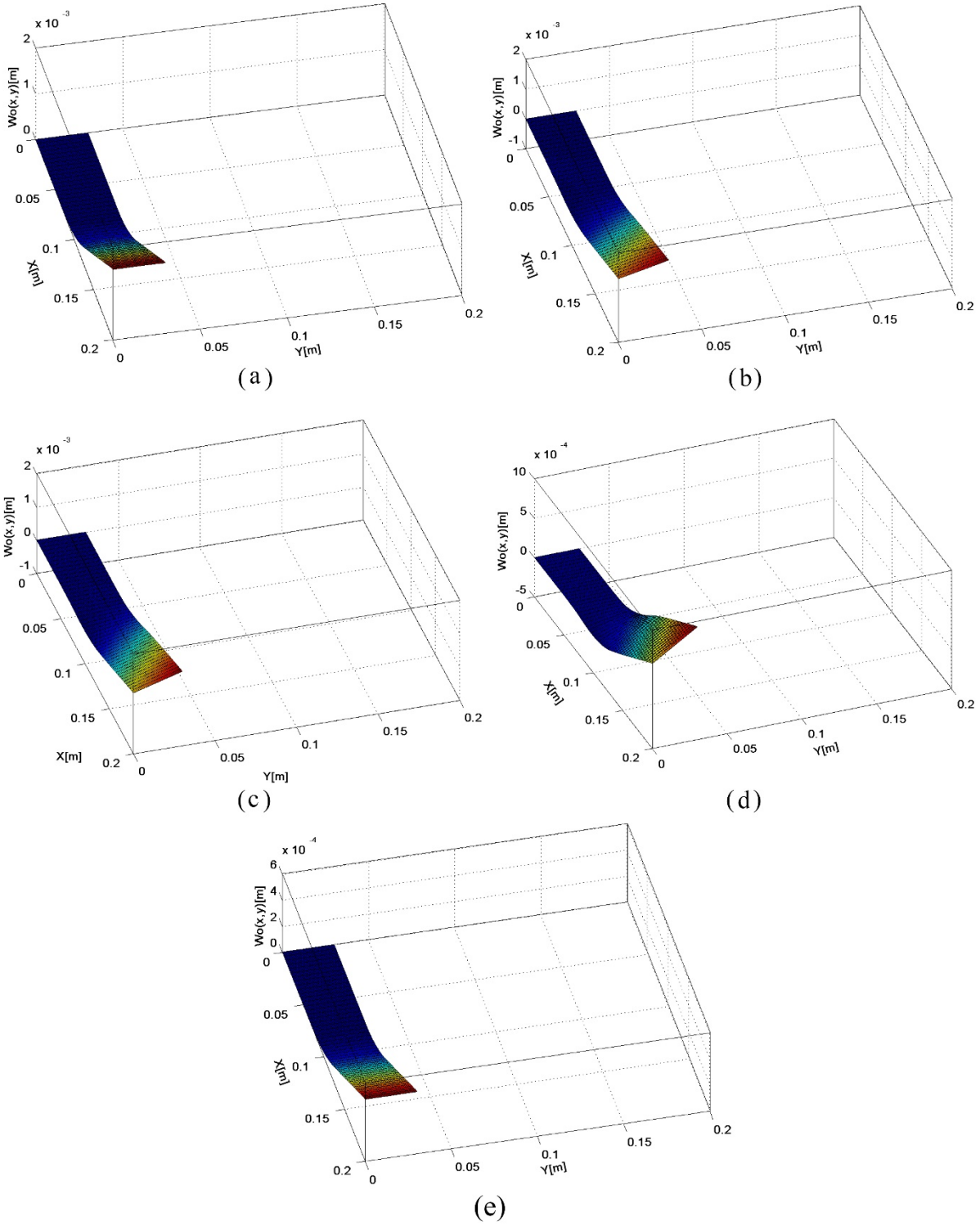

Fig.23. Explicit analysis of various inclination angle effect on shape deformation in the smart cantilever composite plate integrated with inclined double piezoelectric actuator pairs: a) $\theta = 0^o$, b) $\theta = 30^o$, c) $\theta = 45^o$, d) $\theta = 60^o$, e) $\theta = 90^o$.

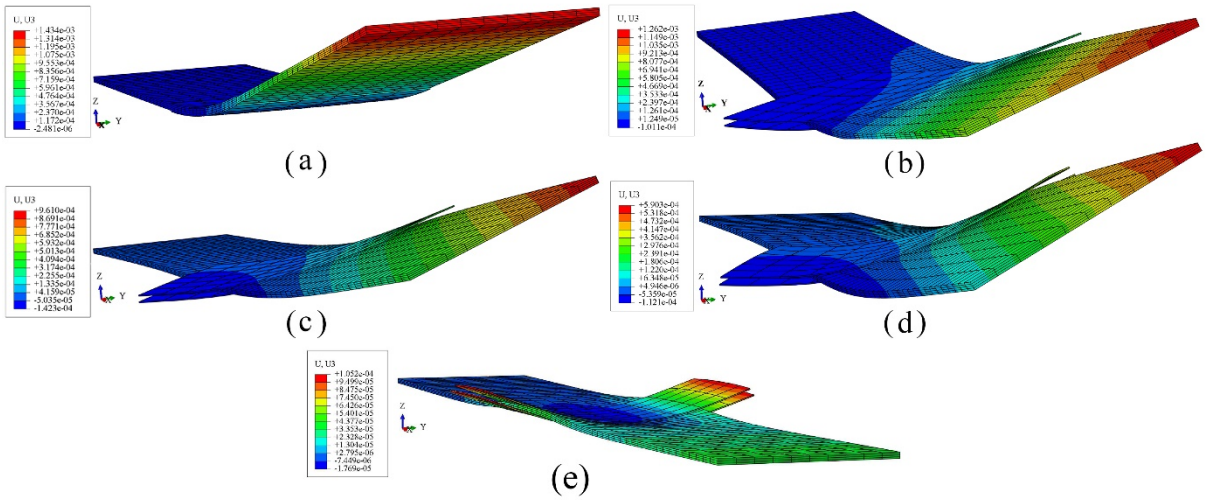

Fig.24. Numerical analysis of various inclination angle effect on shape deformation in the smart cantilever composite plate integrated with inclined double piezoelectric actuator pairs: a) $\theta = 0^o$, b) $\theta = 30^o$, c) $\theta = 45^o$, d) $\theta = 60^o$, e) $\theta = 90^o$.

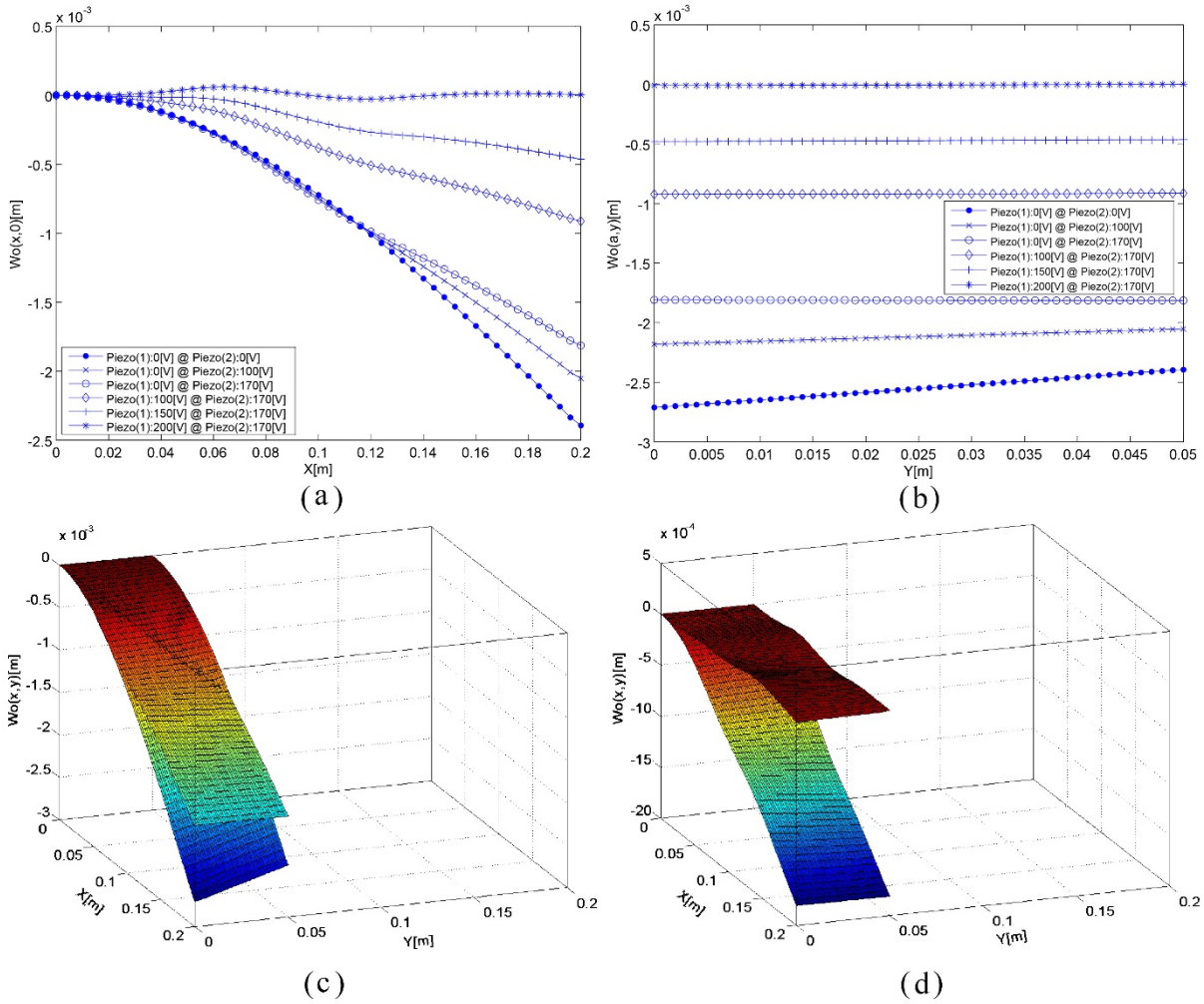

Fig.25. Explicit analysis of shape control task of the smart composite laminate subjected to asymmetrical concentrated load using double inclined bounded piezoelectric actuator pairs: a) $w_o(x,0)$, b) $w_o(a,y)$, c) $w_o(x,y)$: Pure twisting suspension using piezoelectric actuator ② ($\theta = -30^0$), d) $w_o(x,y)$: Pure bending suspension using piezoelectric actuator ① ($\theta = 0^0$).